

Sorbonne Université

2021-2022

Stage de Master 2

Noé Bassel

(Non)-equilibrium molecular dynamics and a Norton method for the estimation of transport coefficients

Projet réalisé en collaboration avec le CERMICS
Ecole Nationale des Ponts et Chaussées
6 et 8 avenue Blaise Pascal
Cité Descartes - Champs sur Marne
77455 Marne la Vallée Cedex 2

Tuteur : Gabriel Stoltz

July 29, 2022

This document is the report for an internship which took place from February 1st to July 31st 2022, at the CERMICS laboratory in the École des Ponts. This is a research unit in applied mathematics, comprising of teams working on problems arising from probability theory and optimization, as well as, more directly relevant to us, material science and molecular simulations. It was conducted under the advisement of Gabriel Stoltz, and had two explicitly stated aims.

One was to engage with Julia and its molecular simulation ecosystem by implementing various methods from equilibrium and non-equilibrium molecular dynamics inside the Molly package. Eventually, this approach resulted in a one-week stay with Molly's main author, to integrate some of the implementations developed during the course of the internship inside Molly.

A second aim, more prospective from the scientific point of view, was to advance the understanding of the Norton method, which is a novel method for the computation of transport coefficients from molecular simulations, based on a dual approach from the standard non-equilibrium method, whereby the response is fixed and the average forcing needed to induce it is measured, instead of the usual reverse situation. As of the end of this internship, we have proposed a numerical integration strategy for a class of Norton dynamics, and applied it to the cases of mobility and shear viscosity computations. Our numerical results suggest several avenues for future theoretical work, which will be continued in the PhD work of Shiva Darshan, starting from the fall of 2022.

The report is divided into five chapters and one appendix. The first chapter is dedicated to a basic introduction to some concepts in statistical mechanics which are relevant to molecular simulation. The second and third chapter are dedicated to equilibrium averages, with the second's focus on a presentation of the different numerical methods involved, and the third's on answering a question that arose when examining's Molly native Langevin integrator, which coincidentally was also under investigation at the same time by a team of theoretical chemists, Bettina Keller and Stefanie Kieninger. It is essentially compiled from the written communication we sent to them, presenting our understanding of the BAOA scheme. The fourth and fifth chapters are dedicated to the non-equilibrium setting, with the fourth centered on a discussion of the standard methods (Thévenin and Green-Kubo), and the fifth on the presentation of the Norton method. All chapters are supplemented with numerical examples, which are destined to illustrate some theoretical properties, or the viability of a given numerical method. We conclude the report by a short appendix which highlight some of the thinking that went into the choice of Molly as a molecular simulation package, as well as pointing the reader to relevant source code.

Every example on a realistic system was implemented within Molly, and thus we wish to thank Joe Greener for creating this very flexible and pleasant to work with package, as well as for inviting us to stay for a fascinating week in Cambridge. We also take advantage of this short introduction to thank Gabriel Stoltz for trusting us with this subject, for his precious advice, and more generally for introducing us to the fun and mathematically rich subject that is molecular simulation.

Notational conventions

We convene that the gradient of a differentiable function $\varphi : \mathbb{R}^n \mapsto \mathbb{R}$ is a column vector-valued function

$$\nabla \varphi : \mathbb{R}^n \rightarrow \mathbb{R}^n := \mathbb{R}^{n \times 1}.$$

Notationally,

$$\nabla = \begin{pmatrix} \partial x_1 \\ \vdots \\ \partial x_n \end{pmatrix}.$$

So that the Hessian operator writes

$$\nabla^2 := \nabla \nabla^\top = \begin{pmatrix} \partial_{x_1, x_1}^2 & \cdots & \partial_{x_1, x_n}^2 \\ \vdots & \ddots & \vdots \\ \partial_{x_n, x_1}^2 & \cdots & \partial_{x_n, x_n}^2 \end{pmatrix}$$

The gradient (also known as the Jacobian matrix) of a vector field $f = (f_1, \dots, f_n)^\top : \mathbb{R}^n \rightarrow \mathbb{R}^n$ is

$$\nabla f = \begin{pmatrix} \nabla^\top f_1 \\ \vdots \\ \nabla^\top f_n \end{pmatrix} = (\nabla \otimes f)^\top, \quad (1)$$

while its divergence is

$$\operatorname{div} f = \partial_{x_1} f_1 + \cdots + \partial_{x_n} f_n = \nabla^\top f.$$

Contents

1	Introduction to molecular dynamics	6
1.1	The microscopic description of atomic systems	6
1.1.1	Classical phase space	6
1.1.2	From microscopic states to macroscopic quantities	7
1.2	Thermodynamic ensembles	8
1.2.1	Microcanonical ensemble	8
1.2.2	Canonical ensemble	9
1.3	Microscopic dynamics	10
1.3.1	Reduced units	11
1.3.2	Ergodic averages	12
2	Sampling equilibrium properties	13
2.1	Microcanonical averages	13
2.1.1	Elementary properties of Hamiltonian dynamics	13
2.1.2	Numerical schemes for Hamiltonian dynamics	16
2.2	Canonical averages	20
2.2.1	Langevin dynamics	20
2.2.2	Invariance of the canonical measure	21
2.2.3	Overdamped limit of Langevin dynamics	23
2.2.4	Convergence to equilibrium	24
2.2.5	Asymptotic variance for ergodic averages	24
2.2.6	Splitting schemes for the Langevin dynamics	25
2.2.7	Error analysis for splitting schemes	28
2.2.8	Unbiased sampling	29
2.2.9	Numerical illustrations	31
3	Study of the BAOA scheme	33
3.1	Relating invariant measures of discretization schemes	34
3.2	Error estimate on the phase space measure	35
3.3	Error estimates on the kinetic marginal distributions	36
3.4	Analysis of the second order error term for kinetic averages under $\mu_{\Delta t, P}$	37
3.5	Analysis of the discrepancy between the dominant error terms on the kinetic marginals	39
3.6	Numerical results	40
3.6.1	Models	41
3.6.2	Equality of marginal configurational distributions	41
3.6.3	Comparison of marginal kinetic distributions	41
3.6.4	Verification of the first-order expansion	43
3.6.5	Example of first-order bias in a BAOA average	43
3.6.6	Effect of the friction parameter	43
4	Non-equilibrium Molecular Dynamics	47
4.1	Non-equilibrium molecular dynamics	47
4.1.1	General framework	47
4.1.2	Numerical implementation	49
4.1.3	Mobility	50
4.1.4	Shear viscosity	50
4.2	The Green–Kubo method	53

4.2.1	Numerical implementation	55
4.2.2	Mobility	56
4.2.3	Shear viscosity	60
5	Norton dynamics	63
5.1	General framework	63
5.2	Norton dynamics for transport coefficients	65
5.2.1	Splitting schemes for numerical integration	66
5.2.2	Physical interpretation	70
5.3	Numerical results	71
5.3.1	Mobility	71
5.3.2	Shear viscosity	72
A	Implementation details	77
A.1	Scaling of the computational cost	77
A.2	Selecting a Molecular Dynamics package	78
A.3	Summary of implementations	78

Chapter 1

Introduction to molecular dynamics

The purpose of this chapter is to introduce a few of the basic ideas from classical and statistical mechanics which enter into the conceptual framework of molecular simulation. We start by describing the classical account of the microscopic state of a system, before motivating and presenting the notion of statistical ensembles, which captures the idea of the macroscopic state of a system with many unknowable microscopic degrees of freedom. Having presented some examples, we finally describe how dynamics on the microscopic level can in principle be thought of as a means to sample from these ensembles, thus allowing the measurement of macroscopic properties from the numerical simulation of the microscopic dynamics.

1.1 The microscopic description of atomic systems

Molecular dynamics, and computational statistical physics at large, aim at simulating on the computer the behavior of physical systems. The hope is that one can infer quantities and properties of real-life interest from observing the results of numerical simulations, which may be relevant to understanding material properties of many-particle systems, or the nature of interactions in complex systems such as those found in biology. Computational simulations can thus act as surrogate experiments in cases where experimental setups are hard to achieve, or measurements are impossible. They can also be seen as surrogate tests of theoretical models, as they allow to test the validity of a mathematical description by comparing numerical predictions to experimental data. Molecular dynamics, in particular, is concerned with simulating atomic systems, most often (and as we shall systematically do) using a classical description.

1.1.1 Classical phase space

We consider a system of N particles evolving in d -dimensional space. The classical description contends that the *state* of a system is the datum of the positions and momenta of every particle in the system. We can interpret this as the statement that, given full knowledge of the positions and momenta at some initial time, and of the forces at play, one can deduce exactly the positions and momenta at any future time. It is often the case in computer simulations that we consider positions which are restricted to a bounded domain by the use of periodic boundary conditions. To that effect, let

$$\mathcal{D} = (L\mathbb{T})^{dN} \text{ or } \mathbb{R}^{dN},$$

where \mathbb{T} is the one-dimensional torus. We call \mathcal{D} the configuration space.

Definition 1 (Phase space). *We describe the positions and momenta of the atoms as vectors*

$$q = (q_{1,1}, \dots, q_{1,d}, \dots, q_{N,1}, \dots, q_{N,d})^\top \in \mathcal{D},$$

$$p = (p_{1,1}, \dots, p_{1,d}, \dots, p_{N,1}, \dots, p_{N,d})^\top \in \mathbb{R}^{dN},$$

where $q_i := (q_{i,1}, \dots, q_{i,d})^\top$ is the position vector of the i -th particle, and similarly for p . Let

$$\mathcal{E} := \mathcal{D} \times \mathbb{R}^{dN}.$$

In this framework, the time evolution of a system can be captured by trajectories

$$(q_t, p_t)_{t \geq 0} \subset \mathcal{E}$$

through phase space. It is not clear *a priori* why we should choose momenta to describe the kinetic quality of the system, rather than velocities, although this is fully justified after the fact because it makes many mathematical properties simpler to state (see for example Proposition 1). However, it is of no importance since we can change from one description to the other via the relation

$$v = M^{-1}p,$$

where $M \in \mathbb{R}^{dN \times dN}$ is a diagonal matrix recording the masses of each particle (d times per particle), and v is the velocity vector. Equipped with this microscopic description, we can now describe the macroscopic state of a system, which we understand as the magnitude of certain observed quantities, in terms of its underlying microscopic configuration.

1.1.2 From microscopic states to macroscopic quantities

The way to relate a macroscopic quantity to a microscopic state is through the general notion of an observable, which is simply a function

$$\varphi : \mathcal{E} \rightarrow \mathbb{R}$$

mapping a microscopic state to a quantity. Of course, the challenge is to define observables which are relevant in explaining pertinent macroscopic behavior. We will not be going into the details of how formulas for these observables can be obtained, since this is a substantial part of classical mechanics. We refer the interested reader to [30, Section 5.7] for an example of such a derivation in the case of pressure, while we simply state some of the observables we will be interested in. Of utmost importance, we define the Hamiltonian, which corresponds to the total energy of the system:

$$H(q, p) = \frac{1}{2} p^\top M^{-1} p + V(q). \quad (1.1)$$

It is the sum of two terms, the kinetic energy on the left, and the potential energy on the right, which also define respective observables of interest in their own right. As we shall see, the Hamiltonian encodes the microscopic dynamics of the system. Let us note that although we restrict our discussion to real-valued observables, we can of course consider vector-valued observables, such as the force ∇V . The kinetic temperature is defined by the following expression:

$$T_\kappa(q, p) = \frac{2}{k_B d N} E_\kappa(q, p).$$

It is, up to a conversion factor of Boltzmann's constant, twice the kinetic energy per degree of freedom. The instantaneous isotropic pressure is defined by

$$P(q, p) = \frac{1}{|\mathcal{D}|} \left(N k_B T_\kappa - \frac{1}{d} \sum_{i=1}^N q_i^\top \nabla_{q_i} V(q) \right).$$

Neglecting the right-hand side gives the famous ideal gas law, $PV = Nk_B T$, which is a good approximation at low densities. The right hand side, otherwise known as the virial, appears to be problematic since the q_i are not periodic functions of q , which would suggest P is not a well-defined observable on \mathcal{D} . However, in the case of a periodic pair interaction of the form (1.12), we can use symmetry arising from Newton's third law to arrive at the following expression:

$$P(q, p) = \frac{1}{d|\mathcal{D}|} \left(\sum_{i=1}^N \frac{|p_i|^2}{m_i} - \sum_{1 \leq i < j \leq N} |q_i - q_j| v'(|q_i - q_j|) \right), \quad (1.2)$$

At this point, we are faced with an apparent paradox: for a system that does not display macroscopic evolution, quantities such as the energy and pressure appear constant, while the microscopic description suggest they should evolve as a function of the underlying microscopic dynamics. A possible solution to this paradox is to move to a probabilistic description. This is the path chosen by statistical mechanics, which we now turn to by introducing the notion of a thermodynamic ensemble.

1.2 Thermodynamic ensembles

The microscopic description is interesting from a theoretical standpoint, but it fails to be relevant when attempting to describe the behavior of atomic systems with a macroscopic number of particles, of the order of Avogadro's number (6.02×10^{23}). Besides the technical impossibility of measuring to a high accuracy the configuration of such systems, and that of recording the information required to track it (coincidentally, the total amount of digitally stored information on Earth is estimated to be 10^{23} bytes as of 2022), it is also the case that knowledge of a system at this level of detail is unnecessary to describe the quantities which are relevant to our macroscopic experience. In the instance of a gas at thermal equilibrium, examples of relevant quantities are total energy, pressure, temperature, density, which, while of course resulting from the internal state of the system, are independent of the minutiae of individual atomic motions: loosely speaking, one may describe the macroscopic state of a system by only a handful of macroscopic variables, loosing track of the myriad of microscopic degrees of freedom. In fact, since real-valued observables map a high dimensional space to a one dimensional space, we can expect that for a given set of macroscopic conditions, there will in general be many microscopic states compatible with these conditions. This motivates, from a purely rational point of view, passing to a statistical description: we define the macroscopic state of the system as an *ensemble* of microscopic conditions compatible with the observed macroscopic constraints. In full generality, we may further distinguish microscopic states by the likelihood they underlie the macroscopic state: this amounts to defining a probability distribution over the ensemble, or in more mathematical terms, to the data of a probability measure μ on phase space. The macroscopic value of an observable φ can now be interpreted as an average over the ensemble,

$$\mathbb{E}_\mu[\varphi] = \int_{\mathcal{E}} \varphi(q, p) \mu(dq, dp). \quad (1.3)$$

This, of course, does not tell us *how* we should choose such a probability measure. However, it seems reasonable to choose, out of all probability measures which are compatible with the macroscopic constraints, that which contains the least information about the microscopic state, or in other words that which makes the least assumptions about it. The mathematical translation of this idea is given by the principle of maximal entropy. Out of all probability distributions ρ , which for convenience we identify with smooth densities on \mathcal{E} , and which are consistent with the macroscopic constraints, we may define the statistical ensemble as the one which maximizes the statistical entropy

$$S(\rho) = - \int_{\mathcal{E}} \rho(x) \ln(\rho(x)) dx. \quad (1.4)$$

For a mathematically rigorous introduction to these ideas, we refer the reader to [5, Chapter 3]. We will be considering two examples of thermodynamic ensembles.

1.2.1 Microcanonical ensemble

The microcanonical ensemble is the suitable model for an isolated system in thermodynamic equilibrium, evolving according to Hamiltonian dynamics. The number of particles N , the volume $V = L^3$, and the energy E are fixed. We will alternatively refer to the microcanonical ensemble as the NVE ensemble. Because the constant energy condition constrains the compatible microstates to level sets of H , which in general will be Lebesgue-negligible subsets of \mathcal{E} , some care must be taken in defining the microcanonical measure, since one cannot express the macroscopic constraints by a family of probability densities. However, under suitable assumptions on V , one can define the microcanonical measure as a weak limit of uniform distributions over level "shells" of H :

$$\int_{\mathcal{E}} \varphi d\mu_{mc,E} := \lim_{\varepsilon \rightarrow 0} \frac{1}{|S(E, \varepsilon)|} \int_{S(E, \varepsilon)} \varphi(q, p) dq dp,$$

where

$$S(E, \varepsilon) = \{(q, p) \in \mathcal{E} \mid H(q, p) \in [E - \varepsilon, E + \varepsilon]\}.$$

This is consistent with the fact that, for a set A with finite Lebesgue measure, the probability distribution on A which maximizes the entropy is the uniform distribution on A . Alternatively, $\mu_{mc,E}$ is uniquely defined by the relation

$$\frac{1}{Z_E} \int_{\mathcal{E}} g(H(q, p)) f(q, p) dq dp = \int_{\mathbb{R}} g(E) \int_{\mathcal{E}} f(q, p) \mu_{mc,E}(dq, dp) dE,$$

for all test functions $g : \mathbb{R} \rightarrow \mathbb{R}$ and $f : \mathcal{E} \rightarrow \mathbb{R}$, and where Z_E is a normalization constant ensuring that $\mu_{mc,E}(\mathcal{E}) = 1$. It is possible, using the coarea formula, to derive an explicit formula for $\mu_{mc,E}$, namely,

$$\mu_{mc,E}(dq, dp) = \frac{1}{Z_E} \frac{\sigma_E(dq, dp)}{|\nabla H(q, p)|}, \quad (1.5)$$

where σ_E is the surface measure induced by the Lebesgue measure on the constant energy manifold

$$S(E) = \{(q, p) \in \mathcal{E} \mid H(q, p) = E\}. \quad (1.6)$$

1.2.2 Canonical ensemble

Isolated systems in thermal equilibrium are not typically those that we encounter in experiments. Instead, it is more common to observe systems which are in thermal equilibrium with respect to their environment, an ambient *heat bath* at a fixed temperature. The total energy of such systems is not fixed: small fluctuations can occur as energy is exchanged back and forth between the heat bath and the system. However, the average energy \bar{E} is fixed. This is the macroscopic constraint that defines the canonical ensemble. For fixed values N, V, \bar{E} , define the density of the the canonical measure as the maximizer:

$$\underset{\rho \in \mathcal{A}}{\operatorname{argmax}} \mathfrak{S}(\rho)$$

where \mathcal{A} is the set of admissible densities

$$\mathcal{A} = \left\{ \rho : \mathcal{E} \rightarrow \mathbb{R}_+ \mid \int_{\mathcal{E}} \rho = 1, \int_{\mathcal{E}} H(q, p) \rho(q, p) dq dp = \bar{E} \right\}.$$

Solving the Euler-Lagrange equation associated with this constrained optimization problem yields that the only admissible solution can be written under the form:

$$\mu(q, p) := \frac{1}{Z} e^{-\beta H(q, p)}. \quad (1.7)$$

Furthermore, one can show that μ is indeed the unique maximizer. Here, $-\beta$ and $1 + \ln Z$ are the Lagrange multipliers associated respectively with the energy constraint and the normalization constraint. Thus

$$Z = \int_{\mathcal{E}} e^{-\beta H(q, p)} dq dp$$

is a normalization constant called the partition function, and β is a tuning parameter related to the value of \bar{E} . The physical interpretation of β is that of an inverse temperature,

$$\beta = \frac{1}{k_B T},$$

where $k_B = 1.38 \times 10^{-23} \text{ J} \cdot \text{K}^{-1}$ is Boltzmann's constant. For obvious reasons, we prefer to refer to the canonical ensemble as the NVT ensemble, rather than the NVE. Besides, it can easily be shown that the canonical average of the kinetic temperature is equal to T , which justifies the terminology.

Remark 1 (Other ensembles). *One could of course go further and remark that when observing a fixed volume of unconfined gas in thermal equilibrium, the total number of particles N is not fixed. Rather, this fluctuates as particles are constantly exchanged with an ambient particle reservoir. Instead, the average number of particles \bar{N} is fixed. The resulting ensemble is called the grand canonical or μVT ensemble. This, and many other constructions are possible, but we will restrict our attention to the NVE and NVT cases.*

Remark 2 (Independence of canonical momenta and configurations). *We can make an observation on μ using the fact that the Hamiltonian 1.1 is separable: it is the sum of a kinetic term involving p and a configurational term involving q . Thus we can write*

$$e^{-\beta H(q, p)} = e^{-\frac{\beta}{2} p^T M^{-1} p} e^{-\beta V(q)},$$

which implies that the canonical measure μ is of tensor form:

$$\mu = \kappa \otimes \nu, \quad (1.8)$$

where κ is a probability measure on \mathbb{R}^{dN} has a density proportional to $e^{-\frac{\beta}{2} p^\top M^{-1} p}$ and ν has a density proportional to $e^{-\beta V(q)}$ on \mathcal{D} . Recognizing a multivariate Gaussian density, we can further write, abusing the notations κ and ν to denote both the laws and their densities,

$$\kappa(p) = \det\left(\frac{M}{2\pi\beta}\right)^{\frac{1}{2}} e^{-\frac{\beta}{2} p^\top M^{-1} p}, \quad (1.9)$$

$$\nu(q) = \frac{1}{Z_\nu} e^{-\beta V(q)}, \quad (1.10)$$

with

$$Z_\nu = Z \det\left(\frac{M}{2\pi\beta}\right)^{\frac{1}{2}}.$$

This implies in particular that the marginal distribution in p of the canonical measure can be sampled easily, using standard algorithms for generating i.i.d. Gaussian variables, such as the Box-Muller method.

The difficult part is thus to sample from ν , as it is generally a complex and high-dimensional probability measure. The strategy we will use, whatever the ensemble $\tilde{\mu}$, is to define a (possibly stochastic) dynamical system whose evolution leaves $\tilde{\mu}$ invariant.

1.3 Microscopic dynamics

In our sense, the most important dynamics is the reference dynamics prescribed by the laws of Newtonian mechanics. Recalling the potential V in (1.1), its gradient with respect to q_i

$$\nabla_{q_i} V := (\partial_{q_{i,d}}, \dots, \partial_{q_{i,d}})^\top$$

gives minus the force vector acting on the i -th particle. In our case we will always take the potential to be independent of the momentum, so that we can think of V as having domain \mathcal{D} . In the case where $\mathcal{D} = (L\mathbb{T})^{dN}$, it will be convenient to think of V as a function from \mathbb{R}^{dN} to \mathbb{R} which is C^1 and L -periodic in each direction. As it encodes the dynamics of the system, the potential V is of paramount importance. Indeed, the time evolution of the system is then described by Newton's second law:

$$M\ddot{q} = -\nabla V(q).$$

It will be convenient for our analysis to use of reformulation of Newton's equations, based on the Hamiltonian of a system. Using the Hamiltonian (1.1), we can rewrite the classical equations of motion as

$$\begin{cases} dq_t = M^{-1} p_t dt = \nabla_p H(q_t, p_t) dt \\ dp_t = -\nabla V(q_t) dt = -\nabla_q H(q_t, p_t) dt \end{cases}, \quad (1.11)$$

The potential energy is the most important part of the microscopic description, and accordingly, the first and foremost problem in establishing a physical model of this kind is to determine find a potential whose corresponding dynamics faithfully reproduce a given desirable macroscopic behavior. The choice of a classical description automatically implies a degree of approximation, since behavior arising from the laws of quantum mechanics, which may be relevant at a microscopic level, have to be reproduced in a Newtonian framework. Furthermore, if the aim is to simulate such systems numerically, computational constraints imply that some compromise has to be reached between theoretical accuracy and computational cost. If, for small systems, it may be possible to simulate all atomic interactions, for larger or more complex systems, it is often only feasible to use potential functions which are both cheap from a computational point of view and empirically shown to be accurate enough for the purpose of a simulation.

Our main numerical example will be the system given by the following empirical potential, and which is often used to describe the microscopic behavior of chemically inert fluids, such as Argon.

Example 1 (The Lennard-Jones fluid). *We fix $L > 0$ and $d = 3$. The Lennard-Jones fluid is the classical system given by the pair-interaction potential*

$$V_{\text{LJ}}(q) = \sum_{1 \leq i < j \leq N} v(|q_i - q_j|), \quad (1.12)$$

where v is the radial function

$$v(r) = 4\epsilon \left(\left(\frac{\sigma}{r}\right)^{12} - \left(\frac{\sigma}{r}\right)^6 \right).$$

The reference energy ϵ and length σ are shape parameters which respectively control the depth of the potential well and the equilibrium distance $2^{1/6}\sigma$. As seen on Figure 1.1, the potential combines two effects. At small interparticular distances, the dominant term is in r^{-12} , which translates into a strongly repulsive force between close pairs of particles, and makes individual particles essentially impenetrable. At long range, the dominant term is in $-r^6$, which translates into a weakly attractive force between distant particles. Contrary to the repulsive term, which is empirical, this scaling has a theoretical origin in the Van der Waals forces. From a computational standpoint, the fact that v is an even function of r allows one to compute the normalized force while sparing the expense of computing a square root, while the identity $r^{12} = (r^6)^2$ allows further economy. The shape parameters σ and ϵ must be chosen empirically to describe the behavior of a particular atomic species.

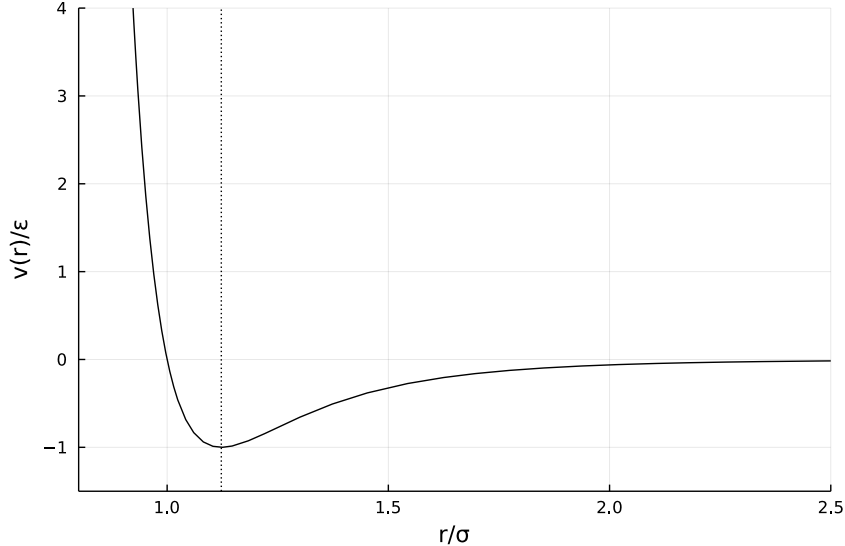


Figure 1.1: The pair potential v , with distances and energy given in reduced units. The equilibrium interparticular distance is indicated by the vertical dotted line.

1.3.1 Reduced units

It is convenient, given an atomic system, to describe quantities therein within a system of units in which they are of order one. This has several advantages. Firstly, like any reasonable system of units, reduced units make quantities easier and more intuitive to reason about. Secondly, from the computational point of view, numerical artifacts due to loss of precision at very large or very small scales and overflow errors can be avoided more often. Thirdly, they may help transfer knowledge about one system to another. For instance, in the Lennard-Jones system, expressing a quantity in reduced units, and knowing the dependency of these units on the parameters (ϵ, σ, M) of the system, one can infer properties about a system with parameters $(\tilde{\epsilon}, \tilde{\sigma}, \tilde{M})$ by applying the inverse transformation, thus effectively yielding equivalence of different systems under different conditions, and sparing the cost of running redundant simulations.

We describe a general procedure to construct a set of reduced units. Our choice, although not necessarily unique, is quite natural, especially when dealing with the Lennard-Jones system. Let us fix a reference mass m_* , a reference energy ϵ_* and a reference length σ_* . Then various reference quantities

can be derived by natural conversions and dimensional analysis:

$$\begin{aligned}
t_* &= \sqrt{\sigma_*^2 m_* \varepsilon_*^{-1}}, & (\text{time}) \\
T_* &= \varepsilon_* k_B^{-1}, & (\text{temperature}) \\
v_* &= \sigma_* t_*^{-1}, & (\text{velocity}) \\
V_* &= \sigma_*^3, & (\text{volume}) \\
A_* &= \sigma_*^2, & (\text{area}) \\
\rho_* &= V_*^{-1}, & (\text{density}) \\
F_* &= m_* \sigma_* t_*^{-2}, & (\text{force}) \\
P_* &= F_* A_*^{-1}, & (\text{pressure})
\end{aligned}$$

and one can of course go on. The point is that if X is a quantity, one can obtain its reduced value X_{red} by dividing X by the reference quantity X_* which is dimensionally compatible with X , and which can be derived as above. For instance, given a pressure P , we obtain

$$P_{\text{red}} = P \sigma_*^3 \varepsilon_*^{-1}.$$

Note this is an adimensional quantity. Note, also that, due to the definition of the reference temperature T_* relative to the reference energy ε_* , energies are now commensurate to temperatures. The Boltzmann factor, which is the conversion factor between units of temperature and units of energy simplifies when expressed in reduced units, a fact we can capture with the maxim $k_B* = 1$. This simplifies many formulae.

For a monatomic Lennard–Jones system, a natural choice for m_* is the atomic mass of the considered species. We also take $\varepsilon_* = \varepsilon$ and $\sigma_* = \sigma$ (although the equilibrium length $\sigma = 2^{1/6}\sigma$ is another possible choice). In the case of Argon, we use the following values:

$$m_* = 6.634 \times 10^{-26} \text{ kg}, \quad \sigma_* = 3.405 \times 10^{-10} \text{ m}, \quad \varepsilon_* = 1.66 \times 10^{-21} \text{ J}.$$

Unless explicitly specified, all numerical results will be in this system of reduced units.

Once a dynamic has been prescribed, and an observable of interest as been fixed, we can describe our strategy to sample from a thermodynamic ensemble.

1.3.2 Ergodic averages

We define a process $(q_t, p_t)_{t \geq 0}$ on \mathcal{E} , either deterministic or stochastic, which is invariant for the target measure $\tilde{\mu}$, in the following sense: for all $t \geq 0$ and all bounded measurable observable φ , we require

$$\int_{\mathcal{E}} \mathbb{E}^{(q,p)} [\varphi(q_t, p_t)] \tilde{\mu}(dq, dp) = \int_{\mathcal{E}} \varphi(q, p) \tilde{\mu}(dq, dp), \quad (1.13)$$

where the superscript in the expectation denotes that the process has value (q, p) at $t = 0$, and the expectation is over realizations of (q_t, p_t) . In other words, this is a process which, given that its initial condition is distributed according to $\tilde{\mu}$, remains distributed according to $\tilde{\mu}$ at any later time. It is then natural to consider average values of φ over the trajectories:

$$\widehat{\varphi}_T := \frac{1}{T} \int_0^T \varphi(q_t, p_t) dt, \quad (1.14)$$

which we may hope will converge to the target ensemble average (1.3). The convergence of ergodic averages to the ensemble average can be shown not to hold in generality, and is something which must be proven on a case by case basis, though general criteria can be derived, see for instance [22]. If the underlying dynamic is stochastic, then the variance of the random variables (1.14) becomes an issue, which one must control by ensuring that time averages are taken over long enough trajectories. Furthermore, since the true invariant dynamics is in general in continuous time, one must generally devise discrete-in-time approximations to the true trajectories. However, empirical practice shows that ergodic averages obtained from computer simulations, even for a modest number of atoms, agrees very well with experimental data for certain types of systems, and even in the absence of theoretical guarantees.

Chapter 2

Sampling equilibrium properties

In this chapter, we discuss techniques to sample static properties of systems in thermodynamic equilibrium. Our focus will be on the microcanonical and canonical ensembles, for which the corresponding sampling dynamics are described by the Hamiltonian and Langevin equations. Consequently, the bulk of this chapter is dedicated to theoretical discussions of their properties, as well as the description of numerical integration strategies.

2.1 Microcanonical averages

We start by describing methods to sample microcanonical averages, first describing a few qualitative properties of Hamiltonian dynamics. These will serve as criteria to determine viable candidate numerical schemes, which will be required to preserve, either exactly or asymptotically, those qualitative properties. We then turn to the description of such structure-preserving schemes, and their energy conservation properties, concluding by a numerical illustration.

2.1.1 Elementary properties of Hamiltonian dynamics

The Hamiltonian dynamics (1.11) rewrites in matrix form, with $X_t = (q_t, p_t)$:

$$dX_t = J \nabla H(X_t) dt, \quad (2.1)$$

where J is the symplectic matrix

$$J = \begin{pmatrix} 0_{dN} & \text{Id}_{dN} \\ -\text{Id}_{dN} & 0_{dN} \end{pmatrix}$$

Applying the chain rule to any smooth function $\varphi : \mathcal{E} \rightarrow \mathbb{R}$, we obtain

$$d\varphi(X_t) = dX_t^\top \nabla \varphi(X_t) = (J \nabla H(X_t))^\top \nabla \varphi(X_t) dt = (\nabla_p H \cdot \nabla_q - \nabla_q H \cdot \nabla_p) \varphi(X_t) dt$$

This motivates the following.

Definition 2 (Generator of the Hamiltonian dynamics). *We define the generator associated with the Hamiltonian dynamics to be the operator \mathcal{L}_H acting on smooth functions as*

$$\mathcal{L}_{\text{ham}} \varphi = (\nabla_p H \cdot \nabla_q - \nabla_q H \cdot \nabla_p) \varphi = (J \nabla H)^\top \nabla \varphi. \quad (2.2)$$

We can split the generator as the sum of two elementary operators,

$$\mathcal{L}_{\text{ham}} = A + B,$$

with

$$A = (M^{-1}p) \cdot \nabla_q \quad B = -\nabla V(q) \cdot \nabla_p. \quad (2.3)$$

The generator allows us to quantify the rate of change of an observable φ under the evolution of the system. If we define, for $t \geq 0$, the evolution operators

$$P_t \varphi(q_0, p_0) = \varphi(\Phi_t(q_0, p_0)),$$

where Φ is the flow associated with the Hamiltonian dynamics, that is the collection of maps $(\Phi_t)_{t \geq 0}$, defined by $\Phi_t(q_0, p_0) = (q_t, p_t)$, the unique solution to (1.11) with initial conditions (q_0, p_0) , then we formally have:

$$\frac{\partial}{\partial t} P_t \varphi(q, p) = \partial_t \varphi(q_t, p_t) = \mathcal{L}_{\text{ham}} \varphi(q_t, p_t) = \mathcal{L}_{\text{ham}} P_t \varphi(q, p) = P_t \mathcal{L}_{\text{ham}} \varphi(q, p).$$

In the following result, we collect certain qualitative properties of Hamiltonian dynamics.

Proposition 1 (Properties of Hamiltonian dynamics). *Assume that the Hamiltonian H (1.1) is C^2 on \mathcal{E} and that the flow Φ_t is globally defined for $t \in \mathbb{R}$. Then the following properties hold.*

i) *Group structure:*

$$\forall t, s \in \mathbb{R}, \quad \Phi_t \circ \Phi_s = \Phi_{t+s}, \quad \Phi_0 = \text{Id}.$$

ii) *Energy preservation:*

$$\frac{dH(q_t, p_t)}{dt} = 0.$$

iii) *Conservation of the Lebesgue measure:*

$$\forall D \in \mathcal{B}(\mathcal{E}), \forall t \geq 0, \quad |\Phi_t(D)| = |D|.$$

iv) *Symplecticity:*

$$\forall t \geq 0, \quad \nabla \Phi_t^\top J \nabla \Phi_t = J.$$

v) *Time reversibility:*

$$\Phi_t \circ \mathcal{R} \circ \Phi_t = \mathcal{R}.$$

The notation ∇ corresponds to (1), and the map \mathcal{R} is the momentum-reversing involution

$$\mathcal{R}(q, p) = (q, -p).$$

Hints of proof. i) This property expresses the fact that the Hamiltonian evolution is autonomous, and follows from uniqueness in the Cauchy–Lipschitz theorem. This allows one to formally interpret the flow as a group action of \mathbb{R} on \mathcal{E} .

- ii) The energy conservation property simply follows from applying \mathcal{L}_{ham} to H .
- iii) This property, known as Liouville’s theorem, holds generally for any divergent-free flow. Its proof is based on a time differentiation of the determinant $\det(\nabla \Phi_t)$, and observing that the Hamiltonian vector field is divergence free:

$$\text{div}(J \nabla H) = \text{div}_q(\nabla_p H) - \text{div}_p(\nabla_q H) = 0.$$

- iv) The property is trivially satisfied at time $t = 0$. A straightforward calculation shows that the time derivative of the symplecticity condition for Φ_t is 0, which proves the claim. Let us remark that this property also implies property iii), since it shows $\det(\nabla \Phi_t)^2 \det(J) = \det(J) \implies |\det(\nabla \Phi_t)| = 1$.
- v) This again follows by uniqueness of trajectories: by observing that, for a fixed initial condition (q_0, p_0) , a time differentiation of the trajectory $(q_{-t}, -p_{-t}) = \mathcal{R} \circ \Phi_{-t}(q_0, p_0)$ shows it is Hamiltonian. Thus it must coincide with $\Phi_t(q_0, -p_0) = \Phi_t \circ \mathcal{R}(q_0, p_0)$. This can be restated as an equality of mappings, $\mathcal{R} \circ \Phi_{-t} = \Phi_t \circ \mathcal{R}$. Precomposing by Φ_t on each side yields the result using property i). \square

Remark 3. Properties i) to iv) above are still valid for any dynamics of the form (2.1), thus it is possible to consider dynamics with more general Hamiltonians, which still obey them, disregarding issues of well-posedness. Property v), however uses the additional property that the classical Hamiltonian is separable into a kinetic and potential part, and that the kinetic part is an even function of p .

Property *ii*) in the proposition above asserts that Hamiltonian trajectories remain on the constant energy manifold $S(H(q_0, p_0))$ defined in (1.6). Since this is the support of the microcanonical measure $\mu_{\text{mc}, E}$, it is natural to ask whether the Hamiltonian dynamics can be used to sample the microcanonical measure, by means of ergodic averages. A minimum requirement for this to hold is that the measure is left invariant under Hamiltonian evolution. This is indeed the case. Consider a Hamiltonian trajectory (q_t, p_t) such that $H(q_0, p_0) = E$. For g and f test functions,

$$\begin{aligned} \int_{\mathbb{R}} g(E) \int_{\mathcal{E}} f(q_t, p_t) d\mu_{\text{mc}, E}(q, p) dE &= \frac{1}{Z_E} \int_{\mathcal{E}} g(H(q, p)) (f \circ \Phi_t)(q, p) dq dp \\ &= \frac{1}{Z_E} \int_{\mathcal{E}} g(H \circ \Phi_{-t}(\tilde{q}, \tilde{p})) f(\tilde{q}, \tilde{p}) d\tilde{q} d\tilde{p} \\ &= \frac{1}{Z_E} \int_{\mathcal{E}} g(H(\tilde{q}, \tilde{p})) f(\tilde{q}, \tilde{p}) d\tilde{q} d\tilde{p} \\ &= \int_{\mathbb{R}} g(E) \int_{\mathcal{E}} f(\tilde{q}, \tilde{p}) d\mu_{\text{mc}, E}(q, p) dE. \end{aligned}$$

the absence of a Jacobian determinant term in the change of variables from the second to the third line follows from property *iii*) in Proposition 1, while the passage from the second to the third line is justified by the energy conservation property. This shows that the microcanonical measure is invariant under the Hamiltonian dynamics, but it is easy to construct examples where ergodic averages fail to converge to the correct value, as the following simple example shows.

Example 2 (A non-ergodic system). *We consider the following one-dimensional system with $\mathcal{E} = \mathbb{T} \times \mathbb{R}$, and the potential given by*

$$V(q) = \cos\left(4\pi\left[q - \frac{1}{2}\right]\right).$$

The constant-energy manifold $S(0)$ consists of two disjoint compact connected components (see Figure 2.1). The observable

$$\varphi(q, p) = \mathbb{1}_{q > \frac{1}{2}} - \mathbb{1}_{q < \frac{1}{2}}$$

is constant on each component of $S(0)$, and has zero average with respect to $\mu_{\text{mc}, 0}$ by symmetry, but ergodic averages do not converge, since

$$\frac{1}{T} \int_0^T \varphi(q_t, p_t) dt = \frac{1}{T} \int_0^T \varphi(q_0, p_0) dt = \varphi(q_0, p_0) \in \{\pm 1\}.$$

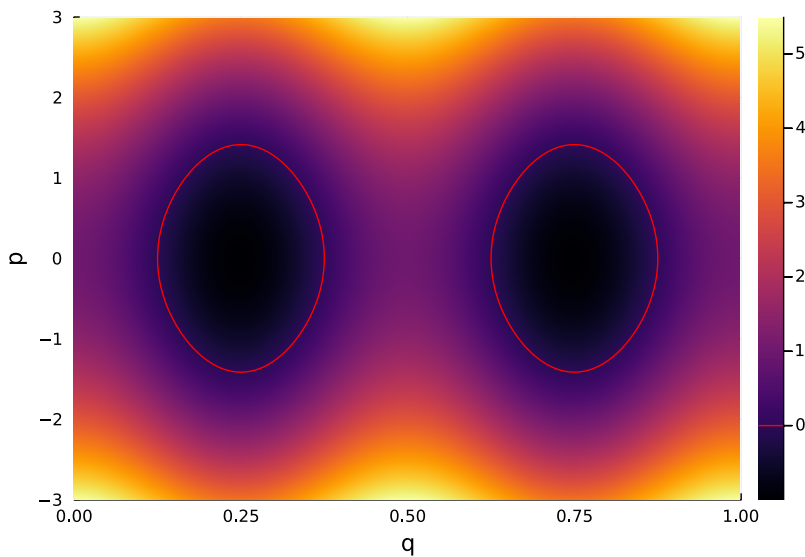


Figure 2.1: The Hamiltonian landscape for the potential V of Example 2 , with $S(0)$ plotted in red.

The issue of ergodicity is in general very hard to tackle for realistic systems, and in practice is often taken as a working hypothesis. Besides, it may happen that for observables satisfying some symmetries in the constant energy manifold converge to the correct microcanonical average even in the absence of ergodicity. This is, for example, the case for the kinetic energy observable in our Example 2.

2.1.2 Numerical schemes for Hamiltonian dynamics

It is not impossible, except for a restricted class of systems, which do not typically arise in practice, to analytically integrate Hamilton's equation (1.11). For this reason, one must resort to numerical schemes, which provide approximations of the flow map over one timestep. More precisely, for a fixed timestep Δt , if one has an approximation of the flow

$$\tilde{\Phi}_{\Delta t} \approx \Phi_{\Delta t},$$

one can deduce discrete approximations of the evolution by iteration:

$$(q^n, p^n) := \tilde{\Phi}_{\Delta t}^n(q_0, p_0) \approx (q_{n\Delta t}, p_{n\Delta t}), \quad (2.4)$$

which can then be used as sample points for the computation of empirical averages, discrete counterparts to the ergodic averages (1.14),

$$\frac{1}{N_{\text{iter}}} \sum_{k=0}^{N_{\text{iter}}} \varphi(q^k, p^k). \quad (2.5)$$

In most common applications involving ordinary differential equations, the aim is to approximate the exact solution as precisely as possible over a given domain. In the case of sampling trajectory averages in molecular dynamics, however, the time domain is usually very large, because simulating long trajectories is a requirement to ensure that a representative portion of phase space is explored. As a consequence, it is in practice impossible to obtain precise solutions over a long time at the level of trajectories, because the evolution's sensitivity to initial conditions will cause small initial errors to rapidly blowup. Furthermore, one does not really *care* about the exact evolution, since the dynamics are merely used as a sampling device. Instead, one key requirement is that the dynamics stay on or close to the constant energy manifold associated with a given initial condition. It can be shown through eigenanalysis that for simple linear systems, this requirement is not satisfied by standard ODE numerical methods such as the explicit and implicit Euler schemes, or the RK4 method, for which the energy may exponentially increase or decrease. This has the practical effect that for reasonably sized atomic systems, numerical instabilities render the simulations nonsensical after only a few time steps, which is far from what is needed to obtain good estimates. One must then devise dedicated numerical methods, guided by the aim to preserve qualitative properties of the Hamiltonian evolution. It turns out that splitting schemes, based on operator splitting approximations of the Hamiltonian evolution operator over one timestep, preserve crucial qualitative properties of the Hamiltonian evolution.

An important observation is that if one considers each part of (2.3) as a generator in its own right, the corresponding elementary dynamics are analytically integrable.

Remark 4. Consider the two dynamics defined by

$$\begin{cases} dq_t^A = M^{-1} p_t^A dt, \\ dp_t^A = 0, \end{cases} \quad (2.6)$$

and

$$\begin{cases} dq_t^B = 0, \\ dp_t^B = -\nabla V(q_t^B) dt. \end{cases} \quad (2.7)$$

These can be analytically solved as

$$\begin{cases} (q_t^A, p_t^A) = (q_0^A + tp_0^A, p_0^A), \\ (q_t^B, p_t^B) = (q_0^B, p_0^B - t\nabla V(q_0^B)). \end{cases} \quad (2.8)$$

Moreover, these evolutions are of Hamiltonian form, with Hamiltonians corresponding respectively to the kinetic part and the configurational part only, and have corresponding generators A and B . We denote by $(\Phi_t^A)_{t \in \mathbb{R}}$ and $(\Phi_t^B)_{t \in \mathbb{R}}$ their respective flow maps.

This observation suggests the following general recipes to construct a class of numerical schemes for the Hamiltonian dynamics, named splitting schemes. We consider approximations of the form

$$\Phi_{\Delta t} \approx \Phi_{\Delta t_k}^{G_k} \circ \cdots \circ \Phi_{\Delta t_1}^{G_1}, \quad (2.9)$$

where $G_i \in \{A, B\}$ for all i and $\sum_{G_i=A} \Delta t_i = \sum_{G_i=B} \Delta t_i = 1$. We will be considering three schemes, the simplest of which are the symplectic Euler schemes. The symplectic Euler schemes are defined by the following update equations:

$$\begin{cases} p^{n+1} = p^n - \nabla V(q^n) \Delta t, \\ q^{n+1} = q^n + M^{-1} p^{n+1} \Delta t, \end{cases} \quad (2.10)$$

and

$$\begin{cases} q^{n+1} = q^n + M^{-1} p^n \Delta t, \\ p^{n+1} = p^n - \nabla V(q^{n+1}) \Delta t. \end{cases} \quad (2.11)$$

These correspond respectively to the splittings $\Phi_{\Delta t}^A \circ \Phi_{\Delta t}^B := \Phi_{\Delta t}^{AB}$ and $\Phi_{\Delta t}^B \circ \Phi_{\Delta t}^A := \Phi_{\Delta t}^{BA}$. The velocity Verlet scheme is based on the symmetric splitting $\Phi_{\Delta t/2}^B \circ \Phi_{\Delta t}^A \circ \Phi_{\Delta t/2}^B := \Phi_{\Delta t}^{BAB}$, Its update equation is given by

$$\begin{cases} p^{n+\frac{1}{2}} = p^n - \frac{\Delta t}{2} \nabla V(q^n) \\ q^{n+1} = q^n + \Delta t M^{-1} p^{n+\frac{1}{2}} \\ p^{n+1} = p^{n+\frac{1}{2}} - \frac{\Delta t}{2} \nabla V(q^{n+1}). \end{cases} \quad (2.12)$$

We have announced above that these numerical schemes preserve some qualitative properties of the Hamiltonian dynamics. We now turn to making this statement precise. Let us fix an evolution operator $\tilde{\Phi}_{\Delta t}$ corresponding to a splitting of the form (2.9) with a timestep $\Delta t > 0$. Recall the properties in 1. Then analogous properties can be stated for each of the schemes. We will refer to these analogous using the same names and indexing, but where Φ_t is replaced by $\tilde{\Phi}_{\Delta t}$ regardless of t . We further say a splitting is *symmetric* if the corresponding order of operators A and B is a palindrome. The velocity Verlet splitting is symmetric, while the symplectic Euler splittings are not. We may then go through the properties in Proposition 1, listing those which apply, and those which have to be modified.

- i) Group structure: the analogous statement is a group action of \mathbb{Z} on \mathcal{E} . This holds if the splitting is symmetric: then, $\tilde{\Phi}_{\Delta t}^{-1} = \tilde{\Phi}_{-\Delta t}$.
- ii) Energy preservation: this does not hold as is, but does in a weakened sense that we discuss below.
- iii) Conservation of the Lebesgue measure: this holds for all splittings.
- iv) Symplecticity: similarly, this holds for all splittings.
- v) Time-reversibility: this holds for all symmetric splittings.

Hints of proofs. For every one of these properties, the strategy is the same. From Proposition 1, each one of them holds for $\Phi_{\Delta t}^A$ and for $\Phi_{\Delta t}^B$. The aim is then to show that these properties are stable, at best under composition, and at worst under symmetric composition.

- i) This simply follows from writing

$$(g_1 \circ g_2 \circ \cdots \circ g_2 \circ g_1)^{-1} = g_1^{-1} \circ g_2^{-1} \circ \cdots \circ g_2^{-1} \circ g_1^{-1},$$

and using property i) applied to $\Phi_{\Delta t}^A$ and $\Phi_{\Delta t}^B$.

- ii) This is a crucial and slightly subtle point, to which we return in more detail below.
- iii) This follows trivially by composition (or alternatively by symplecticity). For any measure preserving measurable maps f and g ,

$$|f \circ g(D)| = |g(D)| = |D|.$$

- iv) This follows from the fact that any composition of symplectic maps is symplectic. This, in turn, follows from the multivariate chain rule below, and applying the symplectic property twice:

$$\nabla(g \circ f) = ((\nabla g) \circ f) \nabla f \implies [((\nabla g) \circ f) \nabla f]^T J [((\nabla g) \circ f) \nabla f] = \nabla f^T J \nabla f = J.$$

v) Fixing $f \circ \mathcal{R} \circ f = g \circ \mathcal{R} \circ g = \mathcal{R}$, we write

$$f \circ g \circ \mathcal{R} \circ g \circ f = f \circ \mathcal{R} \circ f = \mathcal{R},$$

and conclude by induction that the property holds for any symmetric splitting.

□

We have shown that splitting schemes inherit some nice geometrical properties from the underlying Hamiltonian flow, and all the more for symmetric splittings. However our final aim is to sample from the microcanonical measure, hence we should aim to sample points which remain close to the constant energy manifold $S(E)$. Ideally, we would want to guarantee that the Hamiltonian is perfectly preserved under the discrete evolution induced by these schemes. This, it turns out, is too high a hope. It happens, however, that, for each of these schemes, a *perturbed* Hamiltonian is (almost) exactly conserved, which we can interpret as the discrete dynamics (2.4) regularly and (almost) exactly sampling points from a *perturbed* dynamics corresponding to the new Hamiltonian. The order of this perturbation in the timestep Δt then allows one to quantify the error over finite time intervals. The statements and proofs of this kind of results fall under the broad scope of backward numerical analysis. For a clear and more detailed introduction, one can consult [16, Section 4]. The general idea of backward numerical analysis, given an evolution equation and an associated numerical method:

$$\dot{y} = F_0(y), \quad y^{n+1} = \tilde{\Phi}_{\Delta t}(y),$$

is to reinterpret the numerical solution y^1 not as an approximation of the exact solution $y_{\Delta t}$, but as the exact solution $\tilde{y}_{\Delta t}$ of an approximate evolution \tilde{y} , given by the ODE

$$\dot{\tilde{y}} = \tilde{F}(y),$$

where \tilde{F} is given by a perturbative expansion

$$\tilde{F} = F_0 + \Delta t F_1 + \Delta t^2 F_2 + \dots$$

To avoid any convergence issue related to infinite expansions, precise statements usually truncate the expansion at some finite order $\alpha > 0$, and require the exactness of the numerical trajectory up to order $\alpha + 1$, say

$$\tilde{F} = F_0 + \Delta t F_1 + \dots + \Delta t^\alpha F_\alpha, \quad |\tilde{\Phi}_{\Delta t}(y_0) - \tilde{y}_{\Delta t}| = O(\Delta t^{\alpha+2}).$$

Comparing Taylor expansions in powers Δt of $\tilde{\Phi}_{\Delta t}$ and $\tilde{y}_{\Delta t}$ then allows us to explicitly compute the terms in the expansion of \tilde{F} . As an example we compute the first correction term for the symplectic Euler scheme $\Phi_{\Delta t}^{AB}$.

Example 3 (Leading-order correction for $\Phi_{\Delta t}^{AB}$). *Following our strategy, we Taylor-expand our scheme as*

$$\Phi_{\Delta t}^{AB}(q, p) = \begin{pmatrix} q + \Delta t M^{-1} p \\ p - \Delta t \nabla V(q) - \Delta t^2 \nabla^2 V(q) M^{-1} p \end{pmatrix} + O(\Delta t^3).$$

Similarly, expanding the exact solution with initial condition $(q, p) = y_0$ to the second order yields

$$\begin{aligned} \Phi_{\Delta t}(q, p) &= y_0 + \Delta t J \nabla H(y_0) + \frac{\Delta t^2}{2} \nabla [J \nabla H(y_0)] J \nabla H(y_0) + O(\Delta t^3) \\ &= y_0 + \Delta t J \nabla H(y_0) + \frac{\Delta t^2}{2} J \nabla^2 H(y_0) J \nabla H(y_0) + O(\Delta t^3) \\ &= \begin{pmatrix} q + \Delta t M^{-1} p - \frac{\Delta t^2}{2} M^{-1} \nabla V(q) \\ p - \Delta t \nabla V(q) - \frac{\Delta t^2}{2} \nabla^2 V(q) M^{-1} p \end{pmatrix} + O(\Delta t^3). \end{aligned}$$

This shows the scheme is of order one, hence

$$|\Phi_{\Delta t}(q, p) - \Phi_{\Delta t}^{AB}(q, p)| = O(\Delta t^2).$$

Comparing the two expansions allows us to recover the discrepancy term, showing that the solution of the modified equation at time Δt

$$\begin{cases} \frac{d}{dt}q = M^{-1}p + \frac{\Delta t}{2}M^{-1}\nabla V(q) \\ \frac{d}{dt}p = -\nabla V(q) + \frac{\Delta t}{2}\nabla^2 V(q)M^{-1}p \end{cases}$$

agrees with $\Phi_{\Delta t}^{AB}(q, p)$ up to order 2 in Δt . Crucially, this equation is still of Hamiltonian form, for the modified Hamiltonian

$$\tilde{H}(q, p) = H(q, p) - \frac{\Delta t}{2}\nabla V(q)^\top M^{-1}p. \quad (2.13)$$

In fact, it is a general fact that all truncations of the modified dynamics for a symplectic method are of Hamiltonian form. For a more thorough discussion of this fact, we refer to [17, Section IX.4], but for now we simply make note of the fact that given a numerical method, we can construct a modified Hamiltonian equation for which this numerical order is of arbitrarily high order of local consistency. This is important, because, as the following result [17, Theorem IX.8.1] shows, the order of the numerical method is directly related to the long-time energy conservation properties along numerical trajectories.

Theorem 1. *Let H be an analytic Hamiltonian, and $\tilde{\Phi}_{\Delta t}$ a symplectic numerical method of order α . If there is a compact set $K \subset \mathcal{E}$ such that $(q^n, p^n) \in K$ for all $n \geq 0$, then there exists $\tau > 0$ such that for Δt small enough,*

$$H(q^n, p^n) = H(q^0, p^0) + O(\Delta t^\alpha) \quad (2.14)$$

for times $n\Delta t \leq e^{\tau/\Delta t}$.

The fact that the order of the scheme is linked to the local conservation in time of the Hamiltonian is unsurprising. The main content of the above result is that this conservation is valid over very long times, provided the numerical trajectory does not explode and that the timestep is chosen to be small enough.

We have already seen that symplectic Euler methods are of order one, and it can straightforwardly be shown that the Verlet scheme is of order 2 by a Taylor expansion. Hence we expect the fluctuation of the Hamiltonian to be of order Δt for the symplectic Euler methods and of order Δt^2 for the Verlet scheme. Moreover, by construction, symplectic Euler methods are of order 2 for the first-order modified Hamiltonian dynamics, so we expect the fluctuation of the first-order modified Hamiltonian computed in Example 3 to be of order 2 for the symplectic Euler methods. The leading-order correction term for the other Euler symplectic scheme can be computed using the same method, and is given by the opposite of (2.13).

In Figure 2.2, we verify this result numerically. A Lennard–Jones system of 1000 particles was simulated with a temperature $T = 1.5$, for a time $\tau = 1.0$, and at density $\rho = 0.7$. The Lennard–Jones potential was cut off using a cubic spline interpolation between $r_a = 2.0$ and $r_c = 2.5$. We plot the maximal fluctuation of the Hamiltonian

$$\Delta H := \max_{0 \leq n \leq \lceil \tau / \Delta t \rceil} H(q^n, p^n) - \min_{0 \leq n \leq \lceil \tau / \Delta t \rceil} H(q^n, p^n)$$

as a function of the timestep Δt for each of the symplectic splitting schemes. We also plot the maximum fluctuation of the modified Hamiltonian (2.13) for the symplectic Euler schemes, which we denote in the legend by a lowercase \underline{m} . The legend gives the order of the operators in the splitting, along with the slope of the least squares regression line in log-log space, which we superimpose in dotted line. In order for the trajectories to be comparable, every simulation was started from the same precomputed equilibrium starting configuration. The results concur with theoretical prediction.

From a practical point of view, we will always use the Verlet scheme, since it offers the better energy conservation property without any computational overhead compared to the symplectic Euler schemes. Indeed, the force calculation in the last step of (2.12) can be used again in the first step of the next iteration, so that there is only one force calculation per iteration, as in the symplectic Euler method. Finally let us mention that the splitting based on the ordering ABA of the elementary generators yields another symplectic method called the *position* Verlet scheme, which enjoys the same conservation properties as standard (velocity) Verlet. It is, however, rarely used in practice.

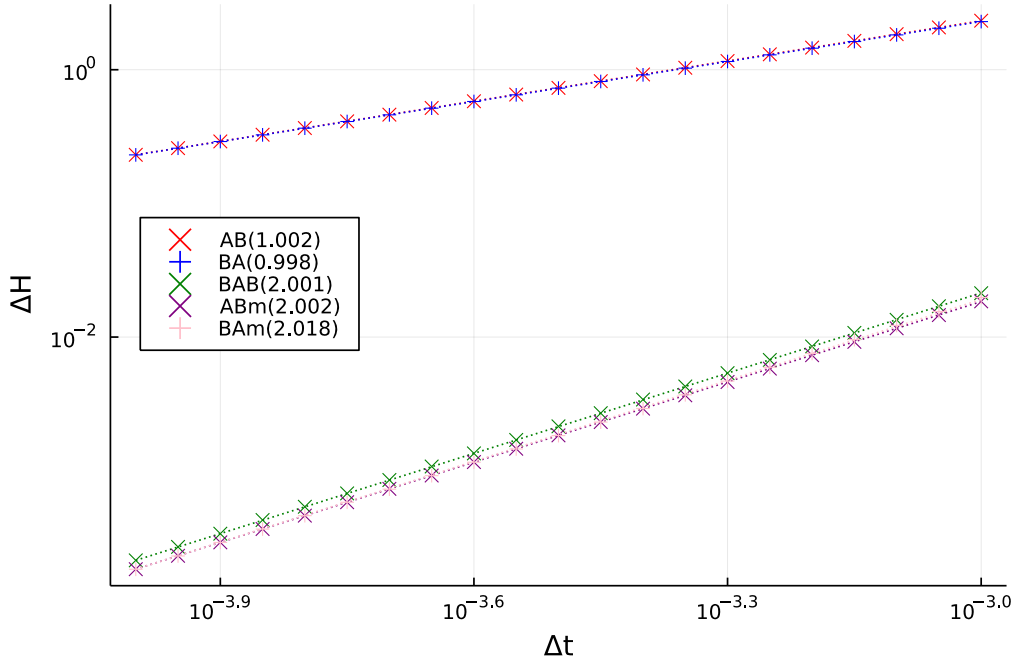


Figure 2.2: Maximal fluctuation of the Hamiltonians and leading-order modified Hamiltonians for the Symplectic Euler and Verlet schemes.

2.2 Canonical averages

We now turn our attention to methods to compute canonical averages, which are expectations of observables with respect to the canonical measure (1.7). As we already alluded to, the sampling strategy will be based on the definition of a stochastic process under whose evolution the canonical measure is invariant. This is the Langevin dynamics. We define it, and discuss some of its theoretical properties which are relevant to the sampling of canonical averages. We then turn to describing a splitting strategy for the discretization of the continuous dynamics, which will serve as our effective sampling tools for canonical averages. We finally give some numerical illustrations of the strategy.

2.2.1 Langevin dynamics

We first consider the inertial Langevin dynamics, defined by the following stochastic differential equation (SDE), where γ, β are fixed positive constants:

$$\begin{cases} dq_t = M^{-1} p_t dt, \\ dp_t = -\nabla V(q_t) dt - \gamma M^{-1} p_t dt + \sqrt{\frac{2\gamma}{\beta}} dW_t, \end{cases} \quad (2.15)$$

where $(W_t)_{t \geq 0}$ is a standard dN -dimensional Brownian motion. This process is a combination of a Hamiltonian evolution with an additional action on the momenta which, if isolated, defines a dN -dimensional Ornstein-Uhlenbeck process.

This additional term be interpreted physically as the combination of two effects: a dissipation term

$$-\gamma M^{-1} p_t dt,$$

which can be understood as the effect of a viscous friction force on the particles, and a fluctuation term,

$$\sqrt{\frac{2\gamma}{\beta}} dW_t,$$

which corresponds to the input of kinetic energy into the system as thermal agitation induced by a surrounding heat bath at temperature $1/(k_B \beta)$.

However, the physical meaning can be forgotten thanks to the fact that, *in fine*, we only require that the canonical measure be invariant under this dynamic: as we shall shortly see, this is indeed the case.

Remark 5 (Generalized Langevin dynamics). *There are several ways to generalize this process: one is to consider a generic, possibly non-separable, Hamiltonians, as in Remark 3, rather than the classical Hamiltonian used above. The other is to allow the fluctuation-dissipation term to be parametrized by coefficients γ and σ depending on the state variable, and which obey a relation ensuring the invariance of μ . Hence in full generality, we could consider the following system of SDEs:*

$$\begin{cases} dq_t = \nabla_p H(q_t, p_t) dt, \\ dp_t = -\nabla_q H(q_t, p_t) dt - \gamma(q_t, p_t) \nabla_p H(q_t, p_t) dt + \sigma(q_t, p_t) dW_t, \end{cases} \quad (2.16)$$

where γ and σ are $dN \times dN$ matrix-valued functions. In fact one can also consider the case where W_t is a r -dimensional Brownian motion and σ is a $dN \times r$ matrix-valued function. The Dissipative Particle Dynamics (DPD, see [6]) is a generalized Langevin equation of this form, where γ and σ are position-dependent and the Brownian motion is $dN(N-1)/2$ -dimensional, which corresponds to the number of pairs of non-orthogonal momentum degrees of freedom.

The generator of the Langevin dynamics is the operator

$$\mathcal{L}_\gamma = M^{-1} p \cdot \nabla_q - \nabla V(q) \cdot \nabla_p - \gamma M^{-1} p \cdot \nabla_p + \frac{\gamma}{\beta} \Delta_p, \quad (2.17)$$

and we denote the evolution operator using exponential notation:

$$(e^{t\mathcal{L}_\gamma} \varphi)(q, p) := \mathbb{E}^{(q,p)} [\varphi(q_t, p_t)], \quad (2.18)$$

where the expectation is over all trajectories of the dynamics (2.15), starting from $(q_0, p_0) = (q, p)$.

2.2.2 Invariance of the canonical measure

Using the generator, one can easily express the evolution of a probability distribution under the Langevin dynamics. We assume for simplicity that the solution $(q_t, p_t)_{t \geq 0}$ to (2.15) has a distribution with a smooth density ρ_t at time t over \mathcal{E} . For any C^∞ compactly supported observable φ , we have

$$\int_{\mathcal{E}} \varphi(q, p) \rho_t(q, p) dq dp = \int_{\mathcal{E}} \mathbb{E}^{(q,p)} [\varphi(q_t, p_t)] \rho_0(q, p) dq dp = \int_{\mathcal{E}} e^{t\mathcal{L}_\gamma} \varphi(q, p) \rho_0(q, p) dq dp,$$

where the superscript is as in (1.13). Thus,

$$\frac{\partial}{\partial t} \left(\int_{\mathcal{E}} \varphi(q, p) \rho_t(q, p) dq dp \right) = \int_{\mathcal{E}} e^{t\mathcal{L}_\gamma} \mathcal{L}_\gamma \varphi(q, p) \rho_0(q, p) dq dp = \int_{\mathcal{E}} \mathcal{L}_\gamma \varphi(q, p) \rho_t(q, p) dq dp$$

If we define $\mathcal{L}_\gamma^\dagger$ as the adjoint of \mathcal{L}_γ on the flat space $L^2(\mathcal{E})$, that is,

$$\int_{\mathcal{E}} (\mathcal{L}_\gamma \varphi) \psi = \int_{\mathcal{E}} \varphi (\mathcal{L}_\gamma^\dagger \psi) \quad \text{for all } \phi, \psi \quad (2.19)$$

compactly supported C^∞ test functions, we have the Fokker–Planck equation,

$$\frac{\partial}{\partial t} \int_{\mathcal{E}} \varphi(q, p) \rho_t(q, p) dq dp = \int_{\mathcal{E}} \varphi(q, p) \mathcal{L}_\gamma^\dagger \rho_t(q, p) dq dp, \quad (2.20)$$

which rewrites formally as

$$\frac{\partial}{\partial t} \rho_t = \mathcal{L}_\gamma^\dagger \rho_t. \quad (2.21)$$

Using this equation, we can easily show that the canonical distribution is invariant under this dynamics, which is equivalent to the condition

$$\mathcal{L}_\gamma^\dagger \mu = 0.$$

In fact, it is useful to reformulate this condition in the weighted space $L^2(\mu)$. Indeed, the stationary Fokker–Planck equation rewrites

$$\int_{\mathcal{E}} \mathcal{L}_\gamma \varphi d\mu = 0 \quad \forall \varphi,$$

or equivalently,

$$\mathcal{L}_\gamma^* \mathbb{1}_{\mathcal{E}} = 0,$$

where \mathcal{L}_γ^* is the adjoint of \mathcal{L}_γ in $L^2(\mu)$ for the scalar product

$$(\varphi, \psi) \mapsto \int_{\mathcal{E}} \varphi \psi \, d\mu.$$

This, in turn, follows easily from the following lemma.

Lemma 1. *The $L^2(\mu)$ adjoints of the elementary differential operators are given by the formulae*

$$\begin{cases} \partial_{q_i}^* = -\partial_{q_i} + \beta \partial_{q_i} V, \\ \partial_{p_i}^* = -\partial_{p_i} + \beta (M^{-1} p)_i. \end{cases} \quad (2.22)$$

These are easily found by integration by parts. In particular, we find that

$$\partial_{q_i} \partial_{p_i}^* - \partial_{p_i} \partial_{q_i}^* = \beta ((M^{-1} p)_i \partial_{q_i} - \partial_{q_i} V \partial_{p_i}),$$

hence, by summing over i ,

$$\mathcal{L}_{\text{ham}} = \frac{1}{\beta} (\nabla_q \cdot \nabla_p^* - \nabla_p \cdot \nabla_q^*), \quad (2.23)$$

which is an antisymmetric operator. Similarly,

$$\partial_{p_i} \partial_{p_i}^* = \beta (M^{-1} p)_i \partial_{p_i} - \partial_{p_i}^2,$$

hence

$$C = -\frac{1}{\beta} \nabla_p \cdot \nabla_p^*, \quad (2.24)$$

which is a symmetric operator. In summary, we have that

$$\mathcal{L}_\gamma^* = -\mathcal{L}_{\text{ham}} + \gamma C = -(A + B) + \gamma C. \quad (2.25)$$

It follows immediately that $\mathcal{L}_\gamma^* \mathbb{1}_{\mathcal{E}} = 0$. Notice that since $\mathcal{L}_{\text{ham}}^* \mathbb{1}_{\mathcal{E}} = 0$, the canonical measure is also invariant under the Hamiltonian dynamics. However, because the latter is restricted to a manifold with zero measure with respect to μ , Hamiltonian ergodic averages cannot in general converge to the correct value.

Remark 6 (Fluctuation-dissipation relation for generalized Langevin dynamics). *We come back to the general Langevin dynamics (2.16). In this case the generator is given by*

$$\mathcal{L}_{\gamma, \sigma} = \mathcal{L}_{\text{ham}} - (\gamma \nabla_p H) \cdot \nabla_p + \frac{1}{2} (\sigma \sigma^\top) : \nabla_p^2.$$

The canonical measure is invariant under the action of the Hamiltonian part, so having

$$\tilde{\mathcal{L}}_{\text{FD}} := -(\gamma \nabla_p H) \cdot \nabla_p + \frac{1}{2} (\sigma \sigma^\top) : \nabla_p^2$$

such that $\tilde{\mathcal{L}}_{\text{FD}}^ \mathbb{1}_{\mathcal{E}} = 0$ is enough to guarantee the invariance of the canonical measure. If γ and σ are momentum-dependent, then this condition is a complicated differential-in- p relation between the coefficients of γ and σ , which can be explicitly computed by integration by parts in the expression*

$$\int_{\mathcal{E}} (\mathcal{L}_{\text{FD}} \varphi) \psi e^{-\beta H},$$

with $\varphi, \psi \in C_c^\infty(\mathcal{E})$ test functions. In the case where γ and σ are only position-dependent however, as is often the case in practice, then the expression simplifies greatly, and becomes simply an algebraic relationship between γ and σ , namely

$$\sigma \sigma^\top = \frac{2\gamma}{\beta}. \quad (2.26)$$

2.2.3 Overdamped limit of Langevin dynamics

As already pointed out, the fact that the kinetic marginal of μ is a Gaussian distribution makes sampling canonical momenta trivial. Instead, the main problem is sampling from ν . It follows directly from the invariance of μ under trajectories of the Langevin dynamics that ν is invariant under the configurational trajectories of the Langevin dynamics. It would be convenient, however, to have at our disposal a dynamics on \mathcal{D} which has ν as an invariant measure. It turns out this is possible, by observing that the invariance of μ is independent of the parameter γ , and taking the limit $\gamma \rightarrow \infty$. This requires a bit of care. Notice the SDE on the momenta in (2.15) rewrites

$$dp_t = -\nabla V(q_t)dt - \gamma dq_t + \sqrt{\frac{2\gamma}{\beta}}dW_t,$$

thus a time integration gives

$$q_t - q_0 = \frac{p_0 - p_t}{\gamma} - \frac{1}{\gamma} \int_0^t \nabla V(q_s)ds + \sqrt{\frac{2}{\gamma\beta}}W_t.$$

The scaling invariance of the Brownian motion $(\sqrt{\alpha}W_{t/\alpha^2})_{t \geq 0} \sim (W_t)_{t \geq 0}$ suggests considering the timescale $\gamma\beta t$, thus

$$q_{\gamma\beta t} - q_0 = \frac{p_0 - p_{\gamma\beta t}}{\gamma} - \frac{1}{\gamma} \int_0^{\gamma\beta t} \nabla V(q_s)ds + \sqrt{2}\widetilde{W}_t,$$

where \widetilde{W} is again a Brownian motion. Using the change of variables $s = \gamma\beta u$ in the integral term yields

$$q_{\gamma\beta t} - q_0 = \frac{p_0 - p_{\gamma\beta t}}{\gamma} - \beta \int_0^t \nabla V(q_{\gamma\beta u})du + \sqrt{2}\widetilde{W}_t, \quad (2.27)$$

At this point, we formally take $\gamma \rightarrow \infty$, which suggests the following SDE for the rescaled in time process,

$$dq_t = -\beta \nabla V(q_t) dt + \sqrt{2} dW_t. \quad (2.28)$$

This equation defines the overdamped Langevin, or Brownian, dynamics. To justify the limit in a rigorous manner, one would hope to show that the rescaled process (2.27) converges in law to a weak solution of the SDE (2.28), in some functional space. However, this is technical overkill, since, we only need to consider dynamics as sampling devices. In fact, the physical interpretation of this equation is not entirely clear in terms of the dimensions of the quantities involved. We can just as well take equation (2.28) as given, and be satisfied by the following fact.

Proposition 2. *The configurational Gibbs measure ν is invariant under the dynamics (2.28).*

This follows along the same lines as for the Langevin dynamics. The generator (now acting on observables defined on \mathcal{D}) is the operator

$$\mathcal{L}\varphi = -\beta \nabla V \cdot \nabla \varphi + \Delta \varphi. \quad (2.29)$$

Again, we consider the weighted space $L^2(\nu)$. Adjoints of elementary differential operators are still given by the first line of (2.22), and it is then easily seen that

$$\mathcal{L} = -\nabla^* \cdot \nabla \quad (2.30)$$

is a symmetric operator. Again we have $\mathcal{L}^* \mathbb{1}_{\mathcal{D}} = 0$, so ν satisfies the stationary Fokker–Planck equation under this dynamics.

Remark 7. *Instead of rescaling time by $\beta\gamma$, we could have rescaled by γ , which would yield the dynamics*

$$dq_t = -\nabla V(q_t)dt + \sqrt{\frac{2}{\beta}}dW_t. \quad (2.31)$$

Which formulation to choose is a matter of preference, since both yield a dynamics invariant under ν , as seen from the identity (where we still write \mathcal{L} for the generator)

$$\mathcal{L} = -\frac{1}{\beta} \nabla^* \cdot \nabla.$$

We end this chapter by stating some key properties of the continuous dynamics, regarding ergodicity and statistical error, before moving to the description of splitting schemes.

2.2.4 Convergence to equilibrium

Once we have shown that the Langevin dynamics and its overdamped limit are reasonable candidates to sample from the canonical measure and its configurational marginal, we should ensure that the target measure is actually sampled, and not simply invariant for the dynamics, as the cautionary example of the Hamiltonian dynamics shows. This is the question of ergodicity, and results of this nature mainly come in two flavors.

- (i) Probabilistic ergodic theorems that ask about the convergence of random variables like (1.14), that give analogs of the Law of Large Numbers for the correlated process $\varphi(q_t, p_t)$.
- (ii) More analytic results which express the convergence of the law of the process at time t towards a stationary solution to the Fokker–Planck equation. These can usually be expressed as decay estimates on the evolution Semigroup (2.18), in a judiciously chosen functional setting.

We will not get into details as these questions can quickly get quite technical, but rather give intuitive ideas of the setting, and point the reader to more thorough sources. Results such as (i) typically leverage the strong Law of Large Numbers by dissecting the trajectory into a discrete number of (loosely) *i.i.d.* excursions through phase space, guaranteeing the almost sure convergence of trajectory averages. As such, proving the positive recurrence of the dynamics is crucial to showing that these excursions are well-behaved, while also implying that the invariant measure is unique. One idea, exploited by Kliemann in [22], is to recast the Langevin dynamics as a control equation (where W_t acts as the control). He is thus able to leverage criteria on \mathcal{L}_γ from geometric control theory to ensure the almost sure convergence of trajectory averages. Results such as (ii) depend on the functional setting. Let us simply state the following result, based on hypocoercive estimates. For an introduction to these ideas, and references, we point to Section 2.1.1 in [24], and [18]. For any measure ρ denote by $L_0^2(\rho)$ the space of square-integrable observables with respect to ρ and zero mean.

Proposition 3 (Exponential decay rate of the Semigroup). *Assume that the potential V is smooth and that the configurational marginal ν of μ satisfies a Poincaré inequality: there exists a constant $R > 0$ such that for all $\varphi \in L_0^2(\nu)$ such that $\nabla \varphi \in L^2(\nu)^{dN}$,*

$$\|\varphi\|_{L^2(\nu)}^2 \leq \frac{1}{R} \|\nabla \varphi\|_{L^2(\nu)}^2. \quad (2.32)$$

Then there exist constants $C_\gamma, \lambda_\gamma > 0$ such that

$$\|e^{t\mathcal{L}_\gamma}\|_{\mathcal{B}(L_0^2(\mu))} \leq C_\gamma e^{-t\lambda_\gamma}. \quad (2.33)$$

For the overdamped case, exponential decay rates can also be obtained (much more directly) under the same conditions. Moreover the Poincaré inequality (2.32) is automatically satisfied in the case of a compact configurational space \mathcal{D} .

2.2.5 Asymptotic variance for ergodic averages

Since ergodic averages are computed over a finite time-interval, the corresponding random variable will have some variance. Let us show how to relate this variance to the dynamics, provided a Central Limit Theorem holds. For simplicity, we assume that $(q_0, p_0) \sim \mu$, and let $\varphi \in H^1(\mu)$ be an observable of interest. We also denote by

$$\Pi\varphi = \varphi - \int_{\mathcal{E}} \varphi d\mu \quad (2.34)$$

the centering projector associated with μ . The Central Limit Theorem asserts that the following convergence in law holds:

$$\frac{1}{\sqrt{T}} \int_0^T \Pi\varphi(q_t, p_t) dt \xrightarrow{\text{law}} \mathcal{N}(0, \sigma_\varphi^2), \quad (2.35)$$

where σ_φ^2 is the asymptotic variance associated to φ under the dynamics, which is thus given by the limit of the variance on the left-hand side. Let us compute:

$$\sigma_{\varphi, T}^2 := \mathbb{E}_\mu \left[\left(\frac{1}{\sqrt{T}} \int_0^T \Pi\varphi(q_t, p_t) dt \right)^2 \right] = \frac{1}{T} \int_0^T \int_0^T \mathbb{E}_\mu [\Pi\varphi(q_t, p_t) \Pi\varphi(q_s, p_s)] ds dt.$$

By stationarity, for $t > s$, $\Pi\varphi(q_t, p_t)\Pi\varphi(q_s, p_s) \sim \Pi\varphi(q_{t-s}, p_{t-s})\Pi\varphi(q_0, p_0)$, hence we may write, by Fubini's theorem,

$$\begin{aligned}\sigma_T &= \frac{2}{T} \int_0^T \int_0^t \mathbb{E}_\mu [\Pi\varphi(q_{t-s}, p_{t-s})\Pi\varphi(q_0, p_0)] \, ds \, dt \\ &= \frac{2}{T} \int_0^T \int_s^T \mathbb{E}_\mu [\Pi\varphi(q_s, p_s)\Pi\varphi(q_0, p_0)] \, dt \, ds \\ &= 2 \int_0^T \mathbb{E}_\mu [\Pi\varphi(q_s, p_s)\Pi\varphi(q_0, p_0)] \left(1 - \frac{s}{T}\right) \, ds \\ &= 2 \int_0^T \mathbb{E}_\mu [(e^{s\mathcal{L}_\gamma}\Pi\varphi)(\Pi\varphi)] \left(1 - \frac{s}{T}\right) \, ds\end{aligned}$$

Using a Cauchy–Schwarz inequality in $L^2(\mu)$ and an exponential decay estimate on the evolution semigroup like (2.33), we obtain a bound of the form

$$\int_0^T \left| \mathbb{E}_\mu [(e^{s\mathcal{L}_\gamma}\Pi\varphi)(\Pi\varphi)] \frac{s}{T} \right| \, ds \leq \int_0^\infty C_\gamma e^{-\lambda_\gamma s} \|\Pi\varphi\|_{L^2(\mu)}^2 \frac{s}{T} \, ds$$

for some positive constants C and α , which converges uniformly to 0 as $T \rightarrow \infty$. It follows that

$$\sigma_\varphi^2 = \int_0^\infty \mathbb{E}_\mu [(e^{s\mathcal{L}_\gamma}\Pi\varphi)(\Pi\varphi)] \, ds. \quad (2.36)$$

We use the following equality of bounded operators on $\mathcal{H}^1(\mu)$, which is the operator:

$$(-\mathcal{L}_\gamma)^{-1} = \int_0^\infty e^{s\mathcal{L}_\gamma} \, ds, \quad (2.37)$$

which again is justified by the exponential decay rate of evolution semigroup, and where the integral on the right is in the Bochner sense, that is a generalization of the Lebesgue integral to functions taking values in a general Banach space. Using this identity, we can write the asymptotic variance more concisely,

$$\sigma_\varphi^2 = \mathbb{E}_\mu [(\Pi\varphi)(-\mathcal{L}_\gamma)^{-1}(\Pi\varphi)]. \quad (2.38)$$

Note that the exact same computations can be performed for the overdamped Langevin dynamics. It follows from [3, Theorem 2.1], that a sufficient condition for a CLT to hold is that $\Pi\varphi \in \text{Ran } \mathcal{L}_\gamma$, which is the case provided we can express the inverse of \mathcal{L}_γ using (2.37).

2.2.6 Splitting schemes for the Langevin dynamics

Similarly to the Hamiltonian case, the generator (2.17) splits into three elementary generators, namely

$$\mathcal{L}_\gamma = A + B + \gamma C = \mathcal{L}_{\text{ham}} + \gamma C,$$

with

$$C = -M^{-1}p \cdot \nabla_p + \frac{1}{\beta}\Delta_p. \quad (2.39)$$

These generators individually give rise to dynamics which we can analytically integrate, defined by the following evolution operators:

$$\begin{cases} e^{tA}\varphi(q, p) = \varphi(q + tM^{-1}p, p), \\ e^{tB}\varphi(q, p) = \varphi(q, p - t\nabla V(q)), \\ e^{t\gamma C}\varphi(q, p) = \mathbb{E} \left[\varphi \left(q, e^{-\gamma M^{-1}t}p + \sqrt{\frac{M}{\beta}(1 - e^{-2\gamma M^{-1}t})}G \right) \right], \end{cases} \quad (2.40)$$

where G is a standard dN -dimensional Gaussian. The third equality is a reformulation of an equality in law between an Itô integral and a Gaussian random variable, and follows by applying Itô's formula to the rescaled process

$$e^{\gamma M^{-1}t}p_t,$$

where p_t is the Ornstein–Uhlenbeck process:

$$dp_t = -\gamma M^{-1} p_t dt + \sqrt{\frac{2\gamma}{\beta}} dW_t, \quad (2.41)$$

then applying the following matrix form of Itô's isometric property

$$\int_0^t A_s dW_s \stackrel{\text{law}}{=} \left(\int_0^t A_s A_s^\top ds \right)^{\frac{1}{2}} \mathcal{G} \quad (2.42)$$

to obtain the equality in law. The dynamics associated with the A and B parts are deterministic Hamiltonian dynamics already identified in (2.8). Just as in the Hamiltonian case, we can define schemes for the Langevin dynamics based on approximating the evolution operator (2.18) over one timestep by splitting the generator \mathcal{L}_γ , and combining the corresponding evolution operators (2.40) in a sequence. We refer to such a splitting approximation by the sequence in which the individual propagators are composed. It is useful at this point to introduce the stochastic flow map associated with the Ornstein–Uhlenbeck dynamics.

$$\Phi_t^C(q, p, \xi) = \left(q, e^{-\gamma M^{-1} t} p + \sqrt{\frac{M}{\beta}(1 - e^{-2\gamma M^{-1} t})} \xi \right), \quad (2.43)$$

where $\xi \in \mathbb{R}^{dN}$. The map is defined so that $\mathbb{E}[\varphi(\Phi_t^C(q, p, G))] = e^{t\gamma C} \varphi(q, p)$ when G is a standard Gaussian random variable. Given an ordering of operators,

$$(R_1, \dots, R_k) \in \{A, B, \gamma C\}^k, \quad (2.44)$$

we can consider the mapping obtained by composing the elementary flows, noted as

$$\Phi^{R_1, \dots, R_k} := \Phi_{\Delta t / n_{R_k}}^{R_k} \circ \dots \circ \Phi_{\Delta t / n_{R_1}}^{R_1}, \quad (2.45)$$

where

$$n_R := \# \{1 \leq j \leq n | R_j = R\}$$

for $R \in \{A, B, \gamma C\}$, and which we may consider by a slight abuse to be the mapping which takes a point in phase space and $n_{\gamma C}$ vectors in $\xi_1, \dots, \xi_{n_{\gamma C}} \in \mathbb{R}^{dN}$, yielding a point in phase space by successively applying the flow, and, if need be, stochastic flow, mappings corresponding to the reverse ordering of (2.44). Applying this mapping with a vector of independent standard Gaussians yields a stochastic mapping, which defines the update rule for the splitting scheme associated with the ordering (2.44). An important property which follows from writing the update rule using the mapping (2.45) is that numerical trajectories formed by iterating this update rule with independent vectors of standard Gaussians form a Markov chain. The hope is that the invariant measure corresponding to this Markov chain (provided it is unique) is a close approximation to the canonical measure, as well as being ergodic. It is less cumbersome to write such schemes at the level of the evolution operator associated with the Markov chain,

$$P_{\Delta t} \varphi(q, p) = \mathbb{E} [\varphi(q^1, p^1) | q^0 = q, p^0 = p]. \quad (2.46)$$

The evolution operator associated with the splitting (2.44) is

$$P_{\Delta t} = e^{\Delta t / n_{R_1} R_1} \dots e^{\Delta t / n_{R_k} R_k}. \quad (2.47)$$

Note that the order is reversed compared to the stochastic flow formulation. While the formulation at the stochastic flow level is slightly complicated to write, it corresponds very closely to how a general splitting integrator for the Langevin dynamics can be implemented. One simply has to compute the timestep corresponding to each operator in the ordering, and apply in successive steps the corresponding flow maps, sampling independent Gaussian variables for each stochastic step. We will refer to such schemes by the name obtained by concatenating the names of each operator appearing in the ordering, using O instead of γC . For instance, the BAOAB scheme corresponds to the case $k = 5$, $n_A = n_B = 2$, and $n_{\gamma C} = 1$, and the ordering $(B, A, \gamma C, A, B)$.

Example 4 (BAOAB scheme). *The update rule is given by the following equations, with additional intermediate coordinate and momentum variables:*

$$\begin{cases} p^{n+\frac{1}{3}} = p^n - \frac{\Delta t}{2} \nabla V(q^n) \\ q^{n+\frac{1}{2}} = q^n + \frac{\Delta t}{2} M^{-1} p^{n+\frac{1}{3}} \\ p^{n+\frac{2}{3}} = \alpha_{\Delta t} p^{n+\frac{1}{3}} + \sigma_{\Delta t} G^n \\ q^{n+1} = q^{n+\frac{1}{2}} + \frac{\Delta t}{2} M^{-1} p^{n+\frac{2}{3}} \\ p^{n+1} = p^{n+\frac{2}{3}} - \frac{\Delta t}{2} \nabla V(q^{n+1}), \end{cases} \quad (2.48)$$

where, again, G^n is a standard dN -dimensional Gaussian.

Now we have a recipe to make an infinite number of numerical schemes, which can easily be implemented in a computer. We could even go further and consider methods with an uneven distribution for the secondary timesteps, the introduction of negative secondary timesteps for the A and B steps, and so on. This room for creativity highlights the need for criteria to assess the quality of such schemes. A tradeoff between various considerations has to be found:

- (i) Our aim is to compute long trajectories, which are needed to ensure that the phase space is properly explored, as well as to obtain better statistical properties for averages (2.5). Thus, for a fixed computational budget, we desire a scheme which allows us to take as large a timestep Δt as possible. This is the issue of numerical stability.
- (ii) The use of a positive timestep Δt implies in general that the invariant measure for the Markov chain corresponding to a given scheme is not the canonical measure. This issue is called systematic error, or bias, and one would desire a scheme which minimizes this bias.
- (iii) The main computational cost in computing iterates of these numerical schemes is the evaluation of the gradient of the potential used for the B steps. As such, it is desirable to have a scheme which requires as few evaluations of this gradient as possible per iteration. Some care must be taken when implementing these, to ensure that already computed gradients are not re-computed: for instance, the gradient in the last step of the BOAB scheme, is equal to the one in the first step of the next iteration.
- (iv) Notice that the parameter γ is free for the practitioner to choose. A natural question is to determine the properties of the marginal dynamics in q in the limit $\gamma \rightarrow +\infty$, and in particular if we obtain a consistent discretization of the overdamped Langevin dynamics. Conversely, one could ask about properties of the dynamics as we take the Hamiltonian limit $\gamma \rightarrow 0$.

Remark 8 (Overdamped and Hamiltonian limits in splitting schemes). *Concern (iv) is simple to address. Since*

$$\lim_{\gamma \rightarrow 0} \alpha_{\Delta t} = 1 \quad \lim_{\gamma \rightarrow +\infty} \alpha_{\Delta t} = 0,$$

every O-step can simply be dropped as $\gamma \rightarrow 0$ from the sequence of operators defining the splitting. This yields a symplectic scheme for the Hamiltonian parts of the dynamics, whose properties can be analyzed as before. For this reason, the ordering of the Hamiltonian parts of the splitting of most commonly used schemes corresponds to that of a velocity Verlet method. As $\gamma \rightarrow \infty$, every O-step reduces to resampling the momentum according to the Maxwell–Boltzmann distribution. The properties of the resulting scheme depend on the particular ordering of the splitting at hand. For instance, if every A step is preceded by an O step, then the potential is entirely ignored by the evolution, and the trajectories form an isotropic random walk. This is for instance the case of the BOA scheme. On the other hand, it may happen that one obtains a discretization of the overdamped Langevin dynamics. For example, the update equation for the overdamped limit of the BAOA scheme in the case $M = \text{Id}$ rewrites

$$q^{n+1} = q^n - \frac{\Delta t^2}{2} \nabla V(q^n) + \frac{1}{2} \sqrt{\frac{\Delta t^2}{\beta}} (G^n + G^{n+1}),$$

with (G^n) an i.i.d. standard Gaussian sequence. Because of the two-step correlations in the Gaussian increments, the numerical trajectories are not Markovian as such. Nevertheless the scheme is reminiscent

of a discretization of the overdamped equation (2.31), but with an effective timestep $\frac{\Delta t^2}{2}$. This quadratic rescaling of the timestep is common, and has to be related to the fact that the overdamped equation is defined through a diffusive rescaling. This discretization also corresponds to the overdamped limit of the BAOAB scheme, which is unsurprising in view of the results of the next chapter.

2.2.7 Error analysis for splitting schemes

We turn our attention to analyzing the error arising from the estimation of canonical expectations by discrete ergodic averages. We consider estimations of the form

$$\widehat{\varphi}_{N_{\text{iter}}} := \frac{1}{N_{\text{iter}}} \sum_{k=0}^{N_{\text{iter}}-1} \varphi(q^k, p^k),$$

where $(q^n, p^n)_{n \geq 0}$ is a numerical trajectory of a Markov chain which is ergodic with respect to a unique stationary distribution $\mu_{\Delta t}$ on \mathcal{E} , which approximates μ . To show the existence of such an invariant distribution, one can rely on general results from the theory of Markov chains, combined with Lyapunov estimates. For a precise result, we refer the reader to [24, Proposition 2.9], for example. For simplicity, we will assume that (q^0, p^0) is distributed according to $\pi_{\Delta t}$, so that the whole numerical trajectory is stationary. This requires in practice that the system be equilibrated before starting to sample the observables of interest. We decompose the error as follows:

$$\widehat{\varphi}_{N_{\text{iter}}} - \int_{\mathcal{E}} \varphi \, d\mu = \widehat{\varphi}_{N_{\text{iter}}} - \int_{\mathcal{E}} \varphi \, d\mu_{\Delta t} + \int_{\mathcal{E}} \varphi \, d\mu_{\Delta t} - \int_{\mathcal{E}} \varphi \, d\mu. \quad (2.49)$$

Two terms contribute to the error.

Statistical Error

The first term

$$\widehat{\varphi}_{N_{\text{iter}}} - \int_{\mathcal{E}} \varphi \, d\mu_{\Delta t}$$

is the statistical error due to the truncation of computed trajectories to a finite time $T_{\text{sim}} := N_{\text{iter}} \Delta t$. By the Central Limit Theorem for Markov Chains, asymptotically, the statistical error is of order $\sigma_{\varphi, \Delta t} / \sqrt{N_{\text{iter}}}$, where $\sigma_{\varphi, \Delta t}$ is the asymptotic variance of the Markov chain, which is given by the following expression, under suitable assumptions, by

$$\sigma_{\varphi, \Delta t}^2 = \text{Var}_{\pi_{\Delta t}}(\varphi) + 2 \sum_{k=1}^{\infty} \text{Cov}_{\pi_{\Delta t}}(\varphi(q^0, p^0) \varphi(q^k, p^k)).$$

The proof of the above expression is in spirit the same as the one in the continuous case, exploiting the stationarity in law of the trajectory. Using the evolution and projection operators associated with the Markov chain, which are respectively defined by

$$P_{\Delta t} \varphi(q, p) = \mathbb{E}[\varphi(q^1, p^1) | (q^0, p^0) = (q, p)], \quad \Pi_{\Delta t} \varphi = \varphi - \int_{\mathcal{E}} \varphi \, d\mu_{\Delta t}, \quad (2.50)$$

we can rewrite the asymptotic variance in a more analytic form, namely

$$\sigma_{\varphi, \Delta t}^2 = 2 \int_{\mathcal{E}} (\Pi_{\Delta t} \varphi)(\text{Id} - P_{\Delta t})^{-1} (\Pi_{\Delta t} \varphi) \, d\mu_{\Delta t} - \int_{\mathcal{E}} (\Pi_{\Delta t} \varphi)^2 \, d\pi_{\Delta t}, \quad (2.51)$$

where we formally used the Neumann series

$$\sum_{k=0}^{\infty} P_{\Delta t} = (\text{Id} - P_{\Delta t})^{-1},$$

which has to be justified rigorously, for instance using the geometric decay estimate for $P_{\Delta t}^n$ from [24, Proposition 2.9]. This implies that

$$\Delta t \sigma_{\varphi, \Delta t}^2 = 2 \int_{\mathcal{E}} (\Pi_{\Delta t} \varphi) \left(\frac{\text{Id} - P_{\Delta t}}{\Delta t} \right)^{-1} (\Pi_{\Delta t} \varphi) \, d\mu_{\Delta t} + O(\Delta t).$$

For reasonable discretizations of the Langevin dynamics, we expect that

$$\frac{\text{Id} - P_{\Delta t}}{\Delta t} = -\mathcal{L}_\gamma + O(\Delta t),$$

which suggests that at dominant order in Δt approaching 0, $\Delta t \sigma_{\varphi, \Delta t}^2$ behaves like

$$2 \int_{\mathcal{E}} (\Pi \varphi) (-\mathcal{L}_\gamma)^{-1} (\Pi \varphi) d\mu = \sigma_\varphi^2,$$

where we recall the asymptotic variance for the continuous dynamics (2.38). Hence the statistical error can be estimated, for Δt small enough, by

$$\frac{\sigma_{\varphi, \Delta t}}{\sqrt{N_{\text{iter}}}} = \frac{\sigma_{\varphi, \Delta t} \sqrt{\Delta t}}{\sqrt{T_{\text{sim}}}} \approx \frac{\sigma_\varphi}{\sqrt{T_{\text{sim}}}}.$$

Loosely speaking, the statistical error for the discrete ergodic estimator is governed at dominant order by the corresponding asymptotic variance for the underlying continuous dynamics, as well as the *physical* time of the simulation. This confirms that to minimize statistical error, and given a fixed budget of simulation steps, one should maximize T_{sim} and thus Δt , as discussed in consideration (i). However, increasing the timestep comes at the following cost.

Systematic Error

The second term in (2.49), namely

$$\int_{\mathcal{E}} \varphi d\mu_{\Delta t} - \int_{\mathcal{E}} \varphi d\mu,$$

is independent of the simulation time, and expresses the fact, highlighted in consideration (ii), that the invariant measure $\pi_{\Delta t}$ for the discrete evolution will in general be different from μ , in the sense that the average of an observable φ under $\pi_{\Delta t}$ can be expressed by an expansion of the form

$$\int_{\mathcal{E}} \varphi(q, p) \pi_{\Delta t}(dq, dp) = \int_{\mathcal{E}} \varphi(q, p) \mu(dq, dp) + \Delta t^\alpha \int_{\mathcal{E}} \varphi(q, p) f_\alpha(q, p) \mu(dq, dp) + O(\Delta t^{\alpha+1}), \quad (2.52)$$

where $\alpha > 0$ and f_α is the dominant correction term, which can be explicitly written down for splitting schemes, although computing them requires solving a high-dimensional partial differential equation. We postpone further discussion of these types of weak error estimates to the next chapter, in which we analyze the systematic error in the BAOA scheme.

2.2.8 Unbiased sampling

It turns out that one can devise schemes which have no systematic error: the Markov chain generating the trajectories has invariant measure exactly μ . These methods are based on the Metropolis–Hastings algorithm, which gives a general method to sample a given target distribution.

The Metropolis–Hastings algorithm

We aim to sample from a given target measure π on some measurable space \mathcal{X} . We suppose we have at our disposal a way to generate proposal points from a given point $y \in \mathcal{X}$. This amounts to defining a transition kernel, the *proposal*, which we may take to be a map

$$T : \mathcal{X} \times \mathcal{X} \longrightarrow \mathbb{R}_+,$$

such that for any $x \in \mathbb{R}^d$, $T(x, \cdot)$ is a probability density on \mathcal{X} , and which is usually inexpensive to sample from (very often, if $\mathcal{X} = \mathbb{R}^d$, these are taken to be some form of Gaussian distribution). We also assume for simplicity that we always have $T(x, y) > 0$. (This is always the case if the kernel is Gaussian). We also fix a function $r : \mathbb{R}_+ \rightarrow (0, 1]$, the acceptance rule, which satisfies the property

$$x \cdot r \left(\frac{1}{x} \right) = r(x) \quad (2.53)$$

We then define a Markov chain by iterating the following algorithm, starting from an arbitrary point $q^0 \in \mathcal{X}$.

Algorithm 1 (Metropolis–Hastings). Starting from an arbitrary point q^0 , iterate on $n \geq 0$:

(1) Sample a proposal \tilde{q}^{n+1} according to the probability law $T(q^n, \cdot)$.

(2) Compute

$$R(\tilde{q}^{n+1}, q^n) = r \left(\frac{\pi(\tilde{q}^{n+1})T(\tilde{q}^{n+1}, q^n)}{\pi(q^n)T(q^n, \tilde{q}^{n+1})} \right).$$

(3) With probability $R(\tilde{q}^{n+1}, q^n)$, set $q^{n+1} = \tilde{q}^{n+1}$, otherwise, set $q^{n+1} = q^n$. Concretely, this is done by sampling a uniform variable $U^n \sim \mathcal{U}([0, 1])$, and setting $q^{n+1} = \tilde{q}^{n+1}$ if $U^n \leq R(\tilde{q}^{n+1}, q^n)$, and $q^{n+1} = q^n$ otherwise.

(4) Go back to step (1) with $q^n \leftarrow q^{n+1}$.

Since T defines a Markov chain, we may always write $\tilde{q}^{n+1} = \Phi(q^n, \xi^n)$ for some family of *i.i.d.* variables $(\xi^n)_{n \geq 0}$. We can then write q^{n+1} in a concise form:

$$q^{n+1} = \Phi(q^n, \xi^n) + \mathbb{1}_{U^n > R(\Phi(q^n, \xi^n), q^n)} (q^n - \Phi(q^n, \xi^n)) = \Psi(q^n, \xi^n, U^n), \quad (2.54)$$

where the U^n are *i.i.d.* uniform on $[0, 1]$, such that the (ξ^n, U^n) are an independent family. This expression is slightly formal since in general addition is not defined on \mathcal{X} , nevertheless, it shows that the algorithm defines a Markov chain. Moreover,

$$\begin{aligned} \pi(x)\mathbb{P}(q^1 = y | q^0 = x) &= \pi(x)T(x, y)R(x, y) \\ &= \pi(x)T(x, y)r \left(\frac{\pi(y)T(y, x)}{\pi(x)T(x, y)} \right) \\ &= \pi(y)T(y, x) \frac{\pi(x)T(x, y)}{\pi(y)T(y, x)} r \left(\frac{\pi(y)T(y, x)}{\pi(x)T(x, y)} \right) \\ &= \pi(y)T(y, x)r \left(\frac{\pi(x)T(x, y)}{\pi(y)T(y, x)} \right) \quad (\text{Using (2.53)}) \\ &= \pi(y)\mathbb{P}(q^1 = x | q^0 = y). \end{aligned} \quad (2.55)$$

Thus, the chain is reversible with respect to π , so that it is an invariant measure. Note that the algorithm is applicable even when we do not know how to evaluate π , but only the ratios $\pi(x)/\pi(y)$, which is in particular the case for Gibbs measures, which are known up to a normalization constant.

The historical and most commonly used acceptance rule is the Metropolis rule:

$$r(x) = \min \{1, x\}. \quad (2.56)$$

Remark 9 (Alternative acceptance rules for Metropolis–Hastings). Other possible choices for r are:

1. The Barker rule,

$$r(x) = \frac{x}{1+x},$$

2. Any combination of the Barker and Metropolis rules of the form, for $\gamma > 0$,

$$r(x) = \frac{x}{1+x} \left(1 + 2 \left(\frac{1}{2} \min \left(r, \frac{1}{r} \right) \right)^\gamma \right).$$

Remark 10 (Issues with Metropolized-schemes). The Metropolis–Hastings algorithm provides a general recipe to define an unbiased Markov chain for the overdamped Langevin dynamics: one only needs to specify a proposition kernel, an acceptance rule, and a way to compute the ratio of the corresponding transition probabilities. For example, the so-called MALA scheme from [29] is very common, and combines a proposal function based on the Euler–Maruyama discretization of the dynamics (2.28) with a Metropolis acceptance rule. The use of the Metropolis–Hastings algorithm does not come for free. Because of the rejection rate, the correlations between samples decays at a slower rate, resulting in a higher asymptotic variance for estimators based on ergodic averages. In fact with regards to asymptotic variance, the choice of the Metropolis rule is optimal, as was shown in [26]. This implies that the use of a Metropolized scheme is only beneficial if the simulation time regime in which the systematic error overcomes the statistical error is computationally attainable. For most systems of interest, this is not the case. Furthermore, the possibility of rejection effectively slows down the dynamics, which may degrade the quality of estimates for dynamical quantities. The effect of the Metropolization procedure with the MALA scheme on the estimation of self-diffusion properties has been analyzed in [10], and improved rules and proposals for the computation of transport properties are discussed in detail in [11].

2.2.9 Numerical illustrations

We now turn to a few numerical illustrations of the discussions above. In Figure 2.3, we compute numerically compute the pressure as a function of the density for the Lennard–Jones fluid, using the parameters for Argon, at two different temperatures. The resulting profile gives a numerical estimation of the equation of state of Argon, and comparison with experimental data shows that the agreement is very good at low densities and room temperature. The size of the systems was $N = 2744$ atoms, using a sharp cutoff at $r_c = 2.5$, and a BOAB splitting scheme with $\Delta t = 0.005$, and $\gamma = 1.0$ was used for the friction parameter. We verified by using the block averaging procedure described in [12] for the trajectories at both ends of the density range that the standard error bars are negligible.

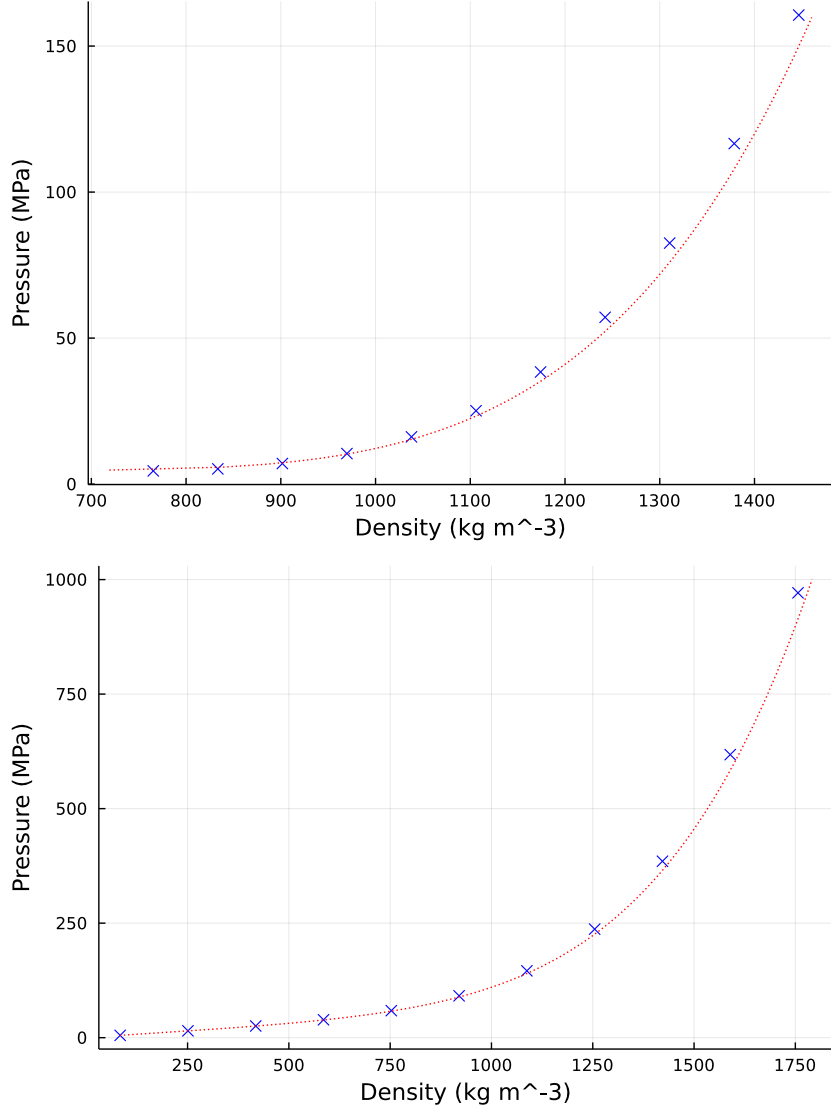


Figure 2.3: Simulated equations of state of Argon at 150 K (liquid phase, top) and 300 K (supercritical phase, bottom). Experimental reference curves obtained from the NIST website [25] are plotted in red, simulated data points correspond to blue crosses.

In Figures 2.4 and 2.5, we highlight the systematic error in several observables. Simulations were run for systems of $N = 27$ Lennard–Jones particles, at a reduced temperature $T = 1.25$ and at a reduced density $\rho = 0.25$. A cutoff of the potential at a distance $r_c = 2.0$ was imposed, with a linear correction term ensuring that V be C^1 . Additionally, regression lines were added by extrapolating the behavior at small Δt based on the theoretical expansions (2.52), and constraining the regression lines to converge to the same value in the limit $\Delta t \rightarrow 0$. This was achieved by a linear least squares regression procedure. The result also illustrate that a possibility to reduce the systematic error is to compute a desired average

for several timesteps, and computing an extrapolated value at $\Delta t = 0$ based on the theoretical knowledge of the behavior of the systematic error as $\Delta t \rightarrow 0$. This is known as Richardson extrapolation, see for instance [27, Section 9.6].

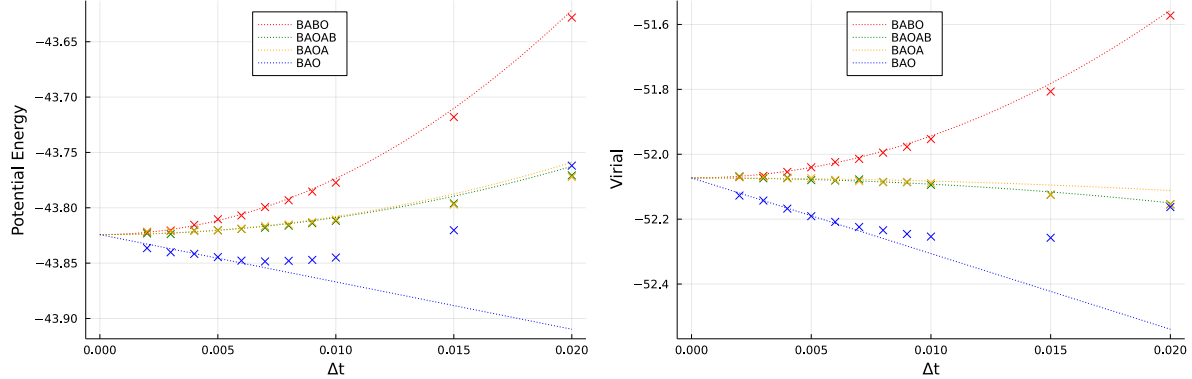


Figure 2.4: Systematic error in configurational quantities for a Lennard–Jones fluid.

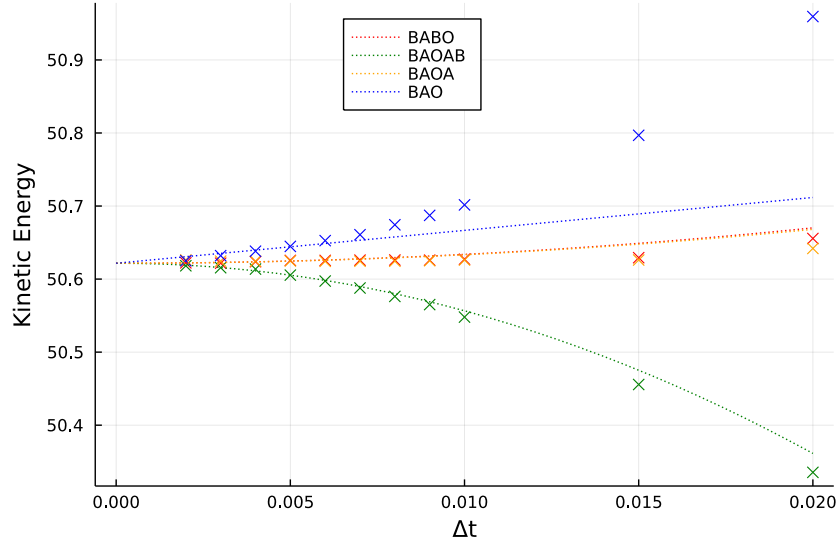


Figure 2.5: Systematic error in kinetic energy for a Lennard–Jones fluid.

For the two configurational quantities we investigated, the virial and potential energy, we observe an overlap in the bias between the BAOAB and BAOA schemes. It so happens that this overlap can be simply explained by a result relating the invariant measures of certain pairs of numerical schemes, see Lemma 2 in the next chapter. In fact, a preprint [21] was recently posted, showing that a certain widely used scheme in the molecular dynamics community was equivalent to the BAOA scheme, and that the latter sampled the same configurational marginal as the BAOAB scheme. This prompted the need for a more thorough investigation of the properties of the BAOA scheme, which we discuss in the next chapter.

Chapter 3

Study of the BAOA scheme

We consider time discretization schemes of underdamped Langevin dynamics known as the BAOA and BAOAB schemes, in order to compare the sampling bias induced by the timestep Δt for these two methods. Like other symmetric splittings, the BAOAB scheme has been well studied, and an analysis of the timestep bias for the BAOAB scheme is for instance given in [24]. Furthermore, it has been shown, see the discussion in [23, Section 7.9.3], that the BAOAB scheme displays a property of superconvergence: the bias on configurational averages becomes $O(\Delta t^4)$ in the overdamped limit $\gamma \rightarrow \infty$. It also enjoys good stability properties. On the other hand, it appeared while studying the native Langevin integrator used by the Molecular Dynamics package Molly [15], itself based on an implementation in OpenMM, corresponds to a BAOA splitting. A recent preprint, [21], further shows that the BAOA splitting is used in the GROMACS Stochastic Dynamics integrator. So it appears that practitioners of molecular simulations have somewhat widely adopted the BAOA scheme, while its bias properties are not so well understood from a theoretical point of view. It has been numerically observed in [21, Section III.B] that the bias on the kinetic marginal distribution is much lower using the BAOA method, while the bias on the configurational marginal as the same as for BAOAB. This gives a plausible explanation for why one might choose BAOA over the more theoretically grounded BAOAB, by comparing errors on kinetic and configurational observables individually. We attempt in this chapter to explain these observations mathematically, before illustrating our results in numerical examples. Building on known results for the BAOAB scheme, we show the following results.

- (i) In Section 3.1, we express the invariant measure of the BAOA scheme in terms of the invariant measure of the BAOAB scheme (Proposition 4), and using this expression, we show, as in [21, Section II.C], the equality between their respective configurational marginal distributions (Corollary 1).
- (ii) In Section 3.2, we show that the dominant error term for BAOA averages is only of order one in Δt , confirming that the BAOAB method is in general of higher order (Corollary 2).
- (iii) We show in Section 3.3 that for kinetic observables, however, the error is of second order in Δt , so that both marginal distributions are second-order accurate (Corollary 3).
- (iv) In Section 3.4, we give an expression for the dominant error term in the kinetic marginal distribution of the BAOA scheme (Proposition 5). In fact, we conjecture that, at least in dimension one, this term cancels, leading to an order of at least Δt^3 (Conjecture 1).
- (v) Lastly, in Section 3.5, we analyze the difference between the kinetic marginal distribution under the BAOA and BAOAB scheme (Proposition 6), and explain why this difference leads to a systematic underestimation of the kinetic variance in BAOAB trajectories (Remark 12).

We consider the two splitting schemes for (2.15) defined by the following evolution operators:

$$\begin{cases} P_{\Delta t} = e^{\Delta t B} e^{\frac{\Delta t}{2} A} e^{\Delta t \gamma C} e^{\frac{\Delta t}{2} A}, \\ Q_{\Delta t} = e^{\frac{\Delta t}{2} B} e^{\frac{\Delta t}{2} A} e^{\Delta t \gamma C} e^{\frac{\Delta t}{2} A} e^{\frac{\Delta t}{2} B}, \end{cases} \quad (3.1)$$

where we recall the notation from (2.40). They correspond respectively to the BAOA and the BAOAB scheme. We also denote by $\mu_{\Delta t, P}, \mu_{\Delta t, Q}$ the invariant measures for the Markov chains associated with (3.1). We assume that they have smooth densities which we also denote by $\mu_{\Delta t, P}, \mu_{\Delta t, Q}$ with some

abuse of notation, and that a certain ergodicity condition holds, see Lemma 2. Additionally we denote by $\nu_{\Delta t, P}, \nu_{\Delta t, Q}, \kappa_{\Delta t, P}, \kappa_{\Delta t, Q}$ the associated marginals and densities in the q and p variables respectively, with obvious notation inspired by (1.8).

3.1 Relating invariant measures of discretization schemes

In this paragraph, we provide a formula for $\mu_{\Delta t, P}$ in terms of $\mu_{\Delta t, Q}$. This result allows one to very simply show the equality in the configurational marginals between these two measures, as noted in [21]. The main tool is the following result, which is a reformulation of the TU lemma [24, Lemma 2.12].

Lemma 2. *Let $P_{\Delta t}, Q_{\Delta t}$ be bounded operators on $B^\infty(\mathcal{E})$. Assume that, for any $n \geq 1$,*

$$R_{\Delta t} P_{\Delta t}^n = Q_{\Delta t}^n S_{\Delta t},$$

where $R_{\Delta t}$ and $S_{\Delta t}$ are bounded operators on $B^\infty(\mathcal{E})$, such that $R_{\Delta t} \mathbb{1} = \mathbb{1}$, and that the following ergodic condition holds: for any $\varphi \in B^\infty(\mathcal{E})$, and almost all $(q, p) \in \mathcal{E}$,

$$\lim_{n \rightarrow \infty} P_{\Delta t}^n \varphi(q, p) = \int_{\mathcal{E}} \varphi(q, p) \mu_{\Delta t, P}(dq, dp),$$

$$\lim_{n \rightarrow \infty} Q_{\Delta t}^n \varphi(q, p) = \int_{\mathcal{E}} \varphi(q, p) \mu_{\Delta t, Q}(dq, dp).$$

Then $\mu_{\Delta t, P}$ and $\mu_{\Delta t, Q}$ are related as follows:

$$\forall \varphi \in B^\infty(\mathcal{E}), \quad \int_{\mathcal{E}} \varphi(q, p) \mu_{\Delta t, P}(dq, dp) = \int_{\mathcal{E}} (S_{\Delta t} \varphi)(q, p) \mu_{\Delta t, Q}(dq, dp). \quad (3.2)$$

Proof. Fix an initial probability measure ρ on \mathcal{E} , absolutely continuous with respect to the Lebesgue measure. Then we may write, using dominated convergence to pass to the limit:

$$\begin{aligned} & \int_{\mathcal{E}} R_{\Delta t} P_{\Delta t}^n \varphi(q, p) \rho(q, p) dq dp \\ &= \int_{\mathcal{E}} P_{\Delta t}^n \varphi(q, p) R_{\Delta t}^\dagger \rho(q, p) dq dp \\ &\xrightarrow{n \rightarrow \infty} \int_{\mathcal{E}} \left(\int_{\mathcal{E}} \varphi(q, p) \mu_{\Delta t, P}(\tilde{q}, \tilde{p}) d\tilde{q} d\tilde{p} \right) R_{\Delta t}^\dagger \rho(q, p) dq dp \\ &= \int_{\mathcal{E}} \varphi(q, p) \mu_{\Delta t, P}(dq, dp) \int_{\mathcal{E}} R_{\Delta t} \mathbb{1} \rho \\ &= \int_{\mathcal{E}} \varphi(q, p) \mu_{\Delta t, P}(q, p) dq dp \end{aligned}$$

Furthermore, applying the ergodic condition to the bounded function $S_{\Delta t} \varphi$ gives

$$\begin{aligned} & \int_{\mathcal{E}} Q_{\Delta t}^n (S_{\Delta t} \varphi)(q, p) \rho(q, p) dq dp \xrightarrow{n \rightarrow \infty} \int_{\mathcal{E}} \left(\int_{\mathcal{E}} S_{\Delta t} \varphi(\tilde{q}, \tilde{p}) \mu_{\Delta t, Q}(\tilde{q}, \tilde{p}) d\tilde{q} d\tilde{p} \right) \rho(q, p) dq dp \\ &= \int_{\mathcal{E}} S_{\Delta t} \varphi(q, p) \mu_{\Delta t, Q}(dq, dp). \end{aligned}$$

Since $R_{\Delta t} P_{\Delta t}^n = Q_{\Delta t}^n S_{\Delta t}$, an identification of the two limits yields (3.2) □

Applying Lemma 2 to (3.1) gives the following result.

Proposition 4. *The densities $\mu_{\Delta t, P}$ and $\mu_{\Delta t, Q}$ satisfy the following equality:*

$$\mu_{\Delta t, P}(q, p) = \mu_{\Delta t, Q} \left(q, p - \frac{\Delta t}{2} V(q) \right). \quad (3.3)$$

Proof. From the expressions (3.1), we immediately get $P_{\Delta t}^n e^{\frac{\Delta t}{2}B} = e^{\frac{\Delta t}{2}B} Q_{\Delta t}^n$, whereby applying Lemma 2, we get for any test function φ ,

$$\int_{\mathcal{E}} e^{\frac{\Delta t}{2}B} \varphi d\mu_{P,\Delta t} = \int_{\mathcal{E}} \varphi d\mu_{Q,\Delta t}. \quad (3.4)$$

Using equation (3.4) with $\psi = e^{-\frac{\Delta t}{2}B} \varphi$ yields an exact expression for $\mu_{\Delta t,P}$ in terms of $\mu_{\Delta t,Q}$:

$$\int_{\mathcal{E}} \varphi d\mu_{\Delta t,P} = \int_{\mathcal{E}} e^{-\frac{\Delta t}{2}B} \varphi d\mu_{\Delta t,Q}. \quad (3.5)$$

Since φ is arbitrary, we infer that at the level of densities,

$$\mu_{\Delta t,P}(q,p) = \left(e^{-\frac{\Delta t}{2}B} \right)^{\dagger} \mu_{\Delta t,Q}(q,p), \quad (3.6)$$

where \dagger denotes the adjoint on the flat space $L^2(\mathcal{E})$. A simple computation shows that $e^{-\frac{\Delta t}{2}B^\dagger} = e^{\frac{\Delta t}{2}B}$, since $B^\dagger = -B$. Hence,

$$\mu_{\Delta t,P}(q,p) = e^{\frac{\Delta t}{2}B} \mu_{\Delta t,Q}(q,p) = \mu_{\Delta t,Q} \left(q, p - \frac{\Delta t}{2} \nabla V(q) \right), \quad (3.7)$$

which is the desired conclusion. \square

Relation (3.7) is sufficient to show an equality between the configurational marginal distributions $\nu_{\Delta t,P}$ and $\nu_{\Delta t,Q}$, as noted in [21].

Corollary 1. *The marginal distributions in the q variable of $\mu_{\Delta t,P}$ and $\mu_{\Delta t,Q}$ coincide:*

$$\nu_{\Delta t,Q}(q) = \nu_{\Delta t,P}(q). \quad (3.8)$$

Proof. Write, for any $q \in \mathcal{D}$,

$$\begin{aligned} \nu_{\Delta t,Q}(q) &= \int_{\mathbb{R}^{dN}} \mu_{\Delta t,Q}(q,p) dp = \int_{\mathbb{R}^{dN}} \mu_{\Delta t,Q} \left(q, p - \frac{\Delta t}{2} \nabla V(q) \right) dp \\ &= \int_{\mathbb{R}^{dN}} \mu_{\Delta t,P}(q,p) dp = \nu_{\Delta t,P}(q), \end{aligned}$$

which proves the claim. \square

3.2 Error estimate on the phase space measure

We now turn to obtaining the dominant order in the sampling bias of $\mu_{\Delta t,P}$, building on previously known results for $\mu_{\Delta t,Q}$, and the relation (3.3). Error estimates on $\mu_{\Delta t,Q}$ have been investigated in [24] (Section 1.4). In particular, the following expansion of $\mu_{\Delta t,Q}$ is derived, which will be central in our analysis.

Theorem 2 ([24], Theorem 13). *There exists a smooth function f_2 such that for any smooth compactly supported ψ ,*

$$\int_{\mathcal{E}} \psi(q,p) \mu_{\Delta t,Q}(q,p) dq dp = \int_{\mathcal{E}} \psi(q,p) \mu(q,p) dq dp + \Delta t^2 \int_{\mathcal{E}} \varphi(q,p) f_2(q,p) \mu(q,p) dq dp + \Delta t^4 r_{\psi,\gamma,\Delta t}, \quad (3.9)$$

where the remainder $r_{\psi,\gamma,\Delta t}$ is uniformly bounded for Δt sufficiently small. Moreover, an expression for the dominant error term is obtained,

$$\begin{cases} f_2 = \tilde{f}_2 - \frac{1}{8}(A+B)g, \\ \mathcal{L}_\gamma^* \tilde{f}_2 = \frac{1}{12}(A+B) \left[\left(A + \frac{B}{2} \right) g \right] \\ g := \beta(M^{-1}p) \cdot \nabla V(q), \end{cases} \quad (3.10)$$

where \mathcal{L}_γ^* is the adjoint of \mathcal{L}_γ on the weighted space $L^2(\mu)$.

Using this expansion, one can derive the dominant order error for the BAOA scheme.

Corollary 2. *For any smooth observable φ ,*

$$\int_{\mathcal{E}} \varphi(q, p) \mu_{\Delta t, P}(q, p) dq dp = \int_{\mathcal{E}} \varphi(q, p) \left(1 + \frac{\Delta t}{2} g(q, p) \right) \mu(q, p) dq dp + O(\Delta t^2), \quad (3.11)$$

where g is given by (3.10).

Proof. Combining (3.9) with (3.3), we get the following estimation for averages with respect to $\mu_{\Delta t, P}$:

$$\int_{\mathcal{E}} \varphi(q, p) \mu_{\Delta t, P}(q, p) dq dp = \int_{\mathcal{E}} \varphi(q, p) \mu \left(q, p - \frac{\Delta t}{2} \nabla V(q) \right) dq dp + O(\Delta t^2). \quad (3.12)$$

Taylor expanding μ gives

$$\mu \left(q, p - \frac{\Delta t}{2} \nabla V(q) \right) = \mu(q, p) \left(1 + \frac{\Delta t}{2} \beta(M^{-1}p) \cdot \nabla V(q) + O(\Delta t^2) \right) = \mu(q, p) \left(1 + \frac{\Delta t}{2} g(q, p) + O(\Delta t^2) \right),$$

hence we get

$$\int_{\mathcal{E}} \varphi(q, p) \mu_{\Delta t, P}(q, p) dq dp = \int_{\mathcal{E}} \varphi(q, p) \mu(q, p) \left(1 + \frac{\Delta t}{2} g(q, p) + O(\Delta t^2) \right) dq dp, \quad (3.13)$$

which proves the claim. \square

3.3 Error estimates on the kinetic marginal distributions

Equation (3.11) expresses the fact that the invariant measure $\mu_{\Delta t, P}$ is only exact at first order in Δt , which is one less than $\mu_{\Delta t, Q}$. So in full generality, one can expect an error of order Δt on averages obtained from BAOA trajectories, versus Δt^2 for averages computed from BAOAB trajectories. However, if we restrict ourselves to marginal observables, that is observables which only depend on the configurational coordinate or the kinetic coordinate, the first order error term vanishes. Indeed, the following result holds.

Corollary 3. *Let $\varphi(q, p) = \varphi(q)$ or $\varphi(q, p) = \varphi(p)$ be a marginal observable. Then*

$$\int_{\mathcal{E}} \varphi d\mu_{\Delta t, P} = \int_{\mathcal{E}} \varphi d\mu + O(\Delta t^2).$$

Proof. By (3.11), it is sufficient to show

$$\int_{\mathcal{E}} \varphi g d\mu = 0. \quad (3.14)$$

This follows from the following cancellations.

$$\int_{\mathbb{R}^{dN}} g(q, p) \mu(q, p) dp = \int_{\mathcal{D}} g(q, p) \mu(q, p) dq = 0. \quad (3.15)$$

Indeed,

$$\begin{aligned} \int_{\mathcal{D}} \beta(M^{-1}p) \cdot \nabla V(q) \mu(q, p) dq &= - \int_{\mathcal{D}} (M^{-1}p) \cdot \nabla_q \mu(q, p) dq = 0, \\ \int_{\mathbb{R}^{dN}} \beta(M^{-1}p) \cdot \nabla V(q) \mu(q, p) dp &= - \int_{\mathbb{R}^{dN}} \nabla V(q) \cdot \nabla_p \mu(q, p) dp = 0, \end{aligned}$$

using integration by parts. By first integrating (3.14) over the coordinate independent of φ , one of the cancellations (3.15) yields the result. \square

Corollary 2 gives no new information concerning configurational observables, since we already know by Corollary 1 that these have the same averages under $\mu_{\Delta t, P}$ and $\mu_{\Delta t, Q}$, and that by Theorem 2, these have error of order Δt^2 . However, kinetic observables may yield different averages.

3.4 Analysis of the second order error term for kinetic averages under $\mu_{\Delta t, P}$

It was observed numerically in [21] that the averages of the kinetic and configurational temperatures computed with a BAOA scheme have a bias of order greater than Δt , as expected from the argument above. In fact, for the kinetic temperature, the order appears to be greater than Δt^2 , in contrast to averages computed with the BAOAB method. Understanding this behavior theoretically requires comparing second order error terms.

We show the following result, which identifies the second-order error term for kinetic observables.

Proposition 5. *Let $\psi(q, p) = \psi(p)$ be a smooth kinetic observable. Then,*

$$\int_{\mathcal{E}} \psi(p) \mu_{\Delta t, P}(q, p) dq dp = \int_{\mathcal{E}} \psi(p) \mu(q, p) dp dq + \Delta t^2 \int_{\mathcal{E}} \psi(p) \tilde{f}_2(q, p) \mu(q, p) dq dp + O(\Delta t^3), \quad (3.16)$$

where \tilde{f}_2 is given by (3.10).

From Theorem 13 of [24], this error term is identical to the dominant error term for OBABO averages, and minus the dominant error term for OABAO averages.

Proof. By writing

$$\int_{\mathcal{E}} \psi(q, p) \mu_{\Delta t, P}(q, p) dq dp - \int_{\mathcal{E}} \psi(q, p) \mu(q, p) dp dq = \int_{\mathcal{E}} \left(\psi(q, p) - \int_{\mathcal{E}} \psi d\mu \right) \mu_{\Delta t, P}(q, p) dq dp,$$

we may assume without loss of generality that ψ has average 0 with respect to μ .

Using (3.9), we get

$$\int_{\mathcal{E}} \psi(p) \mu_{\Delta t, Q}(q, p) dq dp = \Delta t^2 \int_{\mathcal{E}} \psi(p) f_2(q, p) \mu(q, p) dq dp + O(\Delta t^3),$$

so that using our relation (3.3), we get

$$\int_{\mathcal{E}} \psi(p) \mu_{\Delta t, P}(q, p) dq dp = \int_{\mathcal{E}} \psi(p) e^{\frac{\Delta t}{2} B} \mu(q, p) dq dp + \Delta t^2 \int_{\mathcal{E}} \psi(p) e^{\frac{\Delta t}{2} B} [f_2(q, p) \mu(q, p)] dq dp + O(\Delta t^3).$$

The right hand side of the above inequality rewrites, at dominant order,

$$\int_{\mathcal{E}} \psi(p) \mu \left(q, p - \frac{\Delta t}{2} \nabla V(q) \right) dq dp + \Delta t^2 \int_{\mathcal{E}} \psi(p) f_2(q, p) \mu(q, p) dq dp + O(\Delta t^3).$$

Expanding $H \left(q, p - \frac{\Delta t}{2} \nabla V(q) \right)$ to the second order gives

$$H \left(q, p - \frac{\Delta t}{2} \nabla V(q) \right) = H(q, p) - \frac{\Delta t}{2} (M^{-1} p) \cdot \nabla V(q) + \frac{\Delta t^2}{8} (M^{-1} \nabla V(q)) \cdot \nabla V(q) + O(\Delta t^3), \quad (3.17)$$

whereupon expanding $\mu = e^{-\beta H}$ to the second order yields

$$\begin{aligned} & \mu \left(q, p - \frac{\Delta t}{2} \nabla V(q) \right) + O(\Delta t^3) \\ &= \mu(q, p) \left[1 + \beta \frac{\Delta t}{2} (M^{-1} p) \cdot \nabla V(q) + \frac{\Delta t^2}{8} [(\beta M^{-1} p) \otimes (\beta M^{-1} p) \nabla V(q)] \cdot \nabla V(q) - \beta \frac{\Delta t^2}{8} (M^{-1} \nabla V(q)) \cdot \nabla V(q) \right] \\ &= \mu(q, p) \left[1 + \beta \frac{\Delta t}{2} g(q, p) + \frac{\Delta t^2}{8} (g^2(q, p) - \beta (M^{-1} \nabla V(q)) \cdot \nabla V(q)) \right]. \end{aligned}$$

Using $\int \psi d\mu = 0$ and the cancellation (3.15) on q to remove the first order term, we obtain:

$$\int_{\mathcal{E}} \psi(p) \mu_{\Delta t, P}(q, p) dq dp = \Delta t^2 \int_{\mathcal{E}} \psi(p) \left(\frac{1}{8} (g^2(q, p) - \beta (M^{-1} \nabla V(q)) \cdot \nabla V(q)) + f_2(q, p) \right) \mu(q, p) dq dp + O(\Delta t^3). \quad (3.18)$$

Simplifications are possible. First, observe that

$$-\beta(M^{-1}\nabla V(q)) \cdot \nabla V(q) = Bg(q, p),$$

so that, using the expression for f_2 given in (3.10), we get

$$\int_{\mathcal{E}} \psi(p) \mu_{\Delta t, P}(q, p) dq dp = \Delta t^2 \int_{\mathcal{E}} \psi(p) \left(\frac{1}{8} (g^2(q, p) - Ag(q, p)) + \tilde{f}_2(q, p) \right) \mu(q, p) dq dp + O(\Delta t^3). \quad (3.19)$$

Next, we examine the term

$$(g^2(q, p) - Ag(q, p)) \mu(q, p) = \left[\beta^2 ((M^{-1}p) \cdot \nabla V(q))^2 - \beta(M^{-1}p) \cdot (\nabla^2 V(q) M^{-1}p) \right] \mu(q, p),$$

by a straightforward calculation, where ∇^2 denotes the Hessian matrix. This expression is a finite sum of diagonal terms coming from both terms inside the brackets, and off-diagonal terms coming only from the rightmost term inside the bracket. Importantly, these all vanish when integrated against the configurational marginal of μ . To make this precise, we index p and q as

$$p = (p_i)_{1 \leq i \leq dN}, \quad q = (q_i)_{1 \leq i \leq dN}.$$

Fixing indices $i \neq j$, the diagonal term corresponding to i is

$$\left[\beta^2 (M^{-1}p)_i^2 \left(\frac{\partial}{\partial q_i} V(q) \right)^2 - \beta (M^{-1}p)_i^2 \frac{\partial^2}{\partial q_i^2} V(q) \right] \mu(q, p) = (M^{-1}p)_i^2 \frac{\partial^2}{\partial q_i^2} \mu(q, p), \quad (3.20)$$

and the off-diagonal term corresponding to (i, j) is

$$-\beta (M^{-1}p)_i (M^{-1}p)_j \frac{\partial}{\partial q_i} V(q) \frac{\partial}{\partial q_j} V(q) \mu(q, p) = -\frac{1}{\beta} (M^{-1}p)_i (M^{-1}p)_j \frac{\partial^2}{\partial q_i \partial q_j} \mu(q, p). \quad (3.21)$$

Factoring out the q -independent terms, and using the cancellations

$$\int_{\mathcal{D}} \frac{\partial^2}{\partial q_i^2} \mu(q, p) dq = \int_{\mathcal{D}} \frac{\partial^2}{\partial q_i \partial q_j} \mu(q, p) dq = 0, \quad (3.22)$$

which follow by integration by parts, we infer

$$\int_{\mathcal{E}} \psi(p) \mu_{\Delta t, P}(q, p) dq dp = \Delta t^2 \int_{\mathcal{E}} \psi(p) \tilde{f}_2(q, p) \mu(q, p) dq dp + O(\Delta t^3), \quad (3.23)$$

which concludes the proof. \square

Remark 11. Using exponential decay estimates on the evolution semigroup $(e^{t\mathcal{L}_\gamma})_{t \geq 0}$ like (2.33), one can show that the inverse operator \mathcal{L}_γ^{-1} is well-defined for smooth centered observables. Thus $\Psi = \mathcal{L}_\gamma^{-1}\psi$ is well defined. By construction, $\mathcal{L}_\gamma\Psi(q, p) = \psi(p)$. Hence, (3.16) rewrites

$$\begin{aligned} \int_{\mathcal{E}} \psi(p) \mu_{\Delta t, P}(q, p) dq dp &= \Delta t^2 \int_{\mathcal{E}} \mathcal{L}_\gamma\Psi(q, p) \tilde{f}_2(q, p) \mu(q, p) dq dp + O(\Delta t^3) \\ &= \Delta t^2 \int_{\mathcal{E}} \Psi(q, p) \mathcal{L}_\gamma^* \tilde{f}_2(q, p) \mu(q, p) dq dp + O(\Delta t^3) \\ &= \frac{\Delta t^2}{12} \int_{\mathcal{E}} \Psi(q, p) \left[(A + B) \left(A + \frac{B}{2} \right) g \right] (q, p) \mu(q, p) dq dp + O(\Delta t^3), \end{aligned}$$

using (3.10), which provides an alternative expression for the dominant error term. Numerical evidence (see Figure 3.11) suggests that the error on BAOA and BAOAB averages is at dominant order independent of γ . Since the error term on BAOA given in (3.16) *a priori* depends on γ , although not in an explicit manner, this suggests that this term is zero, motivating the following conjecture.

Conjecture 1. For any smooth centered kinetic observable $\psi(p)$, we have

$$\int_{\mathcal{E}} (\mathcal{L}_\gamma^{-1}\psi)(q, p) \left[(A + B) \left(A + \frac{B}{2} \right) g \right] (q, p) \mu(q, p) dq dp = 0. \quad (3.24)$$

This would in particular imply that the kinetic marginal $\kappa_{\Delta t, P}$ is correct at order at least three in Δt , in accordance with numerical results presented in Section 3.6.6, and should be the subject of further investigation.

3.5 Analysis of the discrepancy between the dominant error terms on the kinetic marginals

Numerical evidence presented in [21] shows a significant discrepancy between $\kappa_{\Delta t, P}$ and $\kappa_{\Delta t, Q}$. Specifically, $\kappa_{\Delta t, Q}$ in the case $d = N = 1$ tends to present a sharper peak than $\kappa_{\Delta t, P}$, thus underestimating the variance in the kinetic marginal. We show here that this behavior is generic, in the sense that it does not, up to a shape parameter, depend on V . The arguments above show that

$$\begin{aligned} \int_{\mathcal{E}} \psi(p) \mu_{\Delta t, P}(q, p) dq dp &= \int_{\mathbb{R}^{dN}} \psi(p) \kappa_{\Delta t, P}(p) dp \\ &= \int_{\mathbb{R}^{dN}} \psi(p) \kappa(p) dp + \Delta t^2 \int_{\mathbb{R}^{dN}} \psi(p) \left(\int_{\mathcal{D}} \tilde{f}_2(q, p) \nu(q) dq \right) \kappa(p) dp + O(\Delta t^3), \end{aligned} \quad (3.25)$$

where we used the product form (1.8) for μ . Similarly,

$$\int_{\mathcal{E}} \psi(p) \kappa_{\Delta t, Q}(p) dp = \int_{\mathbb{R}^{dN}} \psi(p) \kappa(p) dp + \Delta t^2 \int_{\mathbb{R}^{dN}} \psi(p) \left(\int_{\mathcal{D}} f_2(q, p) \nu(q) dq \right) \kappa(p) dp + O(\Delta t^3), \quad (3.26)$$

so that

$$\begin{aligned} \int_{\mathcal{E}} \psi(p) (\kappa_{\Delta t, P}(p) - \kappa_{\Delta t, Q}(p)) dp &= \Delta t^2 \int_{\mathbb{R}^{dN}} \psi(p) \left(\int_{\mathcal{D}} (\tilde{f}_2(q, p) - f_2(q, p)) \nu(q) dq \right) \kappa(p) dp + O(\Delta t^3) \\ &= \frac{\Delta t^2}{8} \int_{\mathbb{R}^{dN}} \psi(p) \left(\int_{\mathcal{D}} (A + B) g(q, p) \nu(q) dq \right) \kappa(p) dp + O(\Delta t^3). \end{aligned}$$

Hence, using the expressions for f_2 and \tilde{f}_2 given in (3.10), at the level of densities it holds at dominant order in Δt that

$$\kappa_{\Delta t, P}(p) - \kappa_{\Delta t, Q}(p) = \frac{\Delta t^2 \kappa(p)}{8} \int_{\mathcal{D}} (A + B) g(q, p) \nu(q) dq + O(\Delta t^3).$$

The following proposition gives an alternative expression for this discrepancy term.

Proposition 6. *We have the following expression for the discrepancy term.*

$$\kappa_{\Delta t, P}(p) - \kappa_{\Delta t, Q}(p) = \frac{\Delta t^2}{8} \text{Tr} \left(\left((\beta M^{-1} p)^{\otimes 2} - \beta M^{-1} \right) \text{Cov}_{\nu}(\nabla V) \right) \kappa(p) + O(\Delta t^3). \quad (3.27)$$

Proof. We write:

$$(A + B)g(q, p)\nu(q) = \beta \left[(M^{-1}p) \cdot (\nabla^2 V(q) M^{-1}p) - (M^{-1}\nabla V(q)) \cdot \nabla V(q) \right] e^{-\beta V(q)}. \quad (3.28)$$

Setting $\tilde{p} = M^{-1}p$, we get

$$(A + B)g(q, M\tilde{p})\nu(q) = \beta \left[\tilde{p} \cdot (\nabla^2 V(q)\tilde{p}) - (M^{-1}\nabla V(q)) \cdot \nabla V(q) \right] e^{-\beta V(q)}. \quad (3.29)$$

This is a sum of terms of the form

$$T_{ij}(q, p) = \left[\beta \tilde{p}_i \tilde{p}_j \frac{\partial^2}{\partial q_i \partial q_j} V(q) - \beta M_{i,j}^{-1} \frac{\partial}{\partial q_i} V(q) \frac{\partial}{\partial q_j} V(q) \right] e^{-\beta V(q)}.$$

Upon integrating this term over \mathcal{D} , we can integrate the left-most term by parts (boundary terms cancel out by periodicity or by growth conditions on V), to obtain

$$\int_{\mathcal{D}} T_{ij}(q, p) dq = \int_{\mathcal{D}} \left[\beta^2 \tilde{p}_i \tilde{p}_j \frac{\partial}{\partial q_i} V(q) \frac{\partial}{\partial q_j} V(q) - \beta M_{i,j}^{-1} \frac{\partial}{\partial q_i} V(q) \frac{\partial}{\partial q_j} V(q) \right] e^{-\beta V(q)} dq.$$

Hence,

$$\int_{\mathcal{D}} T_{ij}(q, p) dq = (\beta^2 \tilde{p}_i \tilde{p}_j - \beta M_{i,j}^{-1}) \int_{\mathcal{D}} \frac{\partial}{\partial q_i} V(q) \frac{\partial}{\partial q_j} V(q) e^{-\beta V(q)} dq,$$

so that

$$\int_{\mathcal{D}} (A + B)g(q, p)\nu(q) \, dq = \sum_{i,j} (\beta^2 \tilde{p}_i \tilde{p}_j - \beta M_{i,j}^{-1}) \int_{\mathcal{D}} \frac{\partial}{\partial q_i} V(q) \frac{\partial}{\partial q_j} V(q) e^{-\beta V(q)} \, dq,$$

which we rewrite

$$\left((\beta M^{-1} p)^{\otimes 2} - \beta M^{-1} \right) : \int_{\mathcal{D}} (\nabla V \otimes \nabla V)(q) \nu(q) \, dq = \text{Tr} \left(\left((\beta M^{-1} p)^{\otimes 2} - \beta M^{-1} \right)^T \text{Cov}_{\nu}(\nabla V) \right), \quad (3.30)$$

using the fact that ∇V is a centered observable with respect to ν , and concluding the proof. \square

Remark 12. This expression for the discrepancy term is not particularly useful, however it does explain the behavior observed in [21]. In the case $d = N = \beta = M = 1$, it becomes,

$$\kappa_{\Delta t, P}(p) - \kappa_{\Delta t, Q}(p) = \frac{\Delta t^2}{8} (p^2 - 1) \text{Var}_{\nu}(V') \kappa(p) + O(\Delta t^3),$$

which is, up to a constant, the same correction term for any potential V . We plot this correction profile in figure 3.1. The shape of this profile explains the higher peak observed in $\kappa_{\Delta t, Q}$.

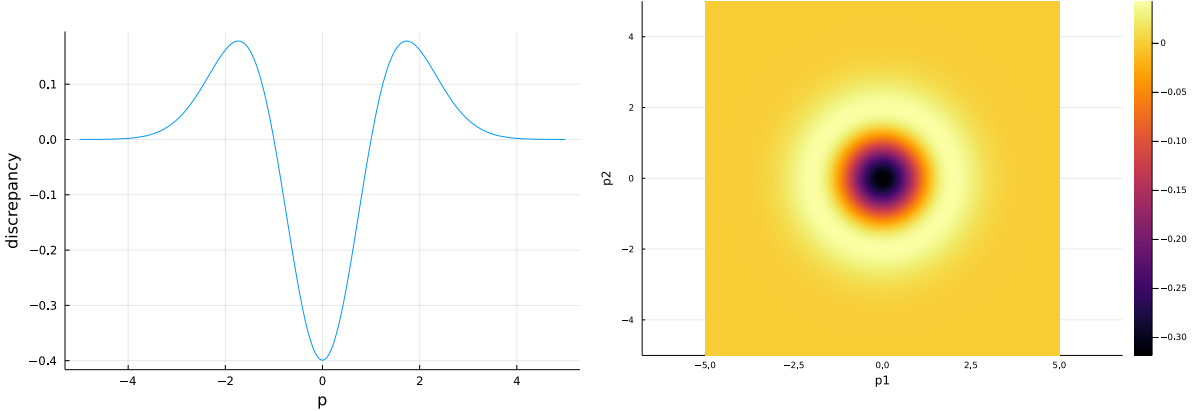


Figure 3.1: Profile of the discrepancy term in one and two dimension, in the case of identity covariances for ∇V .

3.6 Numerical results

We illustrate the results of the previous sections with numerical examples, on toy one dimensional systems.

- (i) In section 3.6.1, we define the potentials used for all the following experiments, and describe the sampling method used.
- (ii) In section 3.6.2, we verify numerically the relation (3.8).
- (iii) In section 3.6.3, we show that there is a significant discrepancy between the two kinetic marginal distributions. We also pinpoint the main, and possibly only source of this error, namely the γ -independent term (3.27).
- (iv) In section 3.6.4, we numerically verify that the first order behavior (3.13) is correct.
- (v) In section 3.6.5, we give an explicit example of an observable for which the BAOA scheme yields a bias of order Δt .
- (vi) Finally, in section 3.6.6, we show that the effect of the parameter γ is undetectable at the level of the kinetic marginals, motivating Conjecture 1.

3.6.1 Models

We take $\beta = 1$, $M = \text{Id}$, and consider four potentials:

- Periodic potential:

$$\mathcal{D} = (\mathbb{R}/\mathbb{Z}), V(q) = \sin(2\pi q),$$

- Quadratic potential:

$$\mathcal{D} = \mathbb{R}, V(q) = \alpha \frac{q^2}{2}, \alpha = 1,$$

- Double well potential:

$$\mathcal{D} = \mathbb{R}, V(q) = \alpha \frac{q^2}{2} + \beta e^{-\frac{q^2}{2\sigma^2}}, \alpha = 1, \beta = 4, \sigma = 0.5,$$

- Tilted double well potential:

$$\mathcal{D} = \mathbb{R}, V(q) = \alpha \frac{q^2}{2} + \gamma q + \beta e^{-\frac{q^2}{2\sigma^2}}, \alpha = 1, \beta = 4, \gamma = 1, \sigma = 0.5.$$

Analytically unknown normalizing constants and reference quantities were obtained through numerical integration of μ , using trapezoid rules with a mesh size of 10^{-6} . For unbounded coordinates, we truncated the domain to the interval $[-5, 5]$. Approximations of $\mu_{\Delta t, P}$, $\mu_{\Delta t, Q}$ were computed by recording the states of 10,000 independently evolving trajectories over 2×10^6 timesteps in a 1000×1000 two-dimensional histogram on the truncated domain. The rare sample points outside of the truncated domain were discarded.

3.6.2 Equality of marginal configurational distributions

On Figures 3.2 and 3.3, we numerically verify the equality (3.8) between the configurational marginal distributions $\nu_{\Delta t, Q}$ and $\nu_{\Delta t, P}$, which holds for any Δt . This point was demonstrated in [21].

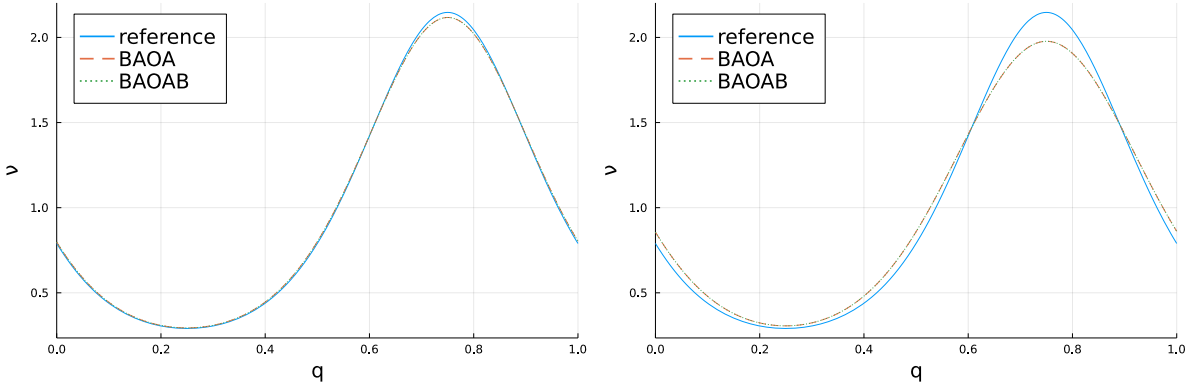


Figure 3.2: Marginal configurational distributions for the periodic potential. Left: $\Delta t = 0.1$. Right: $\Delta t = 0.2$. Even for large timesteps, the distributions perfectly coincide.

3.6.3 Comparison of marginal kinetic distributions

We observe, as in [21], that the kinetic marginal distribution $\kappa_{\Delta t, Q}$ departs from the reference at a faster rate than $\kappa_{\Delta t, P}$, and more precisely appears to underestimate the variance, leading to a sharper distribution. Additionally we observe that removing the part of the bias on BAOAB due to the discrepancy term (3.27) leads to a significant improvement. These corrected marginals are plotted under the label "correction". See Figures 3.4 and 3.5.

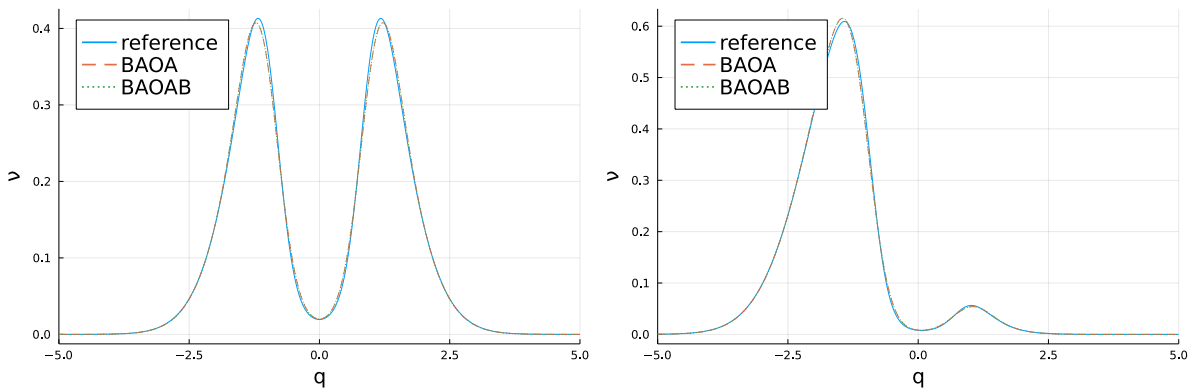


Figure 3.3: Marginal configurational distributions for $\Delta t = 0.4$. Left: double well potential. Right: tilted double well potential.

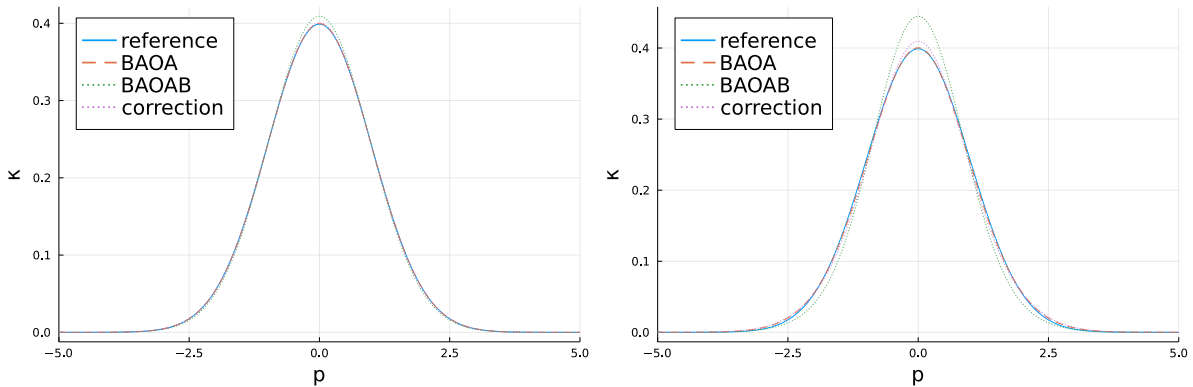


Figure 3.4: Marginal kinetic distributions for the periodic potential. Left: $\Delta t = 0.1$. Right: $\Delta t = 0.2$.

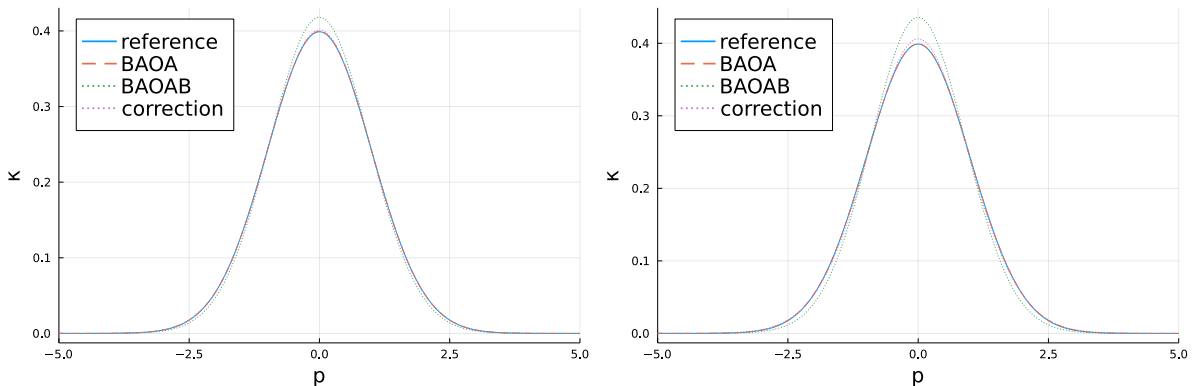


Figure 3.5: Marginal kinetic distributions for the double well potential. Left: $\Delta t = 0.3$. Right: $\Delta t = 0.4$.

3.6.4 Verification of the first-order expansion

We verify the correctness first-order expansion of $\mu_{\Delta,P}$ obtained in (3.13), by comparing the joint distributions obtained from Monte-Carlo simulations with a reference calculation of the first-order expansion for $\mu_{\Delta t,P}$. Additionally, we plot the empirical estimate of $\mu_{\Delta t,Q}$ and μ . The plots show joint likelihoods as a function of the state, using a color mapping. Empirical joint distributions for BAOA and BAOAB trajectories are plotted on the top row of each figure. On the bottom row, a reference computation of μ is plotted on the right, as well as a reference computation of

$$\left(1 + \frac{\Delta t}{2} g\right) \mu$$

on the left. The results visually confirm our result, while suggesting that, as a whole, $\mu_{\Delta t,Q}$ is the superior approximation of μ . See Figures 3.6, 3.7 and 3.8.

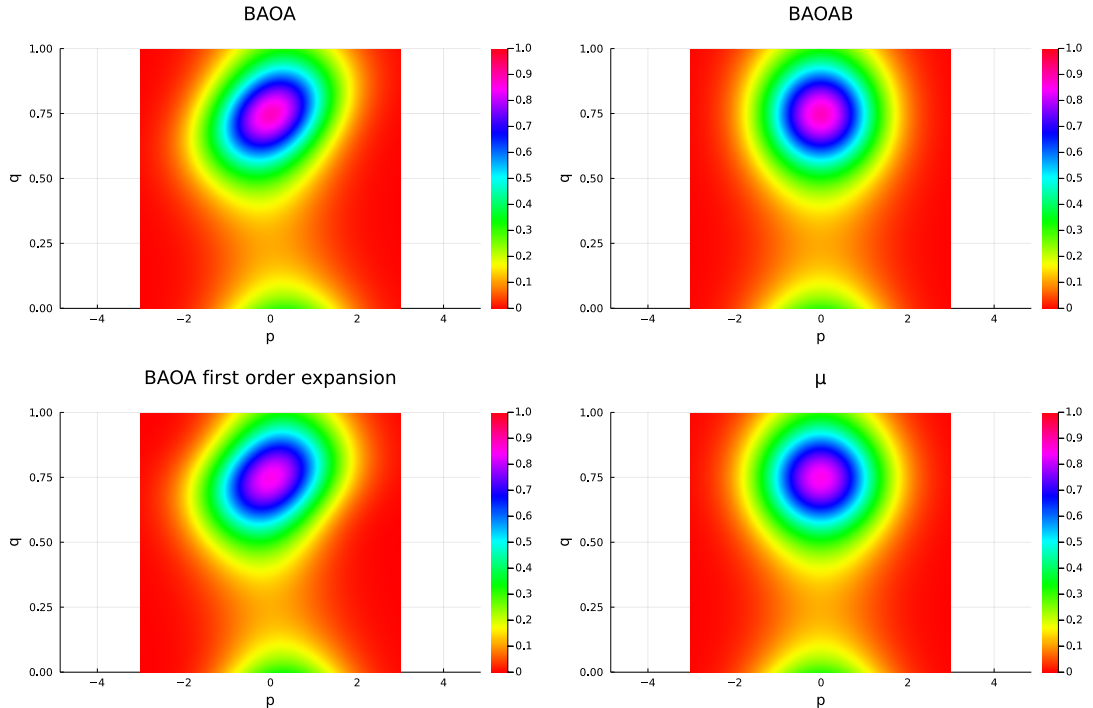


Figure 3.6: Joint distributions for the periodic potential, $\Delta t = 0.1$.

3.6.5 Example of first-order bias in a BAOA average

We demonstrate that for certain observables, BAOA is drastically outperformed by BAOAB, by calculating the average of g for increasing timesteps. Note by (3.15), the true average is 0. Figures 3.9 and 3.10 show the estimated averages as a function of the timestep on the left, and the same data on a log-log plot on the right. The order of the error on the BAOAB averages suggest that the second order error term

$$\int_{\mathcal{E}} g f_2 \, d\mu$$

given in (3.9) cancels out for this specific observable, yielding a fourth-order bias in Δt for BAOAB averages of g .

3.6.6 Effect of the friction parameter

All experiments shown above used a value of $\gamma = 1$ for the friction parameter. In this final experiment, we examine the effect of changing γ . We show the marginal kinetic distributions for three values of $\gamma \in \{0.1, 1, 10\}$. The results show that there is no visually discernable effect of the parameter γ : all

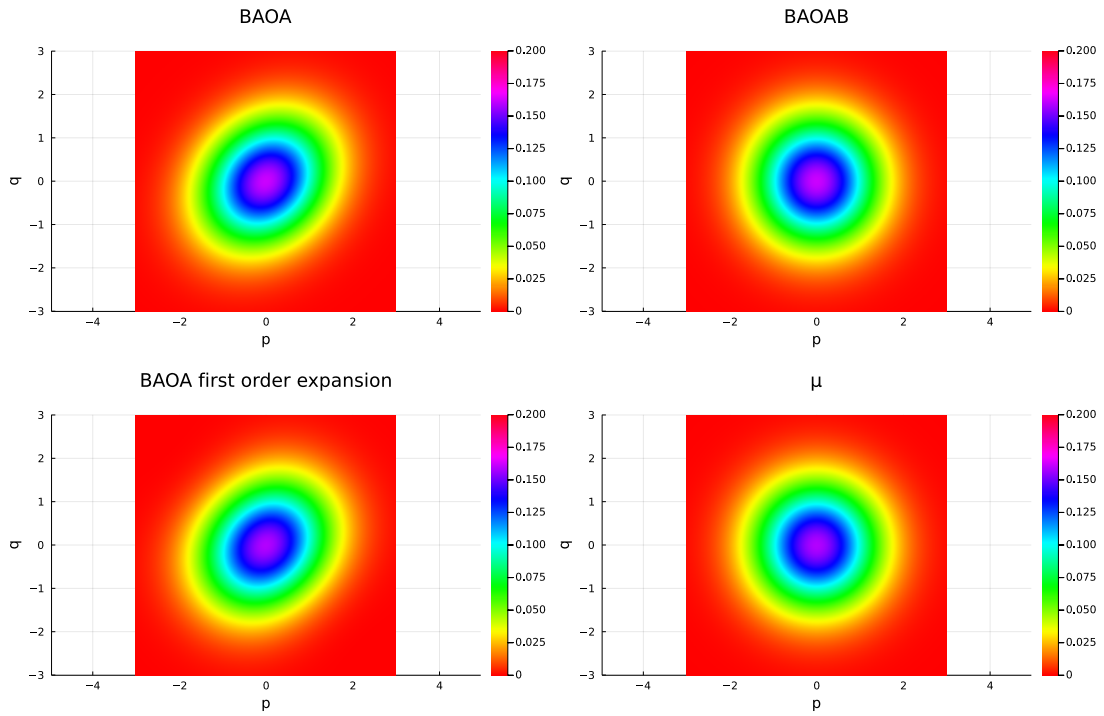


Figure 3.7: Joint distributions for the quadratic potential, $\Delta t = 0.4$.

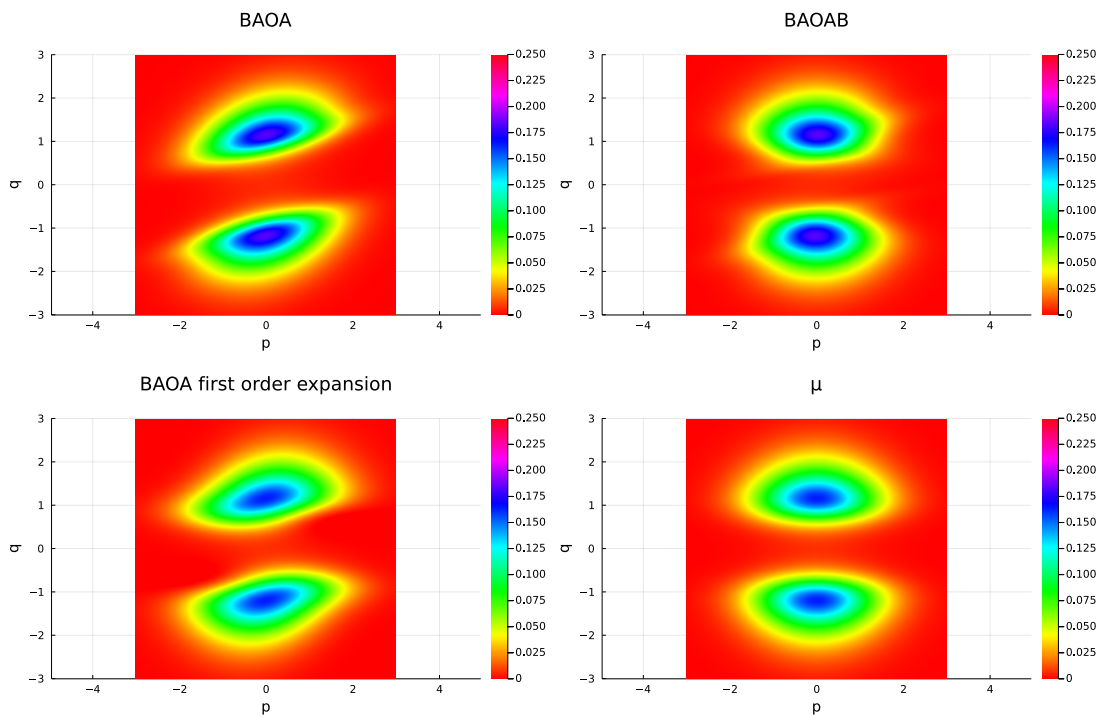


Figure 3.8: Joint distributions for the double well potential, $\Delta t = 0.4$.

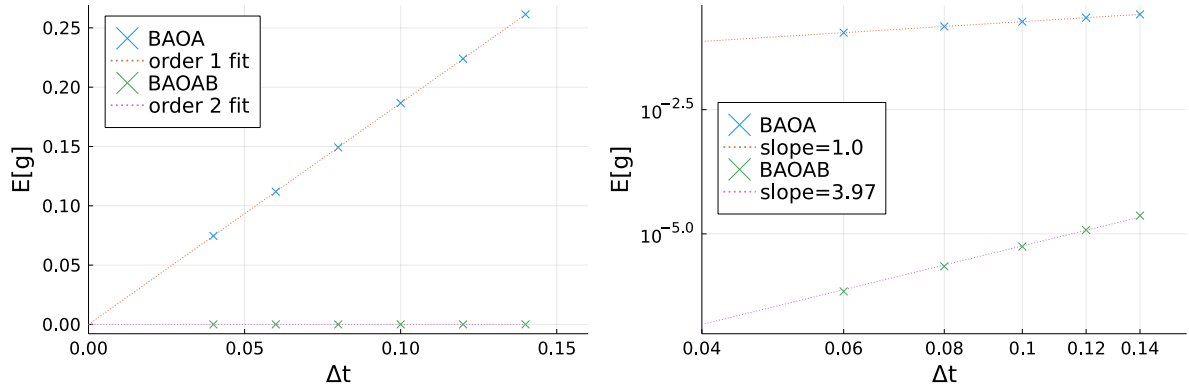


Figure 3.9: Averages of g for the double well potential.

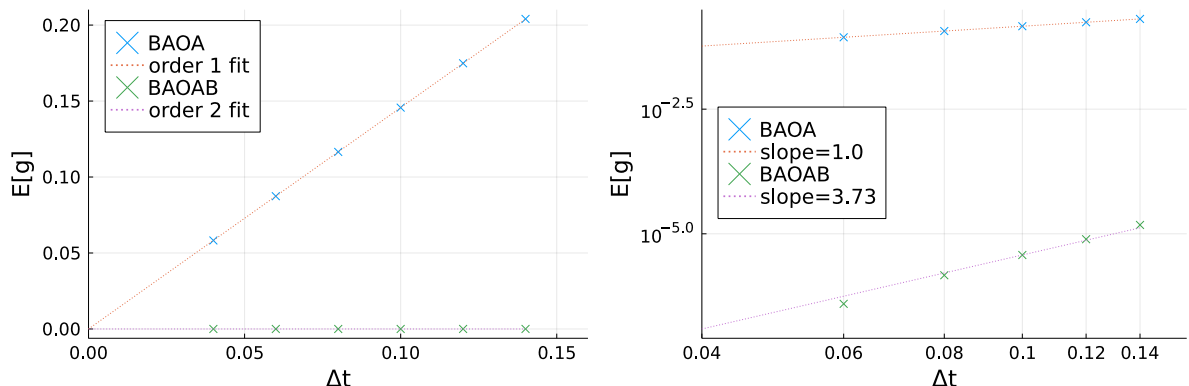


Figure 3.10: Averages of g for the tilted double well potential.

$\kappa_{\Delta t, PS}$ are superposed close to the reference curve, and all $\kappa_{\Delta t, Q}$ s are superposed above. This suggest that most of the error on $\kappa_{\Delta t, Q}$ arises from the additional term

$$-\frac{\Delta t^2}{8} \int_{\mathcal{E}} \varphi(A + B) g \, d\mu,$$

which is the dominant discrepancy term in (3.27), and which is independent of γ . This is the fact we observed numerically on Figures 3.5 and 3.4. See Figure 3.11.

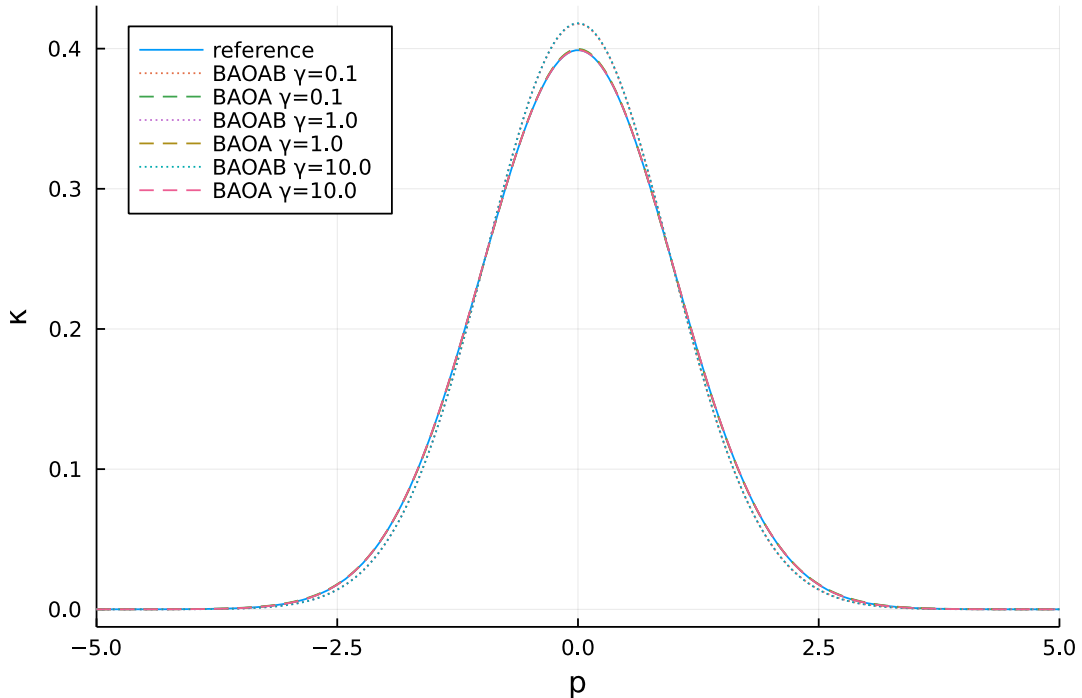


Figure 3.11: Kinetic marginal distributions for $\Delta t = 0.3$ on the double well potential.

Chapter 4

Non-equilibrium Molecular Dynamics

So far, we have only considered methods to sample static averages, which concern quantities at thermodynamic equilibrium. Such techniques yield information about the bulk macroscopic properties of the system, for which there is no discernable macroscopic evolution. We now turn to the next natural question, which is to consider systems in which there is such an evolution, which typically arises from a perturbation of the equilibrium dynamics, either by the introduction of a non-gradient forcing term, or a modification of the fluctuation-dissipation part for which the fluctuation-dissipation relation (2.26) is not satisfied. We will not consider the latter case, which is relevant for instance to the modelling of heat transport within an atomic system, to concentrate on the first case. In general, systems undergoing such a perturbation of the dynamics will reach a new steady state in which there is a net flux in some observable. Mathematically, this translates into the existence of a response observable R which has zero average with respect to the canonical measure μ , but which has a non-zero average with respect to the perturbation steady-state. A natural question is that of the sensitivity of the system to the perturbation: one way to quantify this is to modulate the strength of the perturbation by a positive real parameter $\eta > 0$, and, assuming that the average response is asymptotically linear as $\eta \rightarrow 0$, to compute the linear coefficient linking η and the average response. This quantity is called a *transport coefficient*, and we will dedicate the next two chapters to different methods of computing them using molecular simulation. We consider the most natural method, which is to directly apply a forcing term which does not arise from a potential. The mathematical translation of this idea is a Langevin dynamics with an additional non-gradient forcing term. We start by presenting the general framework of non-equilibrium molecular dynamics (NEMD), the numerical methods we implemented, and the examples of shear viscosity and mobility. We illustrate these examples with numerical results. We then turn to discussing the Green–Kubo method, which allows for the computation of transport coefficients from equilibrium simulations, before applying it to the same examples as in the previous section.

4.1 Non-equilibrium molecular dynamics

4.1.1 General framework

We consider the following modified Langevin dynamics:

$$\begin{cases} dq_t = M^{-1} p_t dt, \\ dp_t = -\nabla V(q_t) dt - \gamma M^{-1} p_t dt + \sqrt{\frac{2\gamma}{\beta}} dW_t + \eta F(q_t) dt, \end{cases} \quad (4.1)$$

perturbed by the configuration-dependent forcing term F , and where the strength of the perturbation is modulated by the parameter $\eta > 0$. Its generator is given by the operator

$$\mathcal{L}_{\gamma,F} = \mathcal{L}_\gamma + \eta F \cdot \nabla_p = \mathcal{L}_\gamma + \eta \tilde{\mathcal{L}}. \quad (4.2)$$

It is also possible to consider non-equilibrium generalized Langevin equations, which are analogous perturbations of (2.16). Given a response of interest R , the transport coefficient is given by the following definition:

$$\rho_{R,F} = \lim_{\eta \rightarrow 0} \frac{\mathbb{E}_\eta[R]}{\eta}, \quad (4.3)$$

where \mathbb{E}_η denotes the expectation with respect to the steady-state probability distribution. If the context makes R clear from the knowledge of F , we will drop it from the notation and simply write ρ_F for the transport coefficient. For this definition to make sense, one has to show that the steady-state with respect to which we take the expectation is well-defined. Since the steady-state is defined by the fact that it is invariant with respect to the dynamics (4.1), this translates into the fact that it is the solution to a stationary Fokker-Planck equation, in the sense of distributions:

$$(\mathcal{L}_\gamma + \eta \tilde{\mathcal{L}})^\dagger \psi_\eta = 0, \quad (4.4)$$

where ψ_η is the steady state measure. Using analytic properties of $\mathcal{L}_{\gamma,F}$ (such as hypoellipticity), one can hope to infer regularity results of its solutions, such as the existence of a smooth density. Existence of the steady-state can hopefully be obtained using Lyapunov techniques. The steady-state measure \mathbb{E}_η is a high-dimensional measure on phase space for which a closed form is generally unavailable. Thus, as usual, one has to resort to ergodic averages under the dynamics (4.1) to compute ensemble averages. This poses another theoretical difficulty, that of showing that the steady-state measure is ergodic, although in principle, uniqueness and ergodicity in the sense of convergence of averages can in principle be recovered following Klieman's method [22].

In fact, for our purposes, F will always be L -periodic, and so we can invoke a special case of Proposition 1 in [19] with time-constant forcings, provided V and F are smooth.

Theorem 3 (Existence of a unique ergodic measure with smooth density). *Let $\eta_* > 0$. For all $\eta \in [-\eta_*, \eta_*]$, the Fokker-Planck equation (4.4) admits a unique solution with a C^∞ density ψ_η . Additionally, the evolution semigroup decays exponentially in a Lyapunov sense: for all $n \geq 1$, there exist $C_n, \lambda_n > 0$ such that*

$$\|e^{t\mathcal{L}_{\gamma,F}} \varphi - \mathbb{E}_\eta[\varphi]\|_{B^\infty(\mathcal{E})} \leq C_n e^{-\lambda_n t} \|\varphi\|_{B_{\mathcal{K}_n}^\infty}, \quad (4.5)$$

where we define the Lyapunov weight functions

$$\mathcal{K}_n(q, p) = 1 + |p|^{2n},$$

and the corresponding B^∞ weighted spaces of bounded functions by the norm

$$\|f\|_{B_{\mathcal{K}_n}^\infty} = \sup \left| \frac{f}{\mathcal{K}_n} \right|.$$

Because of the continuous injections $B^\infty \subset B_{\mathcal{K}_n}^\infty$, this result implies in particular that the operator $(-\mathcal{L}_{\gamma,F})^{-1}$ is well-defined on

$$B_{\mathcal{K}_n,0}^\infty = \{f \in B_{\mathcal{K}_n}^\infty \mid \mathbb{E}_\eta[f] = 0\},$$

with an inverse given by the formula (2.37). Proposition 2 from the same papers also gives the almost-sure convergence of ergodic averages.

Remark 13 (Size of the linear regime). *As $\eta \rightarrow 0$, it is reasonable to expect that the statistical error in ergodic averages for $\mathbb{E}_\eta[R]$ arise at dominant order in η from the asymptotic variance at equilibrium σ_R^2 in (2.38). In particular the finite difference estimator for $\rho_{R,F}$*

$$\frac{\mathbb{E}_\eta[R]}{\eta} \quad (4.6)$$

has, for a fixed simulation time, a variance which scales like $\frac{1}{\eta^2}$ as $\eta \rightarrow 0$. To achieve an acceptable statistical error at minimal cost, one should thus aim to take η as large as possible. On the other hand, if the perturbation is too large, then non-linear effects on R will be observed and (4.6) will give a poor estimation of the transport coefficient. Thus, if one manages to devise another forcing \tilde{F} which does not change the steady-state, but which extends the range of linearity of the response, it may be very beneficial to do so from a computational standpoint. These kinds of methods, sometimes called synthetic forcings, are an area of ongoing research. See for example [8, Section 6.1] for an introduction to these ideas.

4.1.2 Numerical implementation

To integrate the perturbed dynamics, we again rely on a splitting strategy. We split the dynamics into elementary evolutions, whose respective evolution semigroups are given analogously to (2.40). The only difference is in the additional ηF term, which we incorporate into the B step, yielding a $B_{\eta F}$ step, which corresponds to the evolution semigroup

$$e^{tB_{\eta F}}\varphi(q,p) = \varphi(q, p - t[\nabla V(q) - \eta F(q)]). \quad (4.7)$$

Note it would also have been possible to incorporate the forcing term into the Ornstein–Uhlenbeck part of the dynamics, which then corresponds to an Ornstein–Uhlenbeck process with constant drift. However, we will always choose the method described above. We will use the same terminology for these methods, referring to the scheme with evolution operator

$$e^{\frac{\Delta t}{2}B_{\eta F}}e^{\frac{\Delta t}{A}}e^{\Delta t\gamma C}e^{\frac{\Delta t}{2}A}e^{\frac{\Delta t}{2}B_{\eta F}} \quad (4.8)$$

as the BAOAB scheme, for example. Numerical estimates for $\mathbb{E}_\eta[R]$ are then obtained through

$$\widehat{R}_{\eta, N_{\text{iter}}} = \frac{1}{N_{\text{iter}}} \sum_{n=0}^{N_{\text{iter}}-1} R(q^n, p^n), \quad (4.9)$$

where $(q^n, p^n)_{n \geq 0}$ denotes the numerical trajectory under the Markov chain obtained for a chosen splitting of the non-equilibrium dynamics (4.1). To estimate the transport coefficient, we fix different forcing intensities

$$0 < \eta_1 < \dots < \eta_k, \quad \eta := (\eta_i)_{1 \leq i \leq k}$$

all in the linear response regime, and given corresponding estimators

$$\widehat{R} := (\widehat{R}_i)_{1 \leq i \leq k}$$

of the form (4.9), we estimate ρ_F by a least squares linear fit

$$\widehat{\rho}_F = |\eta|^{-2}\eta \cdot \widehat{R} = \operatorname{argmin}_{\rho \in \mathbb{R}} \left| \rho\eta - \widehat{R} \right|^2. \quad (4.10)$$

Note the case $k = 1$ corresponds to the finite difference estimator (4.6). Note that the variance of this estimator is likely to be much smaller than for the latter estimator. In fact, provided $|\eta|^2 \geq 1$, the pitfall of the NEMD technique mentioned in Remark 13 is completely avoided. Indeed, assume that each \widehat{R}_i is an ergodic estimator simulated with $N_{i,\text{iter}}$ timesteps, say

$$\widehat{R}_i = \frac{S_i}{\eta_i N_{i,\text{iter}}}.$$

We assume that the asymptotic regime is reached, thus we may assume that \widehat{R}_i is Gaussian with variance

$$\frac{\sigma_i^2}{\eta_i^2 N_{i,\text{iter}}},$$

where σ_i^2 is the asymptotic variance associated with the ergodic mean $S_i/N_{i,\text{iter}}$. Thus,

$$\operatorname{Var}(\widehat{\rho}_F) = |\eta|^{-4} \sum_{i=1}^k \frac{\sigma_i^2}{\eta_i^2 N_{i,\text{iter}}}. \quad (4.11)$$

If we make the approximation $\sigma_i^2 \approx \sigma_R^2$, which is good at first order in η , and assume $N_{i,\text{iter}} \geq N_{\text{iter}}$, we can estimate an upper bound on the variance,

$$\operatorname{Var}(\widehat{\rho}_F) \lesssim \frac{\sigma_R^2}{|\eta|^2 N_{\text{iter}}}.$$

4.1.3 Mobility

As a first and simplest example, we introduce a method for computing the mobility. In this case the forcing is simply a constant vector, and the response is velocity in the direction F , which we may think of as the particle flux through the hyperplane orthogonal to F . The transport coefficient corresponding to the forcing

$$F \in \mathbb{R}^{dN}, \quad R(q, p) = F \cdot M^{-1}p \quad (4.12)$$

is called the mobility. Let us assume once and for all that $|F|^2 = 1$. For practical computations, we will be considering two cases:

- (i) **Single drift**: this corresponds to a perturbation where the force acts on a single component of the momentum, which we can assume by indistinguishability of the particles to be the x component of the first particle:

$$F_S = (1, 0, \dots)^\top \in \mathbb{R}^{dN}.$$

- (ii) **Color drift** [8, Chapter 6]: this corresponds to a perturbation in which we the force acts on half of the particles in one direction, and on half of the particles in the opposite direction. By isotropy, we may assume this direction is the x direction:

$$F_C = \frac{1}{\sqrt{N}} \underbrace{(1, 0, \dots,}_{d \text{ components}} -1, 0, \dots, 1, 0 \dots)^\top \in \mathbb{R}^{dN}.$$

The color drift method derive its name from the fact that it divides the particles into two categories: the particles with a positive color charge (corresponding to those whose x -component of momentum see a positive force contribution from F), and those with a negative color charge. The equations of motion are analogous to a system of charged particles under a constant electric field, but where the charges do not interact between themselves. Intuitively, we expect the color drift method to be more computationally effective than the single drift method, since the latter should give essentially equilibrium dynamics for the majority of particles outside of the first particle's sphere of influence. On the other hand, the normalization condition implies that the forcing is more dilute in the color drift case, which may make the response more difficult to measure. In fact, numerical evidence presented below shows that the two effects roughly compensate one another.

In order for the two methods to be useful, we need to be able to relate them to a shared dynamical property of the considered system. This is more conveniently done upon reformulating the linear response in terms of integrated autocorrelation functions, a point we postpone to the next section. For now, let us show a few numerical results. In order to compare different methods, we fix a thermodynamical condition, which we give in reduced units below.

$$T = 1.25, \quad \rho = 0.6, \quad \gamma = 1.0, \quad N = 1000. \quad (4.13)$$

Let us also mention here that all simulations for mobility were performed using a BAOAB splitting, a timestep $\Delta t = 10^{-3}$ and a linearly corrected potential with cutoff at distance $r_c = 2.5$. In Figure 4.1, we plot the response profile as a function of the forcing intensity. It appears that the linear response regime is longer for the color drift method. Estimates of ρ_F seem to roughly agree, although we expect a small discrepancy (see Example 5). However this effect should not be detectable because of the persistency of statistical noise.

Estimating the transport coefficients using (4.9) and the variance through (4.11), we obtain

$$\rho_{F_S} = 0.12204 \pm 0.0009, \quad \rho_{F_C} = 0.12128 \pm 0.0009, \quad (4.14)$$

where \pm denotes one standard deviation.

4.1.4 Shear viscosity

As a second example, we discuss the transverse force field method to compute the shear viscosity. The idea was originally introduced in [14], although we base our presentation on the more recent article [20]. We refer to this paper for thorough statements and proofs. Let us assume for notational simplicity that $M = m\text{Id}$. We consider a case of the dynamics (4.1) with a forcing which acts on the longitudinal (x)

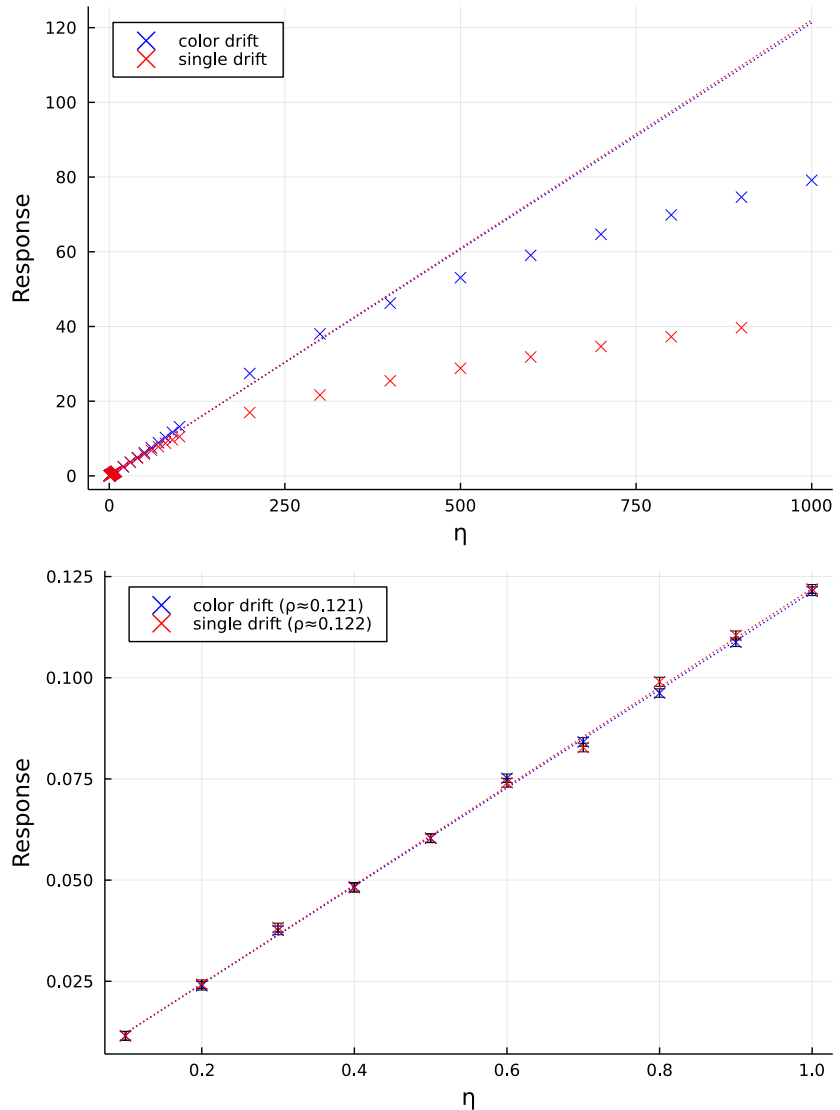


Figure 4.1: Average mobility response against forcing intensity for the Lennard-Jones system (4.13). Extrapolations of the linear response are plotted in dotted lines.

momenta, and is dependent on the transverse (y) positions. More precisely, we fix a reference periodic function $F_y : L\mathbb{T} \rightarrow \mathbb{R}$, and index the state as

$$(q_{i\alpha})_{\substack{1 \leq i \leq N \\ 1 \leq \alpha \leq d}}, \quad (p_{i\alpha})_{\substack{1 \leq i \leq N \\ 1 \leq \alpha \leq d}}.$$

The non-equilibrium dynamics is defined by the following expression for F :

$$\forall 1 \leq i \leq N, \forall 2 \leq \alpha \leq d, \quad F(q)_{i1} = f_y(q_{i2}), \quad F(q)_{i\alpha} = 0. \quad (4.15)$$

The idea is that by imposing a forcing *profile* in the x -direction, we observe a velocity profile in response, which depends on the y -coordinate.

Remark 14 (Anisotropic friction). *In fact the precise model considered in [20] also imposes a separate friction coefficient γ_x for the longitudinal fluctuation-dissipation part of the dynamics. This can be interpreted as a simple case of a generalized Langevin dynamics where the friction coefficient γ is an anisotropic diagonal matrix, which does not pose any difficulties from the theoretical point of view. We therefore restrict our attention to the case where γ is scalar.*

In order to make precise the response of the system, we define

$$u_x(Y) := \lim_{\varepsilon \rightarrow 0} \lim_{\eta \rightarrow 0} \frac{L_y \mathbb{E}_\eta \left[\sum_{i=1}^N p_{i1} \chi_\varepsilon(q_{i2} - Y) \right]}{\eta m N} \quad (4.16)$$

to be the linear response profile in the longitudinal velocity, where $(\chi_\varepsilon)_{\varepsilon > 0}$ is an approximation to the identity (that is a sequence of smooth compactly supported test functions which converge to the Dirac delta function in the sense of distributions). In practice, u_x can be estimated from numerical trajectories by decomposing the domain \mathcal{D} in a finite number of transverse slices, and measuring the average longitudinal velocity in each of these slices. The shear viscosity σ is then defined by the differential equation

$$-\sigma u''_x(Y) + \gamma \rho u_x(Y) = \rho f_y(Y), \quad (4.17)$$

where $\rho = N/L^3$ is the particle density. In fact, the solutions to (4.17) are periodic, thus the magnitude of the linear response can be estimated from its Fourier coefficients. Indeed, writing

$$c_k(h) = \frac{1}{L} \int_0^L h(s) \exp\left(\frac{2ik\pi s}{L}\right) ds \quad (4.18)$$

for the k -th Fourier coefficient of a L -periodic function h , applying c_k to (4.17) gives

$$\begin{aligned} -\sigma c_k(u''_x) + \gamma \rho c_k(u_x) &= \rho c_k(f_y), \\ (\sigma (2k\pi/L)^2 + \gamma \rho) c_k(u_x) &= \rho c_k(f_y), \\ \sigma &= \rho \left(\frac{c_k(f_y)}{c_k(u_x)} - \gamma \right) \left(\frac{L}{2k\pi} \right)^2 \end{aligned} \quad (4.19)$$

using $c_k(h'') = -(2k\pi/L)^2 c_k(h)$ in the second line. The Fourier coefficient $c_k(u_x)$ can then be estimated directly from trajectory averages. this has the advantage of giving an estimation of the linear response in the general framework defined above, and avoiding the discretization error arising from the finite number of transverse slices. To this effect, we define the response observables as empirical Fourier coefficients:

$$R_k(q, p) = \frac{1}{N} \sum_{i=1}^N \frac{p_{i1}}{m} \exp\left(\frac{2ik\pi q_{i2}}{L}\right), \quad (4.20)$$

and the corresponding transport coefficients

$$\rho_{F,k} = \lim_{\eta \rightarrow 0} \frac{\mathbb{E}_\eta[R_k(q, p)]}{\eta}. \quad (4.21)$$

It is easy to show that for the sinusoidal forcing, the response velocity profile, solution to (4.17), is still sinusoidal, so that the Fourier response is a meaningful measure of the magnitude of the response in the velocity profile. In practice, it is sufficient to consider $k = 1$.

f_y	Sinusoidal	Piecewise constant	Piecewise linear
$c_1(f_y)$	$i/2$	$2i/\pi$	$-4/\pi^2$

Figure 4.2: First Fourier coefficients for transverse forcing profiles.

Remark 15. To obtain better statistics, one may for the purpose of numerical simulations want to consider a periodic domain whose unit cell is still a cuboid, but with a side length in the longitudinal direction that is longer than in the transverse direction. In this case we simply replace L by L_y in the response observables, where L_y is the length of the unit cell in the transverse direction.

The shear viscosity can then be computed from equation (4.19), through

$$\sigma = \rho \left(\frac{c_k(f_y)}{\rho_{F,k}} - \gamma \right) \left(\frac{L}{2k\pi} \right)^2, \quad (4.22)$$

again only considering $k = 1$ in practice. Numerically, $\rho_{F,k}$ can be approximated by an estimator of the form (4.10). In our numerical experiments, we consider the same three forcing profiles as in [20], namely:

(i) A sinusoidal forcing profile

$$f_y(u) = \sin \left(\frac{2\pi u}{L} \right),$$

(ii) a piecewise constant forcing profile

$$f_y(u) = \mathbb{1}_{u < \frac{L}{2}} - \mathbb{1}_{u \geq \frac{L}{2}},$$

(iii) and a piecewise linear forcing profile

$$f_y(u) = \frac{4}{L} \left(u - \frac{L}{4} \right) \mathbb{1}_{u < \frac{L}{2}} - \frac{4}{L} \left(\frac{3L}{4} - u \right) \mathbb{1}_{u \geq \frac{L}{2}}.$$

These forcings have the advantage that the Fourier coefficients can be analytically computed. We record in Figure 4.2 the value of the first Fourier coefficient F_1 for each of these forcings. As in the case of mobility, we fix a reference thermodynamic condition,

$$T = 0.8, \quad \rho = 0.7, \quad \gamma = 1.0, \quad N = 1000. \quad (4.23)$$

4.2 The Green–Kubo method

An alternative route to the perturbation method described above leverages a famous expression for the transport coefficient in terms of an integrated correlation function, or, in less technical language, in terms of the fluctuations at equilibrium of the response observable. This is the Green–Kubo method, which we describe in this section. We consider the invariant measure for the non-equilibrium dynamics (4.1). By Theorem 3, there exists a unique invariant measure with density ψ_η . For notational consistency, let us write ψ_0 for the density of the equilibrium measure μ . Then the following result holds.

Theorem 4 (Series expansion for the non-equilibrium steady state). *There exists $r > 0$ such that for all $0 < \eta < r$,*

$$\frac{\psi_\eta}{\psi_0} = \left(1 + \eta (\tilde{\mathcal{L}} \Pi \mathcal{L}_\gamma^{-1} \Pi)^* \right)^{-1} \mathbb{1}_{\mathcal{E}} = \left(1 + \sum_{k=1}^{\infty} (-\eta)^k \left[(\tilde{\mathcal{L}} \Pi \mathcal{L}_\gamma^{-1} \Pi)^* \right]^k \right) \mathbb{1}_{\mathcal{E}}, \quad (4.24)$$

where $\tilde{\mathcal{L}}$ is defined by (4.2), Π is the equilibrium centering projector defined in (2.34), and adjoints are taken in $L^2(\mu)$.

Sketch of proof. The second equality identifies the Neumann series on the right as the resolvent of $1 + (\tilde{\mathcal{L}}\Pi\mathcal{L}_\gamma^{-1}\Pi)^*$, provided η is taken small enough. In fact, from the spectral theory of bounded operators, r can be determined as the spectral radius of $(\tilde{\mathcal{L}}\Pi\mathcal{L}_\gamma^{-1}\Pi)^*$ in the space of bounded operators $\mathcal{B}(L_0^2(\mu))$. The core of the argument lies in making the ansatz

$$\psi_\eta = \psi_0(1 + \eta f_1 + \eta^2 f_2 + \dots). \quad (4.25)$$

The stationary Fokker-Planck equation (4.4) writes

$$(\mathcal{L}_\gamma + \eta \tilde{\mathcal{L}})^\dagger \psi_0(1 + \eta f_1 + \eta^2 f_2 + \dots) = (\mathcal{L}_\gamma + \eta \tilde{\mathcal{L}})^*(1 + \eta f_1 + \eta^2 f_2 + \dots) = 0.$$

Indeed, for an arbitrary test function φ ,

$$\begin{aligned} \int (\mathcal{L}_\gamma + \eta \tilde{\mathcal{L}}) \varphi \psi_\eta &= 0 \\ &= \int [(\mathcal{L}_\gamma + \eta \tilde{\mathcal{L}}) \varphi] (1 + \eta f_1 + \eta^2 f_2 + \dots) d\mu \\ &= \int \varphi [(\mathcal{L}_\gamma + \eta \tilde{\mathcal{L}})^* (1 + \eta f_1 + \eta^2 f_2 + \dots)] d\mu. \end{aligned}$$

By formally identifying terms of the same degree in η , we obtain

$$\begin{aligned} \mathcal{L}_\gamma^* \mathbb{1}_{\mathcal{E}} &= 0, \\ \tilde{\mathcal{L}}^* \mathbb{1}_{\mathcal{E}} + \mathcal{L}_\gamma^* f_1 &= 0, \\ \tilde{\mathcal{L}}^* f_1 + \mathcal{L}_\gamma^* f_2 &= 0, \end{aligned}$$

and so on. Note that the first equality is the equilibrium Fokker-Planck equation. Thus, by induction, again formally, we obtain.

$$\begin{aligned} f_1 &= (-\mathcal{L}_\gamma^*)^{-1} \tilde{\mathcal{L}}^* \mathbb{1}_{\mathcal{E}}, \\ f_2 &= (-\mathcal{L}_\gamma^*)^{-1} \tilde{\mathcal{L}}^* f_1, \\ &\dots \\ f_n &= [(-\mathcal{L}_\gamma^*)^{-1} \tilde{\mathcal{L}}^*]^n \mathbb{1}_{\mathcal{E}}, \end{aligned}$$

whence the formal proof follows, by observing that we can write

$$(-\mathcal{L}_\gamma^*)^{-1} \tilde{\mathcal{L}}^* = -(\tilde{\mathcal{L}}\Pi\mathcal{L}_\gamma^{-1}\Pi)^*.$$

For a rigorous proof, several points should be made precise:

- (i) The convergence of the series (4.24) for sufficiently small η , which can be obtained by showing the boundedness of the operator $(\tilde{\mathcal{L}}\Pi\mathcal{L}_\gamma^{-1}\Pi)^*$ on $L_0(\mu)$.
- (ii) The fact that $\psi_0(1 + \eta(\tilde{\mathcal{L}}\Pi\mathcal{L}_\gamma^{-1}\Pi)^*)^{-1} \mathbb{1}_{\mathcal{E}}$ is indeed a solution to the stationary Fokker-Planck equation, and that it is indeed a probability density. This is done by showing that it is a positive function.

One can then conclude by uniqueness of the steady-state probability measure. \square

The linear response can be read off directly from the first term of the series expansion.

Corollary 4 (Green-Kubo formula). *Let R be any response observable such that $\mathbb{E}_\mu[R] = 0$, and $R \in L_{\mathcal{K}_n}^\infty$ for some n . Then we have the following formula for the linear response*

$$\lim_{\eta \rightarrow 0} \frac{\mathbb{E}_\eta[R]}{\eta} = \int_0^\infty \mathbb{E}_\mu[R(q_t, p_t) S(q_0, p_0)] dt, \quad (4.26)$$

where the expectation on the right hand side is with respect to all equilibrium dynamics trajectories with canonical initial distribution, and S is defined by

$$S = \tilde{\mathcal{L}}^* \mathbb{1}_{\mathcal{E}} = \beta F(q) \cdot M^{-1} p, \quad (4.27)$$

and is called the conjugate response function.

The latter expression follows from a simple integration by parts.

Proof. By Theorem 4, we can write

$$\begin{aligned} \lim_{\eta \rightarrow 0} \frac{\mathbb{E}_\eta[R]}{\eta} &= \int_{\mathcal{E}} R(q, p) \left((-\mathcal{L}_\gamma^*)^{-1} \tilde{\mathcal{L}}^* \mathbb{1}_{\mathcal{E}} \right) (q, p) \psi_0(q, p) dq dp \\ &= \int_{\mathcal{E}} [(-\mathcal{L}_\gamma)^{-1} R] (q, p) S(q, p) \psi_0(q, p) dq dp \\ &= \int_{\mathcal{E}} \int_0^\infty \mathbb{E}^{(q,p)} [R(q_t, p_t) S(q_0, p_0)] \psi_0(q, p) dt dq dp \\ &= \int_0^\infty \mathbb{E}_\mu [R(q_t, p_t) S(q_0, p_0)] dt, \end{aligned}$$

where we rely on an expression like (2.37) for $(-\mathcal{L}_\gamma)^{-1}$. \square

The Green–Kubo formula has a great advantage, in that it allows us to estimate the transport coefficients for as many different perturbations and response observables as we want *from a single equilibrium trajectory*. Indeed, one only needs to compute the corresponding integrated correlation functions (4.26).

4.2.1 Numerical implementation

We now describe a method to compute correlation functions necessary to the Green–Kubo method from a single long numerical trajectory. This method is described by Tuckerman in [30, Section 13.4.2] for Hamiltonian trajectories. In fact we consider a slight extension in which we let R and S to be vector-valued observables. For notational simplicity, we assume that R and S are component-wise centered. The quantities we want to estimate are

$$C(t) = \mathbb{E}_\mu [R(q_t, p_t)^\top S(q_0, p_0)]. \quad (4.28)$$

We let $(q^n, p^n)_{n \geq 0}$ be a numerical trajectory, which we see as the random iterates of the Markov chain associated with a numerical scheme, with a regular timestep $\Delta t > 0$. We further assume that the trajectory is stationary for this Markov chain, which is a realistic assumption if we equilibrate the system using our numerical scheme before recording states. By stationarity, the equality in law

$$(q^n, p^n, q^0, p^0) \xrightarrow{\text{law}} (q^{n+k}, p^{n+k} q^k, p^k)$$

for all $k \geq 0$. Hence we define the following estimator for $C(n\Delta t)$, for $0 \leq n \leq N_{\text{iter}}$:

$$\hat{C}_{N_{\text{iter}}}(n\Delta t) = \frac{1}{N_{\text{iter}} - n + 1} \sum_{k=0}^{N_{\text{iter}}-n} R(q^{n+k}, p^{n+k})^\top S(q^k, p^k). \quad (4.29)$$

Note the quality of the estimators degrades with n . Thus in practice, we fix $N_{\text{corr}} \ll N_{\text{iter}}$, and compute these estimators for $0 \leq n \leq N_{\text{corr}}$. Our implementation can be found in the Molly [15] source code as the `TimeCorrelationLogger` object and associated methods. Using these estimators, we can estimate the transport coefficient through the Green–Kubo formula (4.26). The simplest way is to use a naive Riemann sum, or rectangle rule:

$$\rho_F \approx \Delta t \sum_{k=0}^{N_{\text{corr}}} \hat{C}_{N_{\text{iter}}}(k\Delta t).$$

In fact, the analysis of [24, Corollary 2.3] shows that using a trapezoidal rule reduces the error to $O(\Delta t^2)$ for integration schemes of weak order 2. However, these procedures introduce a truncation in time of the integral in (4.26). Another approach consists in extrapolating the behavior of $\hat{C}_{N_{\text{iter}}}$ by fitting a parametric model

$$C_\theta(t) = \left(\sum_{k=1}^m a_k e^{-\lambda_k t} \cos(f_k t + \omega_k) \right), \quad (4.30)$$

where

$$\theta = (\lambda_k, a_k, f_k, \omega_k) \in (\mathbb{R}_+^* \times \mathbb{R} \times \mathbb{R} \times \mathbb{R})^m$$

is the parameter. The form of this model is justified empirically, although a formal argument based on a diagonalisation of the evolution semigroup can be made, and using the conjugate symmetry property $\mathcal{L}_\gamma \bar{\psi} = \overline{\mathcal{L}_\gamma \psi}$ for ψ a complex-valued observable. Rigorously justifying and quantifying the accuracy of this model requires fine knowledge of the spectrum of \mathcal{L}_γ . At any rate, we can then fit the model in a least-squares sense,

$$\theta^* = \operatorname{argmin}_{\theta \in (\mathbb{R}_+^* \times \mathbb{R} \times \mathbb{R} \times \mathbb{R})^m} \sum_{n=0}^{N_{\text{corr}}} \left| C_\theta(n\Delta t) - \widehat{C}_{N_{\text{iter}}}(n\Delta t) \right|^2, \quad (4.31)$$

using gradient descent, or the Gauss-Newton method, and deduce an estimator for the transport coefficient,

$$\widehat{\rho}_{F,N_{\text{iter}}}^{\text{GK}} = \int_0^\infty C_{\theta^*}(t) dt, \quad (4.32)$$

Using the simple identity

$$a \int_0^\infty e^{-\lambda t} \cos(ft + \omega) dt = a \frac{\lambda \cos \omega - f \sin \omega}{\lambda^2 + f^2}, \quad (4.33)$$

we get a closed form for the estimator,

$$\widehat{\rho}_{F,N_{\text{iter}}}^{\text{GK}} = \sum_{k=1}^m a_k \frac{\lambda_k \cos \omega_k - f_k \sin \omega_k}{\lambda_k^2 + f_k^2}.$$

4.2.2 Mobility

The Green-Kubo formula asserts that

$$\lim_{\eta \rightarrow 0} \frac{\mathbb{E}_\eta[F \cdot M^{-1} p]}{\eta} = \beta \int_0^\infty \mathbb{E}_\mu[(F \cdot M^{-1} p_t) (F \cdot M^{-1} p_0)] dt. \quad (4.34)$$

Using this expression, in the case of a mass-homogeneous system where the potential V is of pair interaction form (1.12), we can relate the transport coefficients for different forcings. As a useful example, we compute an equation relating the transport coefficients for the single drift and color drift forcings. The argument is taken from unpublished notes by Julien Roussel.

Example 5 (Relating linear responses). *We assume $M = m\text{Id}$. Let us define, for $1 \leq i, j \leq N$,*

$$c_{ij} = \frac{\beta}{m^2} \int_0^\infty \mathbb{E}_\mu[p_{i1,t} p_{j1,0}] dt.$$

By the form of the potential (Newton's third law), for all q ,

$$\sum_{i=1}^N \frac{\partial}{\partial q_{i1}} V(q) = 0.$$

This implies upon summing over i the longitudinal p -components of the SDE (2.15) and integrating

$$\begin{aligned} \sum_{i=1}^N p_{i1,t} &= \sum_{i=1}^N \left[p_{i1,0} + \int_0^t \left(-\frac{\partial}{\partial q_{i1}} V(q_s) - \frac{\gamma}{m} p_{i1,s} ds + \sqrt{\frac{2\gamma}{\beta}} dW_{i1,s} \right) \right] \\ &= \sum_{i=1}^N \left[p_{i1,0} - \frac{\gamma}{m} \int_0^t p_{i1,s} ds + \sqrt{\frac{2\gamma}{\beta}} W_{i1,t} \right]. \end{aligned}$$

Multiply by $p_{11,0}$ and take the expectation with respect with the canonical initial distribution, the Brownian terms vanish, and we get

$$\mathbb{E}_\mu \left[\left(\sum_{i=1}^N p_{i1,t} \right) p_{11,0} \right] = \sum_{i=1}^N \left[\mathbb{E}_\mu [p_{i1,0} p_{11,0}] - \frac{\gamma}{m} \int_0^t \mathbb{E}_\mu [p_{i1,s} p_{11,0}] ds \right]. \quad (4.35)$$

By the decay properties of the evolution semigroup, the left hand side converges to 0 as $t \rightarrow \infty$, while the integral is well-defined. Since p_0 has diagonal covariance with respect to μ , we get

$$\sum_{i=1}^N \frac{\gamma}{m} \int_0^\infty \mathbb{E}_\mu [p_{i1,s} p_{11,0}] ds = \mathbb{E}_\mu [p_{11,0}^2] = \frac{m}{\beta}. \quad (4.36)$$

Equivalently,

$$\sum_{i=1}^N c_{i1} = \frac{1}{\gamma}.$$

Using the indistinguishability property

$$c_{ii} = c_{11}, \quad c_{ij} = c_{12}$$

for all $i \neq j$, we can rewrite this identity as

$$c_{12} = \frac{1}{N-1} \left(\frac{1}{\gamma} - c_{11} \right). \quad (4.37)$$

Using this computation, we can relate the linear responses of the single drift and the color drift. By the Green–Kubo formula, the transport coefficient for the single drift is given by c_{11} ,

$$\rho_{F_S} = c_{11}.$$

For the color drift, we expand, by the Green–Kubo formula,

$$\rho_{F_C} = \frac{\beta}{m^2} \int_0^\infty \mathbb{E}_\mu [(F_C \cdot p_t) (F_C \cdot p_0)] dt = \frac{1}{N} \left(\sum_{i=1}^N c_{ii} + 2 \sum_{1 \leq i < j \leq N} (-1)^{i+j} c_{ij} \right)$$

By indistinguishability, and using

$$2 \sum_{1 \leq i \neq j \leq N} (-1)^{i+j} = -2 \left\lfloor \frac{N}{2} \right\rfloor,$$

which is easily seen by induction, we get

$$\rho_{F_C} = c_{11} - \frac{2 \lfloor N/2 \rfloor}{N(N-1)} \left(\frac{1}{\gamma} - c_{11} \right). \quad (4.38)$$

Note that this analysis is consistent with what we observe numerically, although because of persisting statistical uncertainty, much longer trajectories (or smaller systems) have to be considered to confirm this relation numerically. Let us also mention that the discrepancy vanishes in the thermodynamic limit, at rate $O(N^{-1})$. Since the system we consider is isotropic, we also have

$$c_{11} = \frac{\beta}{m^2} \int_0^\infty \mathbb{E}_\mu [p_{i\alpha,s} p_{i\alpha,0}] ds$$

for any $1 \leq i \leq N$ and $1 \leq \alpha \leq d$. Thus, the mobility can be computed through an expression of the form (4.28):

$$\rho_{F_S} = c_{11} = \frac{\beta}{m^2 d N} \int_0^\infty \mathbb{E}_\mu [p_s^\top p_0] ds, \quad (4.39)$$

which is the Green–Kubo relation we use in our numerical experiments. We expect that the expression is much better in terms of asymptotic variance than the naive Green–Kubo estimator based on (4.34). We confirm this fact empirically, in the sense that the estimator based on (4.2.2) converges much quicker, although further work should be undertaken to study this effect systematically. In Figure 4.3, we plot the velocity autocorrelation function used in the estimator (4.2.2), and its integral. We used the same thermodynamics conditions as for the NEMD method (4.13). In Figure 4.4, we show the fitted non-linear least squares model (4.30) for the autocorrelation function, using $m = 4$ modes, trained using the Gauss–Newton algorithm. The estimated correlation function was obtained from a single numerical trajectory with a physical reduced time of $t_{\text{fin}} = 1.628 \times 10^5$. The corresponding estimated values for the mobility are 0.1218 based on a trapezoid quadrature of the truncated autocorrelation function, and 0.1217 for the analytic integral of the parametric model.

We conclude this section on mobility computations by the discussion of a final method, which yields a nice physical interpretation for the mobility.

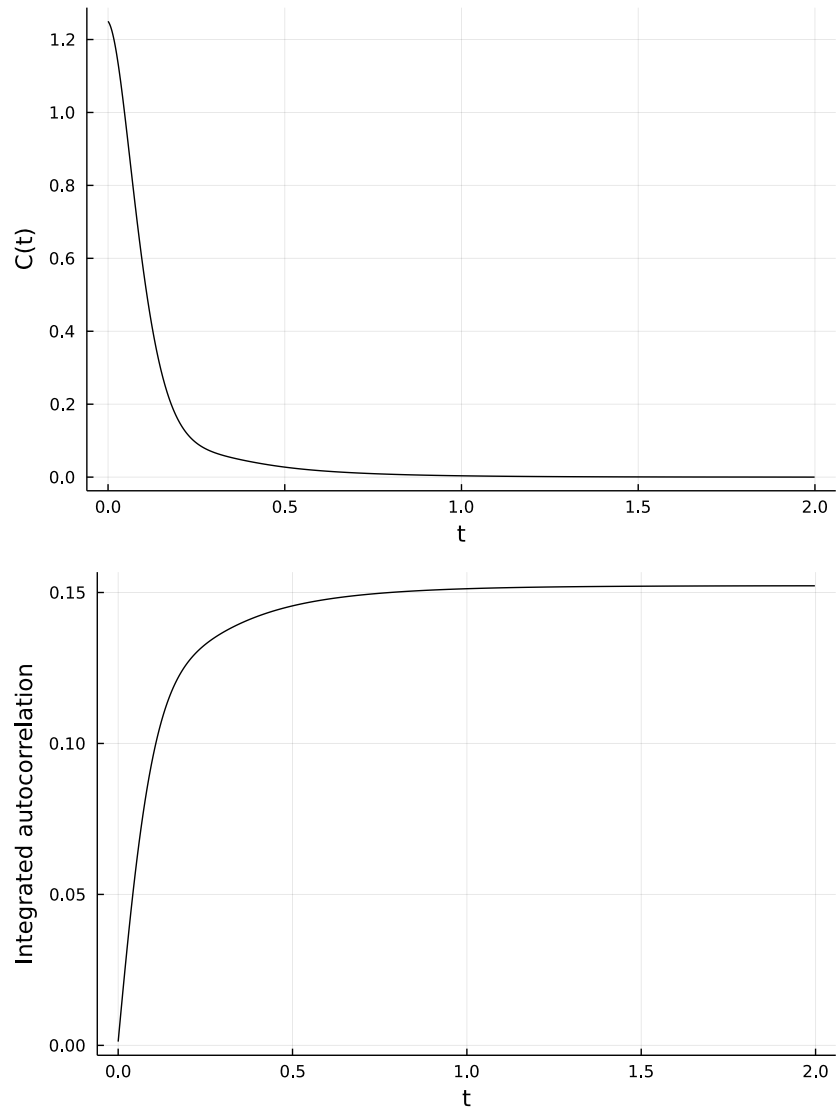


Figure 4.3: Velocity autocorrelation function (top) and its integral (bottom) for the Lennard-Jones system (4.13).

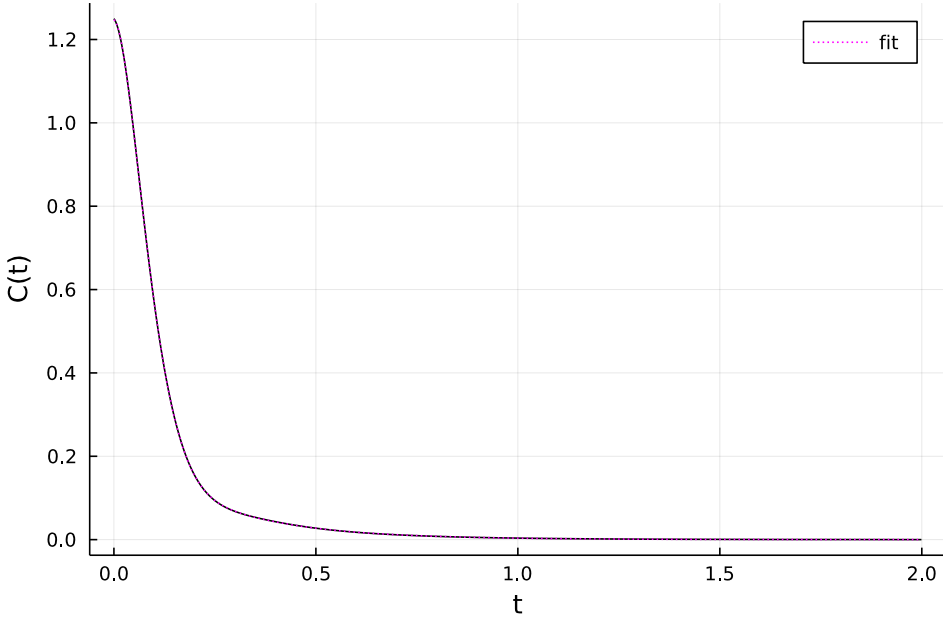


Figure 4.4: Fitted parametric model (4.30) (in dotted line) superimposed on autocorrelation function from Figure 4.3 (in black) for the Lennard-Jones system (4.13).

Remark 16 (Einstein relation for mobility). *Recalling the computations in Section 2.2.5, we can write, for R a centered response observable,*

$$\mathbb{E}_\mu \left[\left(\frac{1}{\sqrt{T}} \int_0^T R(q_t, p_t) dt \right)^2 \right] = 2 \int_0^T \mathbb{E}_\mu [R(q_t, p_t) R(q_0, p_0)] \left(1 - \frac{t}{T} \right) dt. \quad (4.40)$$

Assuming an exponential decay of the evolution semigroup, we get

$$\int_0^\infty \mathbb{E}_\mu [R(q_t, p_t) R(q_0, p_0)] dt = \lim_{T \rightarrow \infty} \frac{1}{2T} \mathbb{E}_\mu \left[\left(\int_0^T R(q_t, p_t) dt \right)^2 \right]. \quad (4.41)$$

This is the Einstein formula. In the case of mobility $R(q, p) = F \cdot M^{-1} p$, the right-hand side rewrites

$$\lim_{T \rightarrow \infty} \frac{1}{2T} \mathbb{E}_\mu \left[(F \cdot (Q_T - Q_0))^2 \right], \quad (4.42)$$

where

$$Q_t = Q_0 + \int_0^t M^{-1} p_s ds = \int_0^t dq_s \quad (4.43)$$

is the so called **self-diffusion** process, which formally satisfies the same SDE as q , but in the unperiodic domain \mathbb{R}^{dN} . Its trajectories corresponds to the unwrapped or unperiodized trajectories of the coordinates, which makes them particularly easy monitor during a numerical simulation. This terminology is justified by a result, [28, Theorem 1], asserting that the diffusively rescaled self-diffusion process

$$\sqrt{\varepsilon} (Q_{\varepsilon^{-1} t} - Q_0)$$

converges in law as $\varepsilon \rightarrow 0$ to a Brownian motion with diffusion matrix \mathfrak{D} characterized by

$$F \cdot \mathfrak{D} F = \lim_{T \rightarrow \infty} \frac{1}{T} \mathbb{E}_\mu \left[(F \cdot (Q_T - Q_0))^2 \right]. \quad (4.44)$$

In the case of an isotropic system, the diffusion matrix is characterized by a single number, the diffusion coefficient, which is given by the half normalized trace of the diffusion matrix.

$$D = \frac{1}{2dN} \text{Tr}(\mathfrak{D}) = \lim_{T \rightarrow \infty} \frac{1}{2dNT} \mathbb{E}_\mu \left[|Q_T - Q_0|^2 \right] \quad (4.45)$$

In view of the Einstein relation (4.42) and of the Green–Kubo relation (4.34), the mobility is related to the diffusion coefficient as

$$\rho_{F_S} = \beta D. \quad (4.46)$$

The formula (4.45) provides a new family of estimators for the mobility, based on a computation of the self-diffusion coordinates expression (4.45). In Figure 4.5 we illustrate the strategy we used to compute the mobility using the Einstein formula, which we proceed to explain. We define the mean-squared deviation as the process

$$M_t = \frac{|Q_t - Q_0|^2}{dN}. \quad (4.47)$$

Fixing a number of independent realizations N_{run} and a number of simulation iterations N_{iter} , we consider, for each $i = 1, \dots, N_{\text{run}}$, a numerical trajectory of regularly sampled points from the mean-squared deviation, $M^i = (M^{i,k})_{0 \leq k \leq N_{\text{iter}}}$. These correspond to points sampled at regular time intervals $T_{\text{samp}} = N_{\text{samp}}\Delta t$, where Δt is the simulation timestep, and computed from the numerical trajectory of the self-diffusion coordinates. We then obtain N_{run} estimators for D by a linear regression on the mean-squared deviation trajectories,

$$\hat{D}_{N_{\text{iter}}}^i = \frac{1}{2|\tau|^2} \tau \cdot M^i, \quad (4.48)$$

where

$$\tau = (kT_{\text{samp}})_{0 \leq k \leq N_{\text{iter}}}$$

is the vector of sampling times. An estimator for D , and thus for ρ_{F_S} , is obtained by averaging over the number of independent runs:

$$\hat{D}_{N_{\text{iter}}} = \frac{1}{N_{\text{run}}} \sum_{i=1}^{N_{\text{run}}} \hat{D}_{N_{\text{iter}}}^i. \quad (4.49)$$

Nearly independent runs can be computed over a single trajectory, using for all $T, t \geq 0$ the stationarity

$$(Q_T - Q_0)_{T \geq 0} \sim (Q_{T+t} - Q_t)_{T \geq 0},$$

and the asymptotic independence, or decorrelation, between $(Q_{T+t} - Q_t)_{T \geq 0}$ and $(Q_s)_{0 \leq s \leq t}$. This can be very simply exploited in a simulation, by resetting the self-diffusion coordinates to zero following each sample run. In practice, one has to take care to take N_{samp} large enough so that the mean-squared deviation behaves approximately linearly over the sample time range $[0, T_{\text{samp}}]$. In Figure 4.5, we illustrate the principle underlying this method. For our final computation, we used $N_{\text{run}} = 545$, $N_{\text{iter}} = 10^6$, $\Delta t = 10^{-3}$, $N_{\text{samp}} = 1$. The estimated mobility is

$$\rho_{F_S} = 0.12157 \pm 0.00011, \quad (4.50)$$

with error bars obtained using the empirical variance.

4.2.3 Shear viscosity

We conclude by applying the Green–Kubo formula to shear viscosity computations. It asserts, with $\rho_{F,k}$ given by (4.21),

$$\rho_{F,k} = \beta \int_0^\infty \mathbb{E}_\mu [R_k(q_t, p_t) (F(q_0) \cdot M^{-1} p_0)], \quad (4.51)$$

where R_k is given by (4.20). At this point, let us remark that we can, similar to the mobility case in (4.2.2), exploit the isotropy of the equilibrium measure to our statistical advantage. To do this let us define versions of the transverse forcing method for any pair of orthogonal canonical directions in \mathbb{R}^d . More precisely, we define, for any $1 \leq \alpha \neq \beta \leq d$,

$$R_{k,\alpha\beta}(q, p) = \frac{1}{N} \sum_{i=1}^N \frac{p_{i\alpha}}{m} \exp\left(\frac{2ik\pi q_{i\beta}}{L}\right),$$

$$F_{\alpha\beta}(q)_{i\alpha} = f_y(q_{i\beta}), \quad F_{\alpha\beta}(q)_{i\delta} = 0, \forall 1 \leq i \leq N, \forall \delta \neq \beta.$$

Then, by isotropy, we have

$$\rho_{F,k} = \frac{\beta}{d(d-1)} \sum_{1 \leq \alpha \neq \beta \leq d} \int_0^\infty \mathbb{E}_\mu [R_{k,\alpha\beta}(q_t, p_t) (F_{\alpha\beta}(q_0) \cdot M^{-1} p_0)]. \quad (4.52)$$

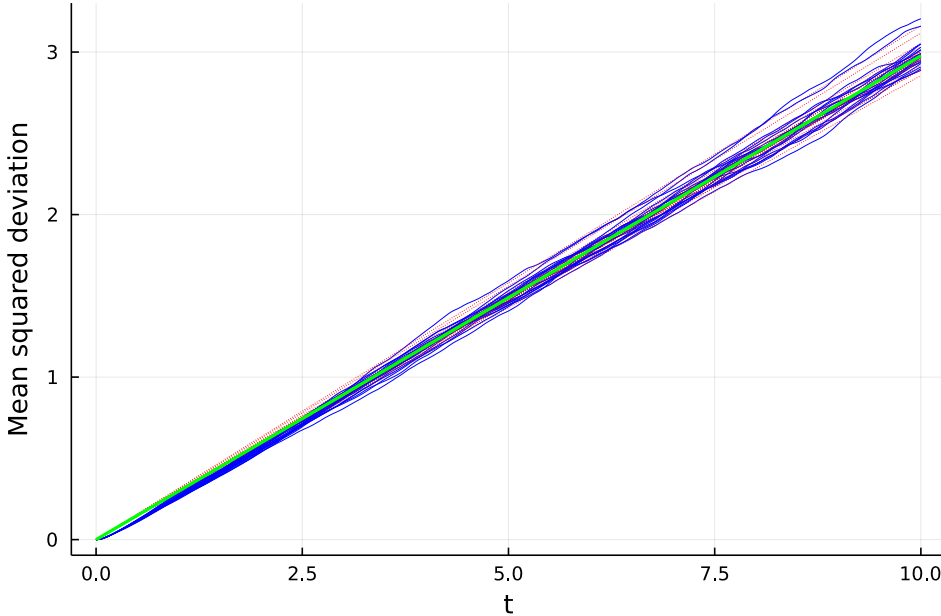


Figure 4.5: Twenty independent realizations of the mean squared-deviation (in blue) superimposed with their corresponding linear regression lines (in red dotted lines). The regression line corresponding to the corresponding estimator (4.49) is plotted in bright green.

This can be rewritten as an expression of the form (4.28), with $d(d-1)$ -dimensional observables. When $d = 3$, the speedup in convergence is appreciable, though we made no attempt to quantitatively measure it. We also take advantage of this opportunity to demonstrate the power of the Green–Kubo method by computing transport coefficients for all three forcing profiles using a single numerical trajectory. In Figure (4.6), we plot the correlation functions and corresponding integral for the three different forcing profiles. We note that the results are roughly consistent with the analytic computations of Figure 4.2, in the sense that the normalized transport coefficient

$$\frac{\rho_{F,k}}{c_k(f_y)}$$

should be real and positive. The persistence of an imaginary component in the estimation of this normalized transport coefficient can be attributed to statistical error, and is useful as a direct empirical non-convergence test for the Green–Kubo estimator. Computations were run under the reference thermodynamic condition (4.23), for a physical simulation time of $t_{\text{fin}} = 2.46 \times 10^4$, with a timestep $\Delta t = 10^{-3}$ and a number of decorrelation steps $N_{\text{corr}} = 10^4$. The corresponding estimates for the normalized transport coefficients are respectively 0.644, 0.645 and 0.655 for the sinusoidal, piecewise constant and piecewise linear forcing profiles.

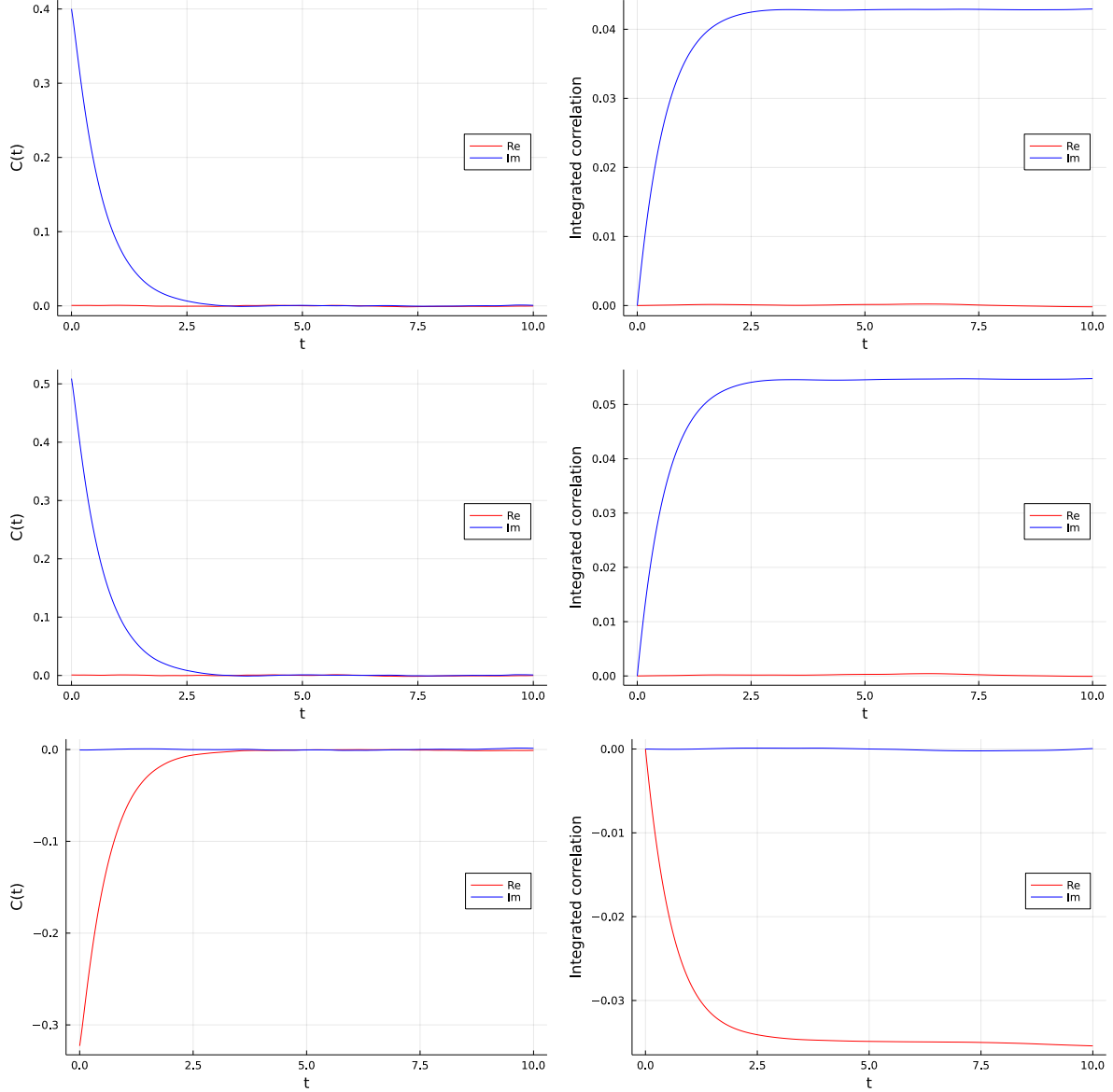


Figure 4.6: Correlation functions (left) and corresponding integrated correlation functions (right) for the shear viscosity dynamics. Top row: sinusoidal forcing, middle row: piecewise constant forcing, bottom row: piecewise linear forcing. Real parts are plotted in red and imaginary parts are plotted in blue. Integrals were obtained with a trapezoid rule.

Chapter 5

Norton dynamics

We have considered so far two general methods for the computation of transport coefficients. The Green-Kubo method, which relies on analysis of autocorrelations in the fluctuation of zero-average equilibrium quantities, and the NEMD method, which relies in measuring the ratio in the average of a given equilibrium-centered response observable under a driven steady-state and the magnitude of the driving force. In the case of mobility, we apply a small constant force, and measure the resulting particle flux in the direction of the perturbation. We can thus think of the mobility ρ_F as measuring how *responsive* the flux is to the forcing on the system. A natural question to ask is whether it is possible to measure the dual quantity, that is, how *resistive* the system is to a given flux. One possible strategy to answer this question, in loose terms, would be to *constrain* the response to be constant, and measure the average magnitude of the forcing needed to maintain it. In the limit of a small response, the linear dependency between these quantities can be hoped to provide an equivalent and reciprocal measure of the transport coefficient. By analogy with the Thévenin and Norton circuit theorems, we will from now on refer to the standard, constant-forcing method as the Thévenin method, and the dual, constant-response method as the Norton method. We will again be using the mobility and the shear viscosity as our examples, so as to leverage our previous calculations as ways to validate our method.

5.1 General framework

We first express the method in full generality, before specializing to the non-equilibrium molecular dynamics context. We consider the stochastic differential equation:

$$\begin{cases} dX_t = b(X_t) dt + \sigma(X_t) dW_t + d\Lambda_t F(X_t) \\ R(X_t) = r, \end{cases} \quad (5.1)$$

where b, σ and F are respectively \mathbb{R}^D , $\mathbb{R}^{D \times E}$ and \mathbb{R}^D -valued functions, and W is a E -dimensional Brownian motion. We interpret F as a perturbation direction for an *equilibrium SDE*, and Λ is the perturbation intensity, which is determined in order to maintain the response observable R constant equal to $r > 0$ along the dynamic's trajectories. The Norton dynamics (5.1) should be thought of as the constant-response counterpart to a corresponding Thévenin dynamics

$$\begin{cases} dX_t = b(X_t) dt + \sigma(X_t) dW_t + \eta F(X_t), \\ \eta > 0, \end{cases} \quad (5.2)$$

which is perturbed in the same direction, but with a constant forcing intensity η . Both these dynamics have a corresponding reference dynamics, respectively for $r = 0$ and $\eta = 0$, with the reference Thévenin dynamics simply being the equilibrium Langevin dynamics. For notational simplicity, let us introduce the following definitions:

$$b_t = b(X_t), \quad \sigma_t = \sigma(X_t), \quad F_t = F(X_t), \quad \nabla R_t = \nabla R(X_t), \quad \nabla^2 R_t = \nabla^2 R(X_t). \quad (5.3)$$

For $A, B \in \mathbb{R}^D$, such that $A \cdot B \neq 0$, we denote by $P_{A,B}$ the projector onto A orthogonally to B

$$P_{A,B} = \frac{A \otimes B}{A \cdot B}. \quad (5.4)$$

Finally, for any projector P , we denote by \bar{P} the complementary projector

$$\bar{P} = \text{Id} - P, \quad (5.5)$$

We can now state the following result, which follows by a simple application of Itô calculus, and gives an expression for the dynamics (5.1) without reference to Λ .

Proposition 7. *Provided it is well-posed, the solution of the following SDE solves (5.1)*

$$dX_t = \bar{P}_{F_t, \nabla R_t} [b_t dt + \sigma_t dW_t] - \frac{1}{2} \frac{\nabla^2 R_t : (\bar{P}_{F_t, \nabla R_t} \sigma_t \sigma_t^\top \bar{P}_{\nabla R_t, F_t})}{F_t \cdot \nabla R_t} F_t dt, \quad (5.6)$$

with Λ_t taken to be an Itô process defined by

$$d\Lambda_t = -\frac{\nabla R_t \cdot b_t}{F_t \cdot \nabla R_t} dt - \frac{\nabla R_t \cdot \sigma_t dW_t}{F_t \cdot \nabla R_t} - \frac{1}{2} \frac{\nabla^2 R_t : (\bar{P}_{F_t, \nabla R_t} \sigma_t \sigma_t^\top \bar{P}_{\nabla R_t, F_t})}{F_t \cdot \nabla R_t}. \quad (5.7)$$

Proof. The proof follows by analysis-synthesis. We first assume that Λ admits a decomposition as an Itô process,

$$d\Lambda_t = \lambda_t dt + d\tilde{\Lambda}_t, \quad (5.8)$$

where λ is a bounded variation process and $\tilde{\Lambda}$ is a martingale, and that R sufficiently regular (say C^2 and bounded). We can apply Itô's formula to the constant response condition, to get

$$\nabla R_t \cdot dX_t + \frac{1}{2} \nabla^2 R_t : \langle \sigma_t dW_t + d\tilde{\Lambda}_t F_t \rangle = 0, \quad (5.9)$$

where the brackets denote the quadratic covariation of an Itô process. By identifying the martingale and bounded variation parts of the above process with 0, we deduce an SDE for Λ_t :

$$\begin{cases} \nabla R_t \cdot (\sigma_t dW_t + F_t d\tilde{\Lambda}_t) = 0 \\ \nabla R_t \cdot (b_t + \lambda_t F_t) + \frac{1}{2} \nabla^2 R_t : \langle \sigma_t dW_t + d\tilde{\Lambda}_t F_t \rangle = 0. \end{cases} \quad (5.10)$$

From the first equation, we deduce the expression of the martingale part of the forcing:

$$d\tilde{\Lambda}_t = -\frac{\nabla R_t \cdot \sigma_t dW_t}{\nabla R_t \cdot F_t}, \quad (5.11)$$

and as a consequence, we may compute the quadratic covariation bracket in (5.9),

$$\langle \sigma_t dW_t + d\tilde{\Lambda}_t F_t \rangle = \left\langle \left(\text{Id} - \frac{F_t \otimes \nabla R_t}{F_t \cdot \nabla R_t} \right) \sigma_t dW_t \right\rangle = \bar{P}_{F_t, \nabla R_t} \sigma_t \sigma_t^\top \bar{P}_{F_t, \nabla R_t}^\top dt, \quad (5.12)$$

where we use $P_{A,B}^\top = P_{B,A}$. Inserting equation (5.12) into (5.10) yields the full SDE for the forcing Λ_t (5.7) and the result follows by inserting the latter in (5.1). \square

As stated above, we propose the Norton dynamics as a possible and alternative means of computing the linear response to a small perturbation of the equilibrium dynamics. We finish this general introduction by evoking a few theoretical questions related to these dynamics.

- (i) Existence of a unique steady-state for the dynamics (5.1) and (5.2). As mentioned in the previous chapter, some results already exist in the Thévenin case.
- (ii) As before, proving the convergence of trajectory averages.
- (iii) With respect to the steady states, whose corresponding expectations we denote by \mathbb{E}_η in the Thévenin case, and \mathbb{E}_r in the Norton case, equality of the transport coefficients

$$\lim_{\eta \rightarrow 0} \frac{\mathbb{E}_\eta[R]}{\eta}$$

and

$$\lim_{r \rightarrow 0} \frac{r}{\mathbb{E}_r[\lambda]}.$$

This is the question of equivalence of the linear responses.

- (iv) Another natural question is that of the equivalence of the Norton and Thévenin equilibrium ensembles. This question asks about the existence of an asymptotic regime, or thermodynamic limit as $D \rightarrow \infty$, for which averages under the two equilibrium steady-states converge to a common value, for a sufficiently rich class of observables.
- (v) On a related note, investigating the equivalence of the non-linear responses, that is the existence of a well-defined $r(\eta)$ such that the graphs $(\eta, \mathbb{E}_\eta[R])$ and $(\mathbb{E}_{r(\eta)}[\lambda], r(\eta))$ either agree or converge to a common value in some asymptotic regime when $D \rightarrow \infty$.
- (vi) Even more ambitiously, full equivalence of the non-equilibrium ensembles.
- (vii) Finally, we mention the question of finding a relation between the Norton equilibrium fluctuations of λ and the linear response, in an analogy with the Green-Kubo formula.

Let us mention that the question of the equivalence of of non-equilibrium ensembles has already been investigated by Evans in [7], although the setting is purely deterministic, and the proof is formal. The purpose of this chapter is to make somewhat rigorous a setting in which these questions are susceptible to find an answer, albeit a probably a difficult one to obtain. Furthermore, the numerical results which we present in the remainder of this report show that these questions do not have obviously negative answers, and thus should be worthy of investigation.

5.2 Norton dynamics for transport coefficients

We now turn to specialising the setting to the Norton counterpart of the dynamics (4.1). It reads

$$\begin{cases} dq_t = m^{-1} p_t dt, \\ dp_t = -\nabla V(q_t) dt - \gamma M^{-1} p_t dt + \sqrt{\frac{2\gamma}{\beta}} dW_t + d\Lambda_t F(q_t), \\ R(q_t, p_t) = r, \end{cases} \quad (5.13)$$

where Λ_t is the magnitude of the perturbation, which is defined by the constraint $R(q_t, p_t) = r > 0$. We may assume γ is a positive semi-definite diagonal matrix, as in the Thévenin case. R is the response observable, which we take of the form

$$R(q, p) = G(q) \cdot p,$$

with G a smooth vector field. Note in particular that $\nabla_p R(q, p) = G(q)$, and $\nabla_p^2 R(q, p) = 0$. Finally note that the forcing acts solely on the momenta. A SDE for Λ_t can be obtained by applying Proposition 7. It immediately implies

$$\begin{cases} dq_t = M^{-1} p_t dt \\ dp_t = \bar{P}_{F_t, G_t} \left[-\nabla V(q_t) - dt \gamma M^{-1} p_t dt + \sqrt{\frac{2\gamma}{\beta}} dW_t \right] - \frac{\nabla_q R_t \cdot M^{-1} p_t}{F_t \cdot G_t} F_t dt, \end{cases} \quad (5.14)$$

with an expression for the forcing term

$$\begin{cases} d\Lambda_t = \lambda_t dt + d\tilde{\Lambda}_t, \\ \lambda_t = \frac{G_t \cdot [\nabla V(q_t) + \gamma M^{-1} p_t] - \nabla_q R_t \cdot M^{-1} p_t}{F_t \cdot G_t}, \\ d\tilde{\Lambda}_t = -\frac{G_t \cdot \sqrt{\frac{2\gamma}{\beta}} dW_t}{F_t \cdot G_t}. \end{cases} \quad (5.15)$$

We use notations identical to (5.4), (5.5) and (5.3) in the expressions above. The bounded and martingale parts of the forcing term can be identified in (5.15), and are given respectively by λ_t and $\tilde{\Lambda}_t$. We record the infinitesimal generator of the dynamics (5.14), which is given by

$$\mathcal{L}_\gamma^{\text{Norton}} \varphi = A\varphi - [\bar{P}_{F,G} (\nabla V + \gamma M^{-1} p)] \cdot \nabla_p \varphi - \frac{\nabla_q R \cdot M^{-1} p}{F \cdot G} F \cdot \nabla_p \varphi + \frac{1}{\beta} \nabla_p^2 \varphi : [\bar{P}_{F,G} \gamma \bar{P}_{G,F}]. \quad (5.16)$$

Note $\bar{P}_{F,G}$ is a function of the coordinate variable in the equation above, and A is as in (2.3).

Remark 17. Note that the $G(q_t) \cdot F(q_t)$ term in the denominator may pose a question of well-posedness of the dynamics. Let us always suppose in our computations that $G(q_t) \cdot F(q_t) > 0$, but this is by no means automatic. Indeed, thinking of the extreme case when F and G are orthogonal everywhere and $V = 0$ highlights the fact that this is an issue of controllability: in that case, by isotropy, the component of the momentum in the direction G will diffuse according to an Ornstein-Uhlenbeck process independent from any forcing applied in the direction F . In this case there is no way to control the response, and thus the dynamics is ill-defined.

Writing the Norton dynamics under the form (5.14) is instructive, since its structure appears clearly: its stochastic increments are comprised of the projected increments of an equilibrium Langevin dynamics, with an additional term involving $\nabla_q R$, which can be interpreted as a correction term enforcing the constant response constraint, in reaction to the configurational dynamics. This fact will become clearer in the following section, where we describe splitting schemes for the Norton dynamics.

5.2.1 Splitting schemes for numerical integration

As in every case we considered so far, we will again rely on the fact that the Norton dynamics (5.14) can be split into three simpler, structure-preserving dynamics, to construct a variety of numerical schemes.

Definition 3 (Splitting of the Norton dynamics). Consider the following dynamics

$$\begin{cases} dq_t = M^{-1} p_t dt \\ dp_t = -\frac{\nabla_q R(q_t, p_t) \cdot M^{-1} p_t}{F(q_t) \cdot G(q_t)} F(q_t) dt \end{cases}, \quad (5.17)$$

$$\begin{cases} dq_t = 0 \\ dp_t = -\bar{P}_{F_t, G_t} \nabla V(q_t) dt \end{cases}, \quad (5.18)$$

and finally

$$\begin{cases} dq_t = 0 \\ dp_t = \bar{P}_{F_t, G_t} \left[\gamma M^{-1} p_t dt + \sqrt{\frac{2\gamma}{\beta}} dW_t \right], \end{cases} \quad (5.19)$$

which additively combine to form the Norton dynamics (5.6). By analogy with the equilibrium setting, we will respectively refer to (5.17), (5.18) and (5.19) as the (Norton) A, B and O dynamics. At the level of the generator (5.16), this corresponds to a splitting into three operators,

$$\mathcal{L}_\gamma^{\text{Norton}} = \mathcal{L}_A^{\text{Norton}} + \mathcal{L}_B^{\text{Norton}} + \mathcal{L}_{\gamma, O}^{\text{Norton}},$$

with

$$\begin{cases} \mathcal{L}_A^{\text{Norton}} \varphi = A\varphi - \frac{\nabla_q R \cdot M^{-1} p}{F \cdot G} F \cdot \nabla_p \varphi, \\ \mathcal{L}_B^{\text{Norton}} \varphi = -(\bar{P}_{F, G} \nabla V) \cdot \nabla_p \varphi, \\ \mathcal{L}_{\gamma, O}^{\text{Norton}} \varphi = -(\bar{P}_{F, G} \gamma M^{-1} p) \cdot \nabla_p + \frac{1}{\beta} (\bar{P}_{F, G} \gamma \bar{P}_{G, F}) : \nabla_p^2 \varphi. \end{cases} \quad (5.20)$$

The claim that these dynamics are structure-preserving is summed up in the following straightforward result.

Lemma 3. Let (q_t, p_t) refer to the solution of any of the Norton A, B or O dynamics. Then if $R(q_0, p_0) = r$, $R(q_t, p_t) = r$ for all $t > 0$.

Proof. The result can be proven by three thoughtless applications of the chain rule or Itô's formula. A quicker and more instructive proof follows from observing that for any $X, q, p \in \mathbb{R}^{dN}$,

$$\begin{aligned} G(q) \cdot \bar{P}_{F(q), G(q)} X &= \bar{P}_{F(q), G(q)}^\top G(q) \cdot X \\ &= \bar{P}_{G(q), F(q)} G(q) \cdot X \\ &= 0, \end{aligned}$$

since $P_{G(q),F(q)}$ is a projector onto the one-dimensional subspace spanned by $G(q)$ and $\bar{P}_{G(q),F(q)}$ is its complement. Hence any dynamics of the form

$$dq_t = 0, \quad dp_t = \bar{P}_{G_t,F_t} [b(q_t, p_t) dt + \sigma(q_t, p_t) dW_t]$$

preserves $R(q_t, p_t) = G(q_t) \cdot p_t$, by applying the Itô formula, since $\nabla_p R(q, p) = G(q)$ and $\nabla_p^2 R = 0$. This implies the result for the B and O dynamics. However, since the Norton dynamics also preserves $R(q_t, p_t)$ by construction, the preservation property for the A dynamics follows immediately, from the response conservation property of the Norton dynamics in the case $V = 0$ and $\gamma = 0$. For the more skeptical reader, we write, with (q_t, p_t) a solution to the A dynamics,

$$\begin{aligned} \frac{d}{dt} R(q_t, p_t) &= \nabla_q R(q_t, p_t) \cdot (M^{-1} p_t) - \nabla_p R(q_t, p_t) \cdot \left(\frac{\nabla_q R(q_t, p_t) \cdot M^{-1} p_t}{F(q_t) \cdot G(q_t)} F(q_t) \right) \\ &= \nabla_q R(q_t, p_t) \cdot (M^{-1} p_t) \left(1 - \frac{G(q_t) \cdot F(q_t)}{F(q_t) \cdot G(q_t)} \right) \\ &= 0 \end{aligned}$$

□

As before, this splitting allows us to define a variety of numerical schemes for the Norton dynamics, following the same strategy as in Section 2.2.6. In order to do so, we must prescribe a way to integrate each of the A,B and O steps individually. This is what we now turn to. In the following, let us fix a timestep $\Delta t > 0$, and a response intensity $r > 0$. Similar to the equilibrium setting, the B step can be integrated analytically, since its trajectories are ballistic. Thus we have the following algorithm.

Algorithm 2 (Norton B step).

$$\begin{cases} \tilde{p}^1 = p^0 - \nabla V(q^0) \\ p^1 = \tilde{p}^1 + \Delta t \lambda^1 F(q^0), \end{cases} \quad (5.21)$$

where λ^1 is determined in order to conserve the response:

$$G(q^0) \cdot p^1 = r \iff \Delta t \lambda^1 = \frac{r - G(q^0) \cdot \tilde{p}^1}{F(q^0) \cdot G(q^0)}. \quad (5.22)$$

We next rely on the fact that the Norton O dynamics is in Ornstein–Uhlenbeck form to compute its exact solution over one timestep, using the following result.

Proposition 8. We consider the following general form of the Norton Ornstein–Uhlenbeck process in \mathbb{R}^{dN} .

$$dp_t = -P\gamma M^{-1} p_t dt + P\sqrt{\frac{2\gamma}{\beta}} dW_t, \quad (5.23)$$

where $P^2 = P$ is a projector (not necessarily orthogonal), γ and M^{-1} are positive definite symmetric matrices, and W is a standard Brownian motion. We denote by \bar{P} the complementary projector $\bar{P} = \text{Id} - P$. Assume also that P and γM^{-1} commute. Then, the analytical solution of (5.23) writes

$$p_t = \bar{P}p_0 + Pp_t^{\text{eq}}, \quad (5.24)$$

where p_t^{eq} is the solution of the coupled equilibrium Ornstein–Uhlenbeck process,

$$\begin{cases} dp_t^{\text{eq}} = -\gamma M^{-1} p_t^{\text{eq}} dt + \sqrt{\frac{2\gamma}{\beta}} dW_t, \\ p_0^{\text{eq}} = p_0. \end{cases} \quad (5.25)$$

Proof. The proof follows the standard strategy of applying Itô’s formula to the process rescaled by $e^{tP\gamma M^{-1}}$. It yields

$$d(e^{tP\gamma M^{-1}} p_t) = e^{tP\gamma M^{-1}} \left(P\gamma M^{-1} p_t dt - P\gamma M^{-1} p_t dt + P\sqrt{\frac{2\gamma}{\beta}} dW_t \right), \quad (5.26)$$

whence, integrating in t and multiplying both sides by $e^{-tP\gamma M^{-1}}$,

$$p_t = e^{-tP\gamma M^{-1}} p_0 + \int_0^t e^{-P\gamma M^{-1}(t-s)} P\sqrt{\frac{2\gamma}{\beta}} dW_s. \quad (5.27)$$

This yields an expression for the solution whatever the particular properties of γ , M^{-1} and P . However, since P is a projector, we can make use of the following useful formula: if A and P are square matrices with $AP = PA$,

$$e^{PA} = \sum_{k=0}^{\infty} \frac{(PA)^k}{k!} = \sum_{k=0}^{\infty} \frac{P^k A^k}{k!} = \text{Id} + P \sum_{k=1}^{\infty} \frac{A^k}{k!} = \text{Id} + P(e^A - \text{Id}) = \bar{P} + Pe^A. \quad (5.28)$$

The second equality follows from the fact that A and P commute, while the third follows from a repeated application of the projector identity $P = P^2 = P^3 = \dots$. This is sometimes referred to as Rodrigue's formula (see for instance [23]chapter 8). Applying's Rodrigue's formula to our analytical form yields

$$p_t = \bar{P}p_0 + Pe^{-t\gamma M^{-1}}p_0 + \int_0^t (\bar{P} + Pe^{-\gamma M^{-1}(t-s)}) P \sqrt{\frac{2\gamma}{\beta}} dW_s. \quad (5.29)$$

expanding the product inside the integral, and using $\bar{P}P = 0$, we get

$$p_t = \bar{P}p_0 + Pe^{-t\gamma M^{-1}}p_0 + \int_0^t Pe^{-\gamma M^{-1}(t-s)} P \sqrt{\frac{2\gamma}{\beta}} dW_s. \quad (5.30)$$

By our commutativity assumption, we can factor out the P s from the integral sign and obtain

$$p_t = \bar{P}p_0 + Pe^{-t\gamma M^{-1}}p_0 + P^2 \int_0^t e^{-\gamma M^{-1}(t-s)} \sqrt{\frac{2\gamma}{\beta}} dW_s = \bar{P}p_0 + P \left(e^{-t\gamma M^{-1}}p_0 + \int_0^t e^{-\gamma M^{-1}(t-s)} \sqrt{\frac{2\gamma}{\beta}} dW_s \right), \quad (5.31)$$

regrouping the terms in P and using again $P^2 = P$. The result follows by simply recognizing the parenthesized term as p_t^{eq} . \square

Remark 18. *The commutativity assumption may seem overly restrictive, but in fact it is enough in the cases we consider. For instance, in the case of shear viscosity computations with anisotropic friction, M is a scalar multiple of the identity and γ is diagonal and constant with respect to longitudinal coordinates, so that the commutativity condition is indeed verified.*

As a consequence of this computation, we may define a numerical strategy to integrate the fluctuation-dissipation part of the Norton dynamics.

Algorithm 3 (Norton O step).

$$\begin{cases} \tilde{p}^1 = \alpha_{\Delta t} p^0 + \sigma_{\Delta t} \mathcal{G}^1, \\ p^1 = \tilde{p}^1 + \Delta t \lambda^1 F(q^0), \end{cases} \quad (5.32)$$

where \mathcal{G}^1 is a standard dN -dimensional Gaussian, $\alpha_{\Delta t}$, $\sigma_{\Delta t}$ are given by (??), and λ^1 is again determined by equation (5.22) in order to conserve the response.

Unfortunately, the A dynamics (5.17) cannot be solved analytically. However, its general form is that of an infinitesimal Hamiltonian increment on the position coordinate, with an additional correction term in the direction F on the momentum coordinate. Furthermore, we know the response is conserved by the A dynamics. This naturally suggests the following scheme.

Algorithm 4 (Norton A step).

$$\begin{cases} q^1 = q^0 + \Delta t M^{-1} p^0, \\ p^1 = p^0 + \Delta t \lambda^1 F(q^1), \end{cases} \quad (5.33)$$

where λ^1 is determined by

$$G(q^1) \cdot p^1 = r \iff \Delta t \lambda^1 = \frac{r - G(q^1) \cdot p^0}{F(q^1) \cdot G(q^1)} \quad (5.34)$$

to enforce the constant response constraint.

An advantage of schemes for the Norton dynamics formed by chaining and iterating steps of (5.33), (5.21) and (5.32) is that they immediately yield a discretization of the forcing intensity $d\Lambda_t$, and thus

an estimation of the average $\mathbb{E}_r[\lambda]$, which is the quantity of prime interest to us. Indeed, observe from equation (5.15) that we can write

$$d\Lambda_t = \lambda_t^A dt + \lambda_t^B dt + d\Lambda_t^O, \quad (5.35)$$

with

$$\left\{ \begin{array}{l} \lambda_t^A = -\frac{\nabla_q R(q_t, p_t) \cdot G(q_t)}{F(q_t) \cdot G(q_t)}, \\ \lambda_t^B = -\frac{\nabla V(q_t) \cdot G(q_t)}{F(q_t) \cdot G(q_t)}, \\ d\Lambda_t^O = -\frac{\left[-\gamma M^{-1} p_t dt + \sqrt{\frac{2\gamma}{\beta}} dW_t \right] \cdot G(q_t)}{F(q_t) \cdot G(q_t)}. \end{array} \right. \quad (5.36)$$

These individual parts can be interpreted individually as the forcing intensities in the direction $F(q_t)$ applied to each of the A,B and O dynamics, relative to the corresponding equilibrium dynamics. This yields a natural interpretation of the λ^n terms along numerical trajectories, as discretizations of (5.36), and thus one can use these ergodic averages for the average forcing. As a full example, we record the BABO-like scheme we used in our simulations, as well as the corresponding estimator of $\mathbb{E}_r[\lambda]$. This procedure can of course be generalized to other orderings of the operators in the splitting. The impact of such a choice on the discretization error of the mean force should be the subject of future investigation.

Example 6 (Estimation of the mean force using a BABO scheme.). *The numerical scheme is implemented, for a fixed timestep $\Delta t > 0$, by iterating*

$$\left\{ \begin{array}{l} \tilde{p}^{n+\frac{1}{4}} = p^n - \frac{\Delta t}{2} \nabla V(q^n) \\ \frac{\Delta t}{2} \lambda^{n+\frac{1}{4}} = \frac{r - G(q^n) \cdot \tilde{p}^{n+\frac{1}{4}}}{F(q^n) \cdot G(q^n)} \\ p^{n+\frac{1}{4}} = \tilde{p}^{n+\frac{1}{4}} + \frac{\Delta t}{2} \lambda^{n+\frac{1}{4}} F(q^n) \\ q^{n+1} = q^n + \Delta t M^{-1} p^{n+\frac{1}{4}} \\ \Delta t \lambda^{n+\frac{1}{2}} = \frac{r - G(q^{n+1}) \cdot p^{n+\frac{1}{4}}}{F(q^{n+1}) \cdot G(q^{n+1})} \\ p^{n+\frac{1}{2}} = p^{n+\frac{1}{4}} + \Delta t \lambda^{n+\frac{1}{2}} F(q^{n+1}) \\ \tilde{p}^{n+\frac{3}{4}} = p^n - \frac{\Delta t}{2} \nabla V(q^{n+1}) \\ \frac{\Delta t}{2} \lambda^{n+\frac{3}{4}} = \frac{r - G(q^{n+1}) \cdot \tilde{p}^{n+\frac{3}{4}}}{F(q^{n+1}) \cdot G(q^{n+1})} \\ p^{n+\frac{3}{4}} = \tilde{p}^{n+\frac{3}{4}} + \frac{\Delta t}{2} \lambda^{n+\frac{3}{4}} F(q^{n+1}) \\ \tilde{p}^{n+1} = \alpha_{\Delta t} p^{n+\frac{3}{4}} + \sigma_{\Delta t} \mathcal{G}^{n+1} \\ \Delta t \lambda^{n+1} = \frac{r - G(q^{n+1}) \cdot \tilde{p}^{n+1}}{F(q^{n+1}) \cdot G(q^{n+1})} \\ p^{n+1} = \tilde{p}^{n+1} + \Delta t \lambda^{n+1} F(q^{n+1}). \end{array} \right. \quad (5.37)$$

If the scheme is iterated N_{iter} times, the mean force can be estimated by

$$\hat{\lambda}'_{N_{\text{iter}}} = \frac{1}{N_{\text{iter}}} \sum_{k=0}^{N_{\text{iter}}-1} \left(\frac{\lambda^{k+\frac{1}{4}} + \lambda^{k+\frac{3}{4}}}{2} + \lambda^{k+\frac{1}{2}} + \lambda^{k+1} \right). \quad (5.38)$$

Note that the λ^{k+1} also account for the part of the correction due to the Gaussian increment \mathcal{G}^{k+1} . In practice, it may be possible to replace λ^{k+1} with an estimation of the bounded variation part of $d\Lambda^O$,

$$\lambda_t^O = \frac{\gamma M^{-1} p_t \cdot G(q_t)}{F(q_t) \cdot G(q_t)},$$

to obtain an estimator with a lower variance. For example, in our simulations, we took $M = m\text{Id}$ and a constant γ , so that using the constant-response condition,

$$\lambda_t^O = \frac{\gamma m^{-1}}{F(q_t) \cdot G(q_t)},$$

so that the mean force estimator we considered in practice was

$$\hat{\lambda}_{N_{\text{iter}}} = \frac{1}{N_{\text{iter}}} \sum_{k=0}^{N_{\text{iter}}-1} \left(\frac{\lambda^{k+\frac{1}{4}} + \lambda^{k+\frac{3}{4}}}{2} + \lambda^{k+\frac{1}{2}} + \frac{\gamma m^{-1}}{F(q^k) \cdot G(q^k)} \right). \quad (5.39)$$

5.2.2 Physical interpretation

We conclude this theoretical discussion by pointing out a property of the Norton dynamics (5.14) in the deterministic case $\gamma = 0$, and when the forcing direction F is proportional to the response direction G . Without loss of generality, we assume $F = G$, since changing the proportionality constant amounts to changing the scale of the response. We also assume that the system is homogeneous, so that we may take $M = \text{Id}$. In this case the projectors P_{G_t, F_t} and the like all become orthogonal projectors onto the one-dimensional subspace spanned by F_t , or its orthogonal complement. We show that in this particular case there is a physical interpretation for the dynamics

Proposition 9 (Gauss's principle of least constraint). *Consider the deterministic version of the Norton dynamics,*

$$\begin{cases} \dot{q} = p, \\ \dot{p} = -\bar{P}_{F(q)} \nabla V(q) - \frac{\nabla F(q)p \cdot p}{|F(q)|^2}, \end{cases} \quad (5.40)$$

where the constraint is given by

$$F(q_t) \cdot p_t = F(q_0) \cdot p_0 = r,$$

and where we write \bar{P}_F for $\bar{P}_{F,F}$. The rightmost term in the equation for \dot{p} comes from writing $\nabla_q R(q, p) = \nabla G(q)p$. Then Gauss's principle of least constraint is satisfied:

$$\begin{cases} \dot{q} = p, \\ \dot{p} = \underset{f \cdot F(q) + \nabla F(q)p \cdot p = 0}{\operatorname{argmin}} | -\nabla V(q) - f |^2. \end{cases} \quad (5.41)$$

In other words, the force applied to the system undergoing the Norton dynamics minimizes at each point in time the Euclidean distance to the force applied to the same system undergoing the Hamiltonian dynamics (1.11), subject to the constant response constraint.

Proof. Firstly, let us make clear that the constraint in the minimization problem actually expresses the constant response constraint. Since

$$r = F(q) \cdot p,$$

a differentiation in time yields

$$0 = \nabla F(q)\dot{q} \cdot p + F(q) \cdot \dot{p} = \nabla F(q)p \cdot p + F(q) \cdot \dot{p}. \quad (5.42)$$

Since the force applied to the system is equal to \dot{p} , this effectively yields a constraint on the set of possible forces applied to the Norton system. This is analogous to the case of a Hamiltonian system subject to a set of holonomic constraints, which depend only on the position q . In this case, a so-called hidden or shadow constraint on the set of admissible forces can be obtained by twice-differentiating the constraint condition. For a pedagogical discussion of this case, we refer the reader to [23], section 4.3. In our non-holonomic case (the constraint also depends on p), a single time-differentiation is enough. We can then compute the minimizer

$$\underset{f \cdot F(q) + \nabla F(q)p \cdot p = 0}{\operatorname{argmin}} | -\nabla V(q) - f |^2. \quad (5.43)$$

Since the constraint is affine in f , the unique solution, provided $F(q) \neq 0$, is given by an orthogonal projection of $-\nabla V(q)$ onto the hyperplane (in the variable f)

$$f \cdot F(q) + \nabla F(q)p \cdot p = 0,$$

whose normal direction is given by $F(q)$. Hence the minimizer f^* can be written

$$f^* = -\nabla V(q) - \lambda F(q) \quad (5.44)$$

for some Lagrange multiplier λ , which is determined by

$$f^* \cdot F(q) + \nabla F(q)p \cdot p = 0.$$

Substituting our tentative expression for f^* , we get

$$(-\nabla V(q) - \lambda F(q)) \cdot F(q) + \nabla F(q)p \cdot p = 0.$$

This gives

$$\lambda = -\frac{\nabla V(q) \cdot F(q)}{|F(q)|^2} + \frac{\nabla F(q)p \cdot p}{|F(q)|^2}, \quad (5.45)$$

and finally

$$f^* = -\bar{P}_{F(q)} \nabla V(q) - \frac{\nabla F(q)p \cdot p}{|F(q)|^2} F(q),$$

which concludes the proof. \square

This result gives a nice physical interpretation of the deterministic Norton dynamics: it corresponds to a *physical* trajectory of a Hamiltonian system subject to the constant-response non-holonomic constraint. Indeed, Gauss's principle of least constraint [13] is equivalent to the Legendre-d'Alembert principle, which can be used to derive the equations of motion for constrained classical systems. The use of Gauss's principle of least constraint to enforce thermodynamic constraints for non-equilibrium molecular dynamics was already discussed in [9]. It is not yet clear to us how to extend this result to the case where F and G are non-colinear, and when the system is inhomogeneous, although it seems likely in this case Gauss's principle should have to be stated with respect to some modified scalar product. Another interesting direction would be to extend the principle to the properly Langevin case $\gamma > 0$. At any rate, we now turn to presenting our numerical results. As before, we will be using the two examples of mobility and shear viscosity computations.

5.3 Numerical results

5.3.1 Mobility

The Norton dynamics for mobility is recovered by setting F to be constant

$$F \in \{F_C, F_S\},$$

and taking

$$G = M^{-1}F$$

indeed, the response

$$R(q, p) = M^{-1}F \cdot p = F \cdot M^{-1}p,$$

since M is symmetric, which corresponds to the response observable for the mobility. Since F is constant in the q variable, the correction term in the A dynamics (5.17) is 0. Hence the A step (5.33) is analytically correct, with a vanishing Lagrange multiplier. We thus estimate the mean force through the estimator (5.39) with $\lambda^{k+\frac{1}{2}} = 0$. An estimator of

$$\lim_{r \rightarrow 0} \frac{\mathbb{E}_r[\lambda]}{r}$$

can then be obtained in the same way as (4.10), by

$$\hat{\rho}_F = |\hat{\lambda}|^{-2} \hat{\lambda} \cdot r = \operatorname{argmin}_{\rho \in \mathbb{R}} \left| \rho \hat{\lambda} - r \right|^2, \quad (5.46)$$

where $\hat{\lambda} \in \mathbb{R}^k$ is a vector of k ergodic averages of the form (5.39), and r is a vector containing the corresponding response intensities. Assuming, for simplicity's sake, that all ergodic averages are computed with the same number N_{iter} of time steps, and that $\hat{\lambda}$ has a (diagonal) matrix of asymptotic

variances Σ_λ^2 , applying the delta-method to (5.46) yields the following estimator for the asymptotic variance of $\hat{\rho}_F$

$$\sigma_{\rho_F}^2 = \nabla g(\hat{\lambda})^\top \Sigma_\lambda^2 \nabla g(\hat{\lambda}),$$

where

$$g(y) = |y|^{-2} y \cdot r,$$

which yields, after computation,

$$\sigma_{\rho_F}^2 = \sum_{i=1}^k \Sigma_{\lambda,ii}^2 \left(\frac{r_i |\hat{\lambda}|^2 - 2\hat{\lambda}_i (\hat{\lambda} \cdot r)}{|\hat{\lambda}|^4} \right)^2. \quad (5.47)$$

In the case $k = 1$, this becomes

$$\sigma_{\rho_F}^2 = \sigma_\lambda^2 r^2 \hat{\lambda}^{-4}. \quad (5.48)$$

In Figure 5.1, we plot the response-forcing diagram in the linear regime. The estimated transport coefficient from the color drift is consistent with the results obtained from the Thévenin method. For the single drift, we observe a discrepancy in the linear response. In Figure 5.2, we plot the response-forcing curve in the non-linear regime, and superimpose the data obtained from the Thévenin method. For the color drift, the two computed equations of state coincide perfectly. For the single drift, we again observe a small discrepancy. This leads us to speculate that the equivalence of non-linear responses may only hold in the thermodynamic limit, and for forcings which act on the bulk of the system, contrarily to the single drift forcing. In Figure 5.3, we show the computed asymptotic variance for estimators of ρ_F based on the Thévenin methods and the Norton methods. Asymptotic variances for estimators of the response and mean force were computed using block averages as in [12], and the corresponding asymptotic variance for the Norton estimator of ρ_F was obtained using (5.48). It appears that the two methods are roughly equivalent in terms of asymptotic variance, and that the variance for the finite-difference estimator scales like the inverse square of the forcing intensity, consistent with the result expected in the Thévenin case, as noted in Remark 13.

The final estimates for the transport coefficients using the Norton method are

$$\rho_{F_C} = 0.1211 \pm 0.0006, \quad \rho_{F_S} = 0.1089 \pm 0.0005.$$

Estimates of the transport coefficients were obtained using (5.46), and statistical error was estimated using (5.47)

5.3.2 Shear viscosity

The NEMD response observable (4.20) for shear viscosity can be recovered in the form

$$R_k(q, p) = \tilde{G}_k(q) \cdot p$$

by setting

$$\forall 1 \leq i \leq N, \forall 2 \leq \alpha \leq d, \quad \tilde{G}_k(q)_{i1} = \frac{1}{m} \exp\left(\frac{2ik\pi q_{i2}}{L}\right), \quad \tilde{G}_k(q)_{i\alpha} = 0. \quad (5.49)$$

Thus we can apply the Norton method. In practice, to avoid dealing with a complex exponential, we rather define

$$\forall 1 \leq i \leq N, \forall 2 \leq \alpha \leq d, \quad G_k(q)_{i1} = \frac{1}{m} \sin\left(\frac{2k\pi q_{i2}}{L}\right), \quad G_k(q)_{i\alpha} = 0. \quad (5.50)$$

This can be achieved at no cost to generality by considering an appropriate translation of the forcing profile with respect to the results of Figure 4.2. Estimators for the transport coefficient (4.21) and estimates of the statistical error can be obtained identically to the mobility case. All simulations were run in the reference thermodynamics condition (4.23) for a minimum length of 8×10^7 timesteps.

In Figure 5.4, we plot the normalized response

$$\frac{R_1}{c_1(f_y)}$$

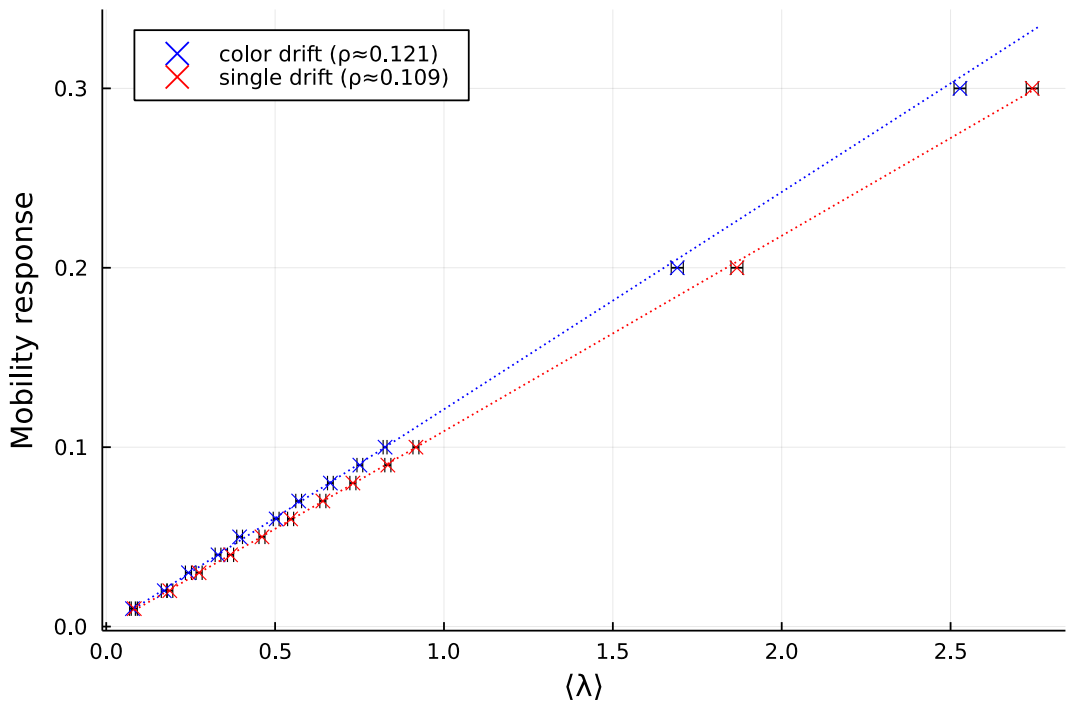


Figure 5.1: Mobility response versus average forcing intensity in the linear regime. Least squares linear regression lines are plotted in dotted line, and the estimated transport coefficients are indicated in the legend.

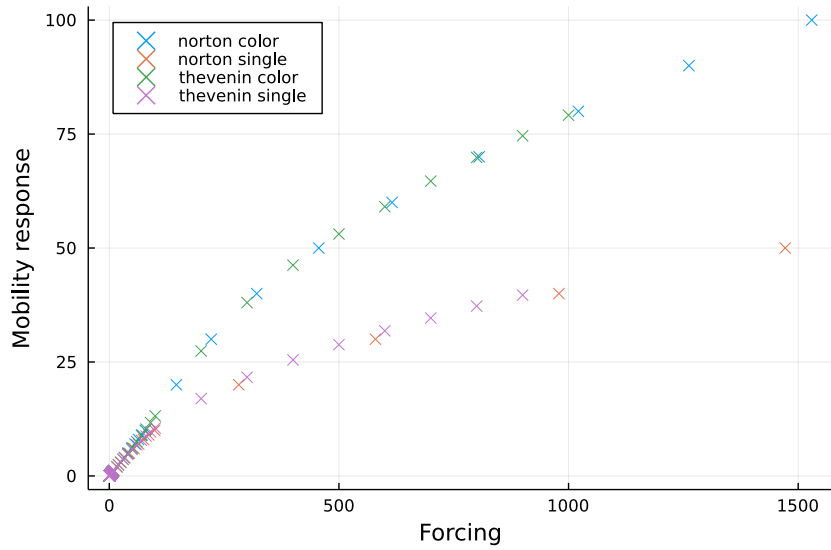


Figure 5.2: Comparison of the Thévenin and Norton mobility equations of state.

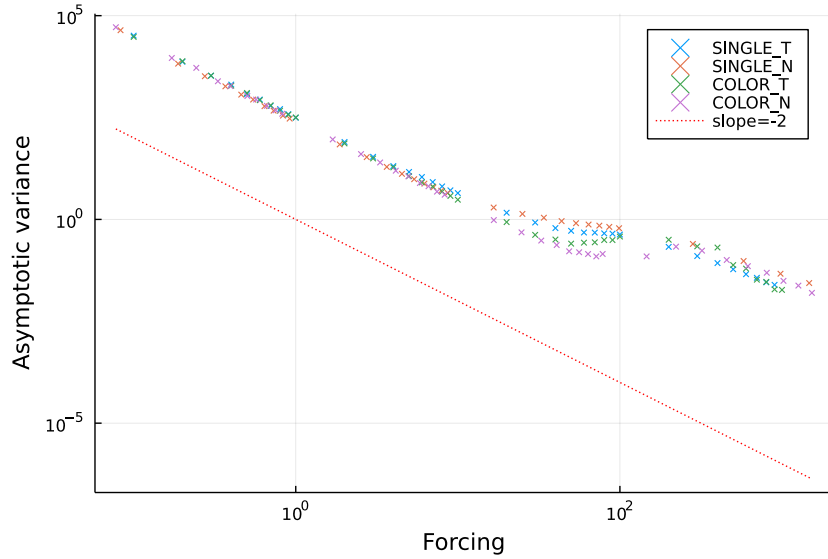


Figure 5.3: Plot of the asymptotic variance as a function of the forcing intensity for the different methods, on a log-log plot. Results corresponding to a Thévenin estimator are denoted with a T, and those corresponding to the Norton estimator are denoted with a N.

against the estimated average forcing $\langle \lambda \rangle$ in the linear regime, for the different forcing profiles. The estimated transport coefficients are consistent with one another, and agree with those obtained in the Thévenin and Green–Kubo setting. In Figure 5.6, we compare the non-linear response profiles between the Thévenin and Norton methods, for each of the forcing profiles. In every case, the responses coincide perfectly throughout. In Figure 5.5 we compare asymptotic variances of the finite difference estimators of the normalized response $\rho_{F,1}/c_1(f_y)$ using the Thévenin and Norton method. The asymptotic variance was estimated directly from the response time series in the Thévenin case, using a block averaging procedure, and for the Norton method, a block averaging procedure on the forcing time series was combined with a delta-method. We find that the Norton estimators consistently outperform their Thévenin counterparts. Furthermore, it appears not all forcing profiles are equal in terms of asymptotic variance.

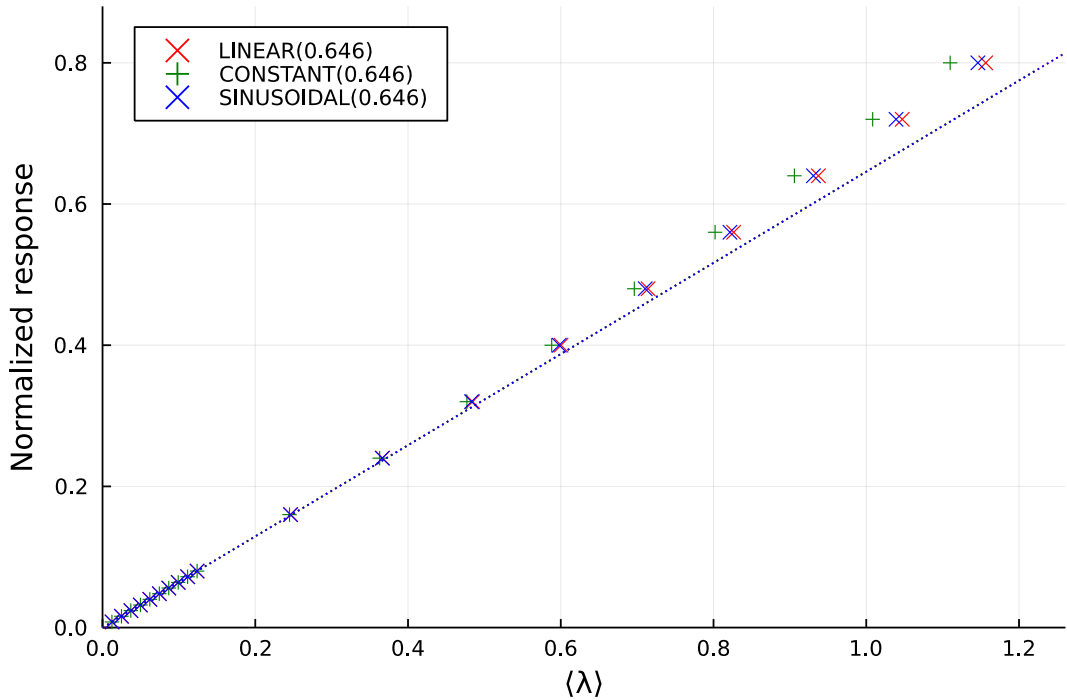


Figure 5.4: Normalized Fourier response versus forcing intensity for the three transverse forcing profiles. The size of the linear response regime is roughly the same for every type of forcing. Least squares linear regression lines on the 10 first values are plotted in dotted line, and estimated normalized transport coefficients are indicated in the legend.

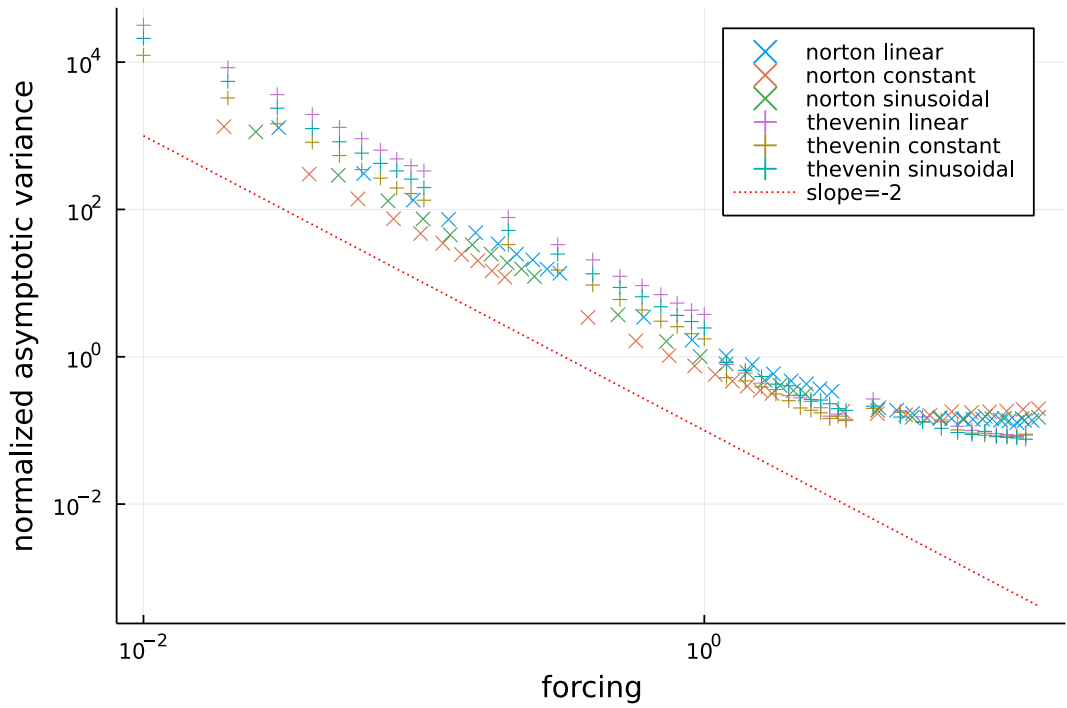


Figure 5.5: Scaling of the asymptotic variance for the finite difference estimator of the normalized transport coefficient for shear viscosity

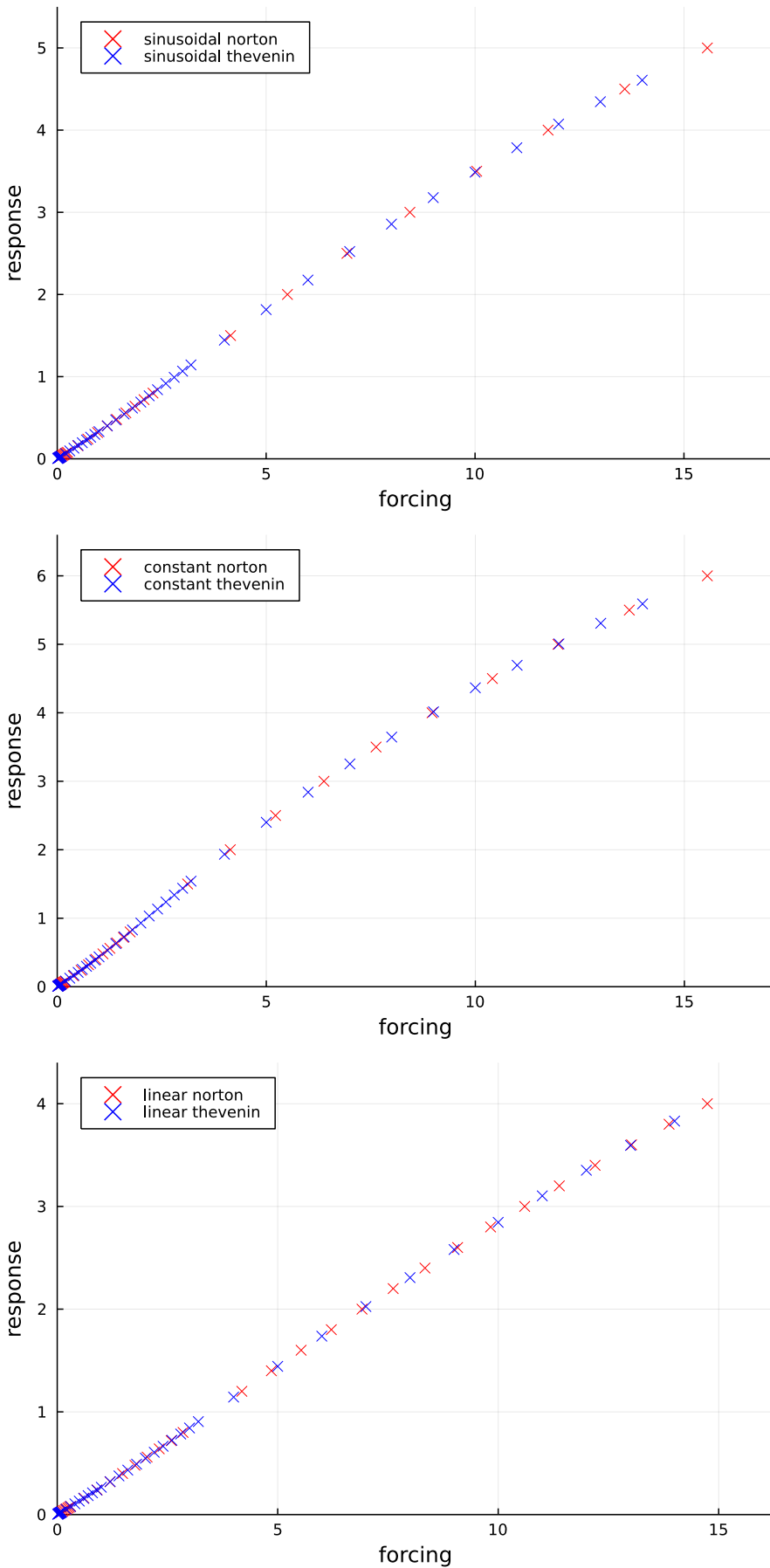


Figure 5.6: Norton and Thévenin equations of state for the shear-viscosity Fourier response, for each type of forcing profile.

Appendix A

Implementation details

We conclude this report by a short appendix dedicated to providing some details about the concrete implementation of the methods we discussed throughout this report. We start by giving some informal ideas about where the computational cost of a molecular simulation is concentrated, before discussing the process of choosing a software to implement various non-equilibrium methods. We finally give a short summary of the implementations we made, pointing the reader to the relevant sources.

A.1 Scaling of the computational cost

Throughout this document, the reader will notice that little is said about ∇V , meaning the methods we described simply invoked ∇V where it is needed, without getting into the specifics of *how* it is computed. For a pair interaction potential of the form (1.12), the naive method of summing over all pairs of particles incurs a cost of

$$\frac{N(N-1)}{2} = \mathcal{O}(N^2)$$

evaluations of the pair interaction function v . Another point we alluded to is that the statistical error on the computation of averages usually dissipates at a rate $\mathcal{O}(1/\sqrt{\Delta t N_{\text{iter}}})$. Furthermore, for averages to be physically meaningful, N must be taken large enough for the thermodynamic limit to be considered reached. In practice, a quadratic scaling of the computational cost of computing ∇V may render essentially impossible the computation of long numerical trajectories. Instead, one has to rely on approximate evaluations of ∇V . For instance, in the case of a Lennard-Jones interaction, the pair interaction potential decays quickly, in $\mathcal{O}(r^{-6})$ as a function of the interparticular distance r . In this case, a reasonable approximation consists on imposing a fixed maximal interaction distance r_c , called the *cutoff* distance, and asserting that particles which are further apart than r_c do not interact. This amounts mathematically to replacing the pair interaction function $v(r)$ by a cut-off version $v(r)\mathbb{1}_{r < r_c}$, effectively modifying the potential. There are various ways to alter this procedure in order to make the modified potential continuous or C^1 , for instance using spline interpolation. Of course, this procedure alone does not solve anything, since one still needs to determine *which* pairs of particles are neighbors, meaning they are closer apart than r_c , which still amounts to $\mathcal{O}(N^2)$ computations of the (squared) Euclidean norm. To make this viable, one has to store a list of neighbor pairs in an efficient data structure which only needs to be updated once every few simulation iterations, since the set of neighboring pairs tend not to drastically change over short time intervals. In practice, and depending on the timestep, the meaning of the word *few* can sometimes be understood to be as large as 50. There are various strategies to implement such a data structure, such as Verlet lists or cell lists, which are described in detail in [1, Section 5.3]. At any rate, since the number of neighbors to a given particle should on average be close to $4\pi\rho r_c^3/3 = \mathcal{O}(1)$, where ρ is the particle density, the cost of computing ∇V becomes (ideally) **linear** in N , which makes long time simulations a practical possibility. We mention the issue of short-range interactions since all our molecular simulations used V of the Lennard-Jones form, but other methods exist in the case where V decays slowly like the Coulomb electrostatic potential, relying in this case on a fast decay property in Fourier space. Of course, many more tricks exists, which collectively form the whole craftsmanship of Molecular Dynamics (MD) simulations: finding efficient, approximate ways to compute V and ∇V .

A.2 Selecting a Molecular Dynamics package

The process of implementing from scratch these methods is time consuming, and unnecessary given the number of freely available MD packages. However, some of these packages are quite ancient and heavily optimized so that the process of implementing new methods comes with quite a heavy learning overhead, as well as being harder to debug. Instead, we chose to make use of a Julia package for MD simulation, thus taking this opportunity to learn the programming language Julia [2], which has been gaining a lot of traction in the scientific computing user base, in part because it offers the shared benefit of performance comparable to that of C or C++, as well as possessing a rich ecosystem of highly intercompatible packages, powered by a strong community and a design philosophy centered around generic, type-agnostic, interfaces.

The first step in the internship consisted in choosing a package between two contenders, NBodySimulator [31], and Molly [15]. NBodySimulator, in summary, acts as a wrapper around the native differential equations Julia framework, constructing a differential equation or stochastic differential equation from the specification of a molecular system. As such, it aims to compute *exact* solutions to the dynamics, or at least exact evaluations of V . On the other hand, Molly offers a number of neighbor-finding strategies, such as the cell list method, a parallelized naive iteration over all pairs of neighbors, as well as a tree-search based method. In Figure A.1, we show the results of a comparison of the scaling of the simulation time as a function of the system size, for NBodySimulator and Molly’s various neighbor finding strategies. We find that, if for very small systems, NBodySimulator outperforms Molly, the advantage quickly disappears, for $N \geq 750$ approximately, in the case of the cell list method. Interestingly, even the naive double loop for Molly overtakes NBodySimulator in performance. This is because by default, Molly parallelizes the force computation, while there is no parallelization in NBodySimulator.

On this basis, we chose to implement our methods in Molly.

A.3 Summary of implementations

Along the way, some of our implementations were integrated in the Molly source, in large part during a one-week stay in the MRC Laboratory of Molecular Biology in Cambridge, where the main author of Molly’s source code, Joe Greener, works. These integrations include:

- i) A cutoff strategy based on a cubic spline interpolation,
- ii) A general Langevin integrators, which works for all splitting orderings (2.44) and in the (non)-equilibrium setting,
- iii) A logger to efficiently estimate time correlations functions of the form (4.28),
- iv) A logger to track the self-diffusion coordinates (4.43) for Einstein mobility computations,
- v) A refactoring of Molly’s general logging architecture, for more flexibility and extensibility,
- vi) The addition of a parameter for Boltzmann’s constant, allowing for fully consistent sets of user-defined custom systems of units,
- vii) An online ergodic average and asymptotic variance estimator for a user-specified observable.

These were additionally documented, and non-regression tests were implemented for each of them. We refer the reader to the Molly documentation and source code for more details. Other implementations were too use-specific, not general or not mature enough to be integrated. These include

- i) A pressure observable based on (1.2),
- ii) The implementation of NEMD force fields for mobility and shear viscosity computations,
- iii) The implementation of an integrator for the Norton method,
- iv) Various logging and visualization utilities.

These implementations are available in the repository [4], although we apologize in advance to the interested reader for the poorly organized, largely uncommented mess that lies within. We expect, especially for the pressure observable, that a future integration in Molly will be possible, for instance once

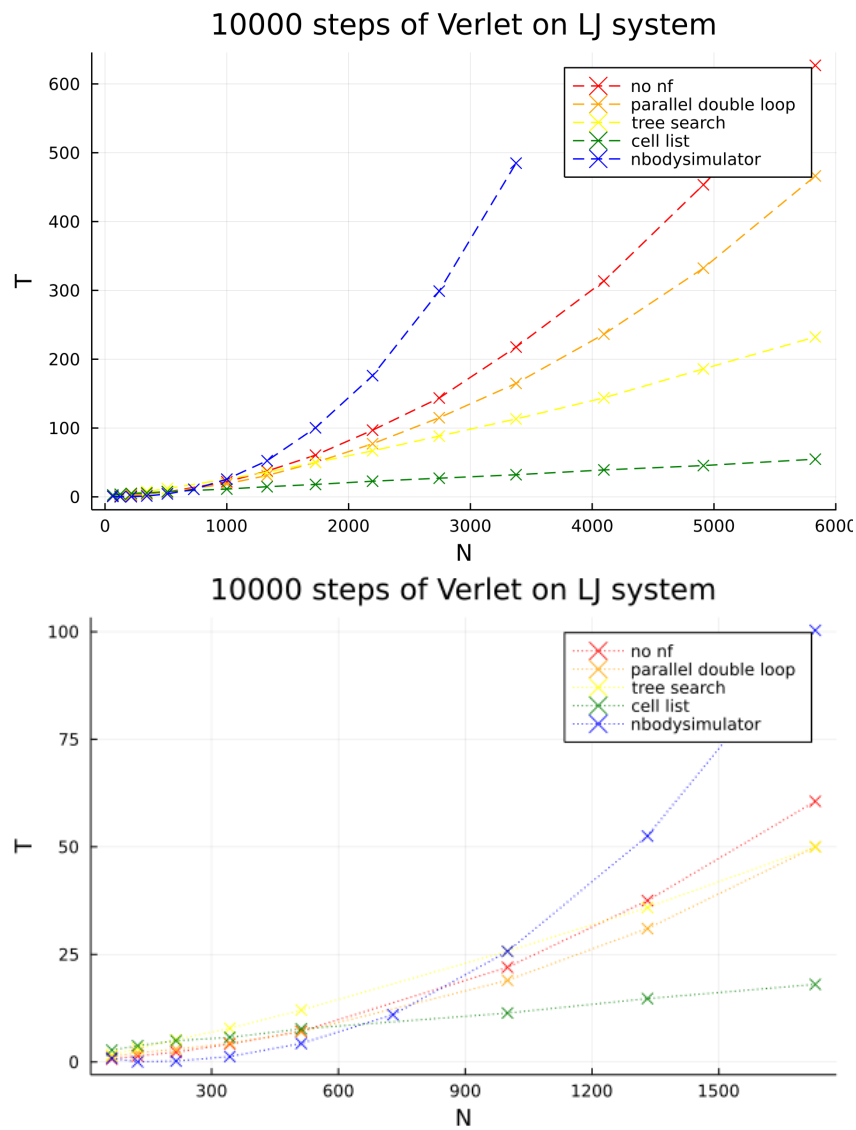


Figure A.1: Comparison of world clock time for the simulation of 10000 steps of a Lennard-Jones system. The "no nf" corresponds to the naive double loop. Top: full curve. Bottom: zoom on the small system regime.

long-range force contributions are implemented, as well as a more flexible interface for force computations. This will be a necessary step in the implementation of barostats, which are important in the context of biomolecular simulation, a use case Molly is particularly attuned to. On the other hand, non-equilibrium methods are unlikely to have a place in a general-purpose MD package. Instead, we might consider publishing in the future a standalone package that extends Molly for transport coefficient computations, once our understanding of the Norton method has cohered.

Bibliography

- [1] M.P. Allen and D.J. Tildesley. *Computer Simulation of Liquids*. Oxford Science Publications. Clarendon Press, 1989.
- [2] Jeff Bezanson et al. “Julia: A fresh approach to numerical computing”. In: *SIAM review* 59.1 (2017), pp. 65–98. URL: <https://doi.org/10.1137/141000671>.
- [3] R.N. Bhattacharya. “On the Functional Central Limit Theorem and the Law of the Iterated Logarithm for Markov Processes”. In: *Zeitschrift für Wahrscheinlichkeitstheorie und verwandte Gebiete* 60 (2 1982), pp. 185–201.
- [4] N. Bassel. *Internship repository*. 2022. URL: <https://github.com/noebassel/MolecularDynamicsJulia>.
- [5] R.S. Ellis. *Entropy, Large Deviations, and Statistical Mechanics*. Classics in Mathematics. Springer Berlin Heidelberg, 2007.
- [6] P Espa  ol and P Warren. “Statistical Mechanics of Dissipative Particle Dynamics”. In: *Europhysics Letters (EPL)* 30.4 (1995), pp. 191–196.
- [7] D.J. Evans. “The equivalence of Norton and Th  venin ensembles”. In: *Molecular Physics* 80 (1 1993), pp. 221–224.
- [8] D.J. Evans and G. Morriss. *Statistical Mechanics of Nonequilibrium Liquids*. Cambridge University Press, 2008.
- [9] D.J. Evans et al. “Nonequilibrium molecular dynamics via Gauss’s principle of least constraint”. In: *Physical Review A* 28 (2 1983), pp. 1016–1021.
- [10] M. Fathi, A.A. Homman, and G. Stoltz. “Error Analysis of the Transport Properties of Metropolized Schemes”. In: *ESAIM Proc.* 48 (2015), pp. 341–363.
- [11] M. Fathi and G. Stoltz. “Improving dynamical properties of metropolized discretizations of overdamped Langevin dynamics”. In: *Numerische Mathematik* 136 (2 2016), pp. 545–602.
- [12] H. Flyvbjerg and H. G. Petersen. “Error estimates on averages of correlated data”. In: *The Journal of Chemical Physics* 91.1 (1989), pp. 461–466.
- [13] Carl Friedrich Gau  . “  ber ein neues allgemeines Grundgesetz der Mechanik.” In: (Jan. 1829). DOI: 10.1515/crll.1829.4.232. URL: <https://doi.org/10.1515/crll.1829.4.232>.
- [14] E.M. Gosling, I.R. McDonald, and K. Singer. “On the calculation by molecular dynamics of the shear viscosity of a simple fluid”. In: *Molecular Physics* 26.6 (1973), pp. 1475–1484.
- [15] J. Greener. *Molly*. 2020. URL: <https://github.com/JuliaMolSim/Molly.jl>.
- [16] E. Hairer, C. Lubich, and G. Wanner. “Geometric numerical integration illustrated by the St  rmer-Verlet method”. In: *Acta Numerica* 12 (2003), pp. 399–450.
- [17] E. Hairer, C. Lubich, and G. Wanner. *Geometric Numerical Integration: Structure-Preserving Algorithms for Ordinary Differential Equations*. Springer Series in Computational Mathematics. Springer Berlin Heidelberg, 2013.
- [18] “Hypocoercivity for linear kinetic equations conserving mass”. In: *Transactions of the American Mathematical Society* 367.6 (2015), pp. 3807–3828.
- [19] R. Joubaud, G.A. Pavliotis, and G. Stoltz. “Langevin dynamics with Space-Time Periodic Nonequilibrium Forcing”. In: *Journal of Statistical Physics* 158 (2015), pp. 1–36.
- [20] R. Joubaud and G. Stoltz. “Nonequilibrium Shear Viscosity Computations With Langevin Dynamics”. In: *Multiscale Modelling & Simulation* 10 (1 2012), pp. 191–216. DOI: <https://doi.org/10.1137/110836237>.

- [21] B.G. Keller and S. Kieninger. “GROMACS Stochastic Dynamics and BAOAB are equivalent configurational sampling algorithms”. URL: <https://arxiv.org/abs/2204.02105v1>.
- [22] W. Kliemann. “Recurrence and Invariant Measures for Degenerate Diffusions”. In: *The Annals of Probability* 15 (2 1987), pp. 690–707.
- [23] B. Leimkuhler and C. Matthews. *Molecular Dynamics With Stochastic and Deterministic Methods*. Interdisciplinary Applied Mathematics. Springer, 2015.
- [24] B. Leimkuhler, C. Matthews, and G. Stoltz. “The computation of averages from equilibrium and nonequilibrium Langevin molecular dynamics”. In: *IMA Journal of Numerical Analysis* 36 (1 2016).
- [25] NIST. *Thermophysical Properties of Fluid Systems*. URL: <https://webbook.nist.gov/chemistry/fluid/>.
- [26] P.H. Peskun. “Optimum monte-carlo sampling using markov chains”. In: *Biometrika* 60.3 (1973), pp. 607–612.
- [27] A. Quarteroni, R. Sacco, and F. Saleri. *Numerical Mathematics*. Texts in Applied Mathematics. Springer Berlin Heidelberg, 2010.
- [28] H. Rodenhausen. “Einstein’s relation between diffusion constant and mobility for a diffusion model”. In: *Journal of Statistical Physics* 55 (1989), pp. 1065–1088.
- [29] P. J. Rossky, J. D. Doll, and H. L. Friedman. “Brownian dynamics as smart Monte Carlo simulation”. In: *The Journal of Chemical Physics* 69.10 (1978), pp. 4628–4633.
- [30] M. Tuckerman. *Statistical Mechanics: Theory and Molecular Simulation*. Oxford University Press, 2010.
- [31] M. Vaganov and C. Rackauckas. *NBodySimulator*. 2018. URL: <https://github.com/SciML/NBodySimulator.jl>.